Microchannel technology in cancer cell confined-migration study and its application in drug screening

by

Qionghua Shen

Presented to the Faculty of the Graduate School of

The University of Texas at Arlington in Partial Fulfillment

of the Requirements

for the Degree of

DOCTOR OF PHILOSOPHY IN BIOMEDICAL ENGINEERING

The University of Texas at Arlington

August 2020

ACKNOWLEDGEMENTS

Abstract

Microchannel technology in cancer cell confined-migration study and its application in drug screening

The University of Texas at Arlington, 2020

Supervising Professor: Dr. Young-tae Kim.

PDMS-based microchannel device has been explored to extend the basic platform for three-dimensional (3D) culture models of cell motility study because of its relevant stiffness and designable shape. Moreover, it is easy to add multi-functions (physical cures and biochemical cures) to one single device and provide a more physiologically relevant context to cells migrating inside channels. As recent cell motility studies have proved that cells show different migration strategies in physiologically confined three-dimensional (3D) space compared to a two-dimensional (2D) culture system. Besides, far from unique, when cancer cells are underling the migrating stage, they show increased resistance to chemo- and radio-therapies compared to non-migrating cells. Therefore, it is consequential to understand the invasion mechanism of migratory cancer cells (for example, GBMs) and explore the insight link between metastasis under physical confinement and acquired therapeutic resistance, in order to devise efficient therapeutic strategies. To choose/ design suitable tools for confined migration study is the fundamental step. In the past four years, I have been focusing on using microchannel platforms to study cancer cell's confined-migration behavior and its correlation with metastatic cancer's therapeutic resistance. Above this, I also try to design a suitable microchannel platform to combine cell motility study with a high-throughput screening method to address issues from cancer tissue's heterogeneity. I have published one article in a peer-reviewed journal and had two manuscripts in the submission that are related to this. All the above-mentioned works are summarized in the following chapters.

Chapter 1: **Shen, Q.**, Hill, T., Cai, X., … & Kim, Y.T. (2020) Physical Confinement during Cancer Cell Migration Triggers Therapeutic Resistance and Cancer Stem Cell-like Behavior.

Chapter 2: **Shen, Q.**, Germain, A., & Kim, Y.T. (2020) Migration and Physical Confinement are Two Indispensable Elements for Upregulating GBM's Chemotherapeutic Resistance.

Chapter 3: **Shen, Q**., Niederstrasser, H., Barakat, R., … & Kim, Y. T. (2020). Single-cell-level screening method for migratory cancer cells and its potential feasibility in high-throughput manner. *Biofabrication*, *12*(3), 035019.

Motivations

Recently existing anticancer therapy is challenged by two major events in cancer progress: 1) the metastatic dissemination of tumor cells leading to multi-organ invasion [1]; 2) active resistance to therapy triggered by tumor microenvironment stress during tumor progression [2]. Traditionally, these two processes are considered as distinct processes and are widely studied separately. However, a recently increasing number of indirect evidence suggests that tumor resistance to treatment may be triggered by or involved in invasion and metastasis process as in response to microenvironmental stress [2]. This may provide a new approach for generating resistant cancer cells which can be used in developing anticancer strategies.

In cancer metastasis, cell migration is the fundamental step. Cancer cells can migrate away from the original tumor mass, through surrounding extracellular matrices, invade into distal sites (where the secondary tumor will form) [3]. Far from unique, when those cancer cells are underling migrating stage, they show increased resistance to chemo- and radio- therapies compared to non-migrating cells [4,5]. Therefore, the development of resistance to therapeutic methods during invasion and metastasis of cancer cells can be considered as the main contribution to cancer intractability [6]. For example, as a typically migratory cancer, glioblastoma cells (GBMs) can be used to illustrate the diffuse and antitherapeutic nature of those cancer cells. As the most malignant and highly aggressive malignant gliomas, patients have GBM have normally short life expectancy (only 12-15 months) [7], mainly due to the treatment failure followed by tumor recurrence [8]. This is caused by diffused GBM cells invasive into the surrounding brain tissue. 1-2 cm healthy brain tissue infiltration is not a rare situation that can be observed in GBM patients [9]. Unsurprising, those diffused GBM cells are highly resistant to common anti-cancer therapies (chemo- and/or radio-therapies) [10]. Therefore, it is critical to understand the invasion mechanism of migratory cancer

cells (for example, GBMs) and explore the insight link between metastasis and therapeutic resistance, in order to devise efficient therapeutic strategies.

Generally, metastatic dissemination largely results from microenvironmental factors [11]. But resistance is believed to be mostly controlled by molecular genetics [12, 13]. Whereas, if viewed in detail, there is an overlap of signaling networks of cancer invasion and resistance (Figure 1) [4].
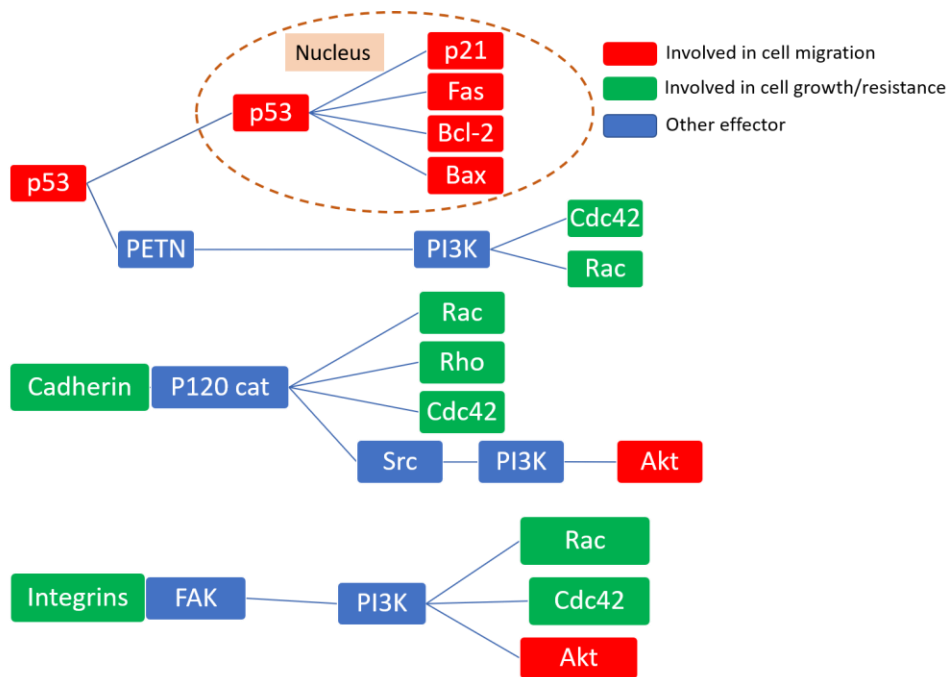

Figure 1. Crosstalk of signaling pathways for invasion and resistance. This tree diagram shows different pathways are involved in both migration/invasion and survival/resistance behavior of tumor cells. Red icons indicate factors that regulate cell migration behavior. Green icons indicate factors influence cell growth. Blue icons label factors with other effects.

The natural microenvironment of an organism is a complex three-dimensional structure. Cells live inside the ECM need to make contact with surrounding components. Therefore, they need to respond to various physical stimuli (e.g., matrix dimensionality and mechanical properties). What's more, the intracellular biochemical activity will also be influenced by these extracellular physical signals. This process is known as mechanotransduction. Various molecules play

important roles during this process. They are activated by outside stimuli and link the cell's ECM to the internal cytoskeleton to allow mechanical signals from the outside to be propagated into the cell[14, 15]. Glioma cells also have a special system that helps them sense and respond to micron-scale gradients of mechanical rigidity throughout the brain. Multiple receptors, such as integrins, G-protein-coupled receptors, and CD44 work together to transduce mechanical signals, including confinement[16, 17]. Inherently, most of those receptors also involved in cancer cells' increased therapeutic resistance.

For example, the adhesion class of G-protein-coupled receptors (GPCR) are involved in cell migration. This class of GPCRs can help glioma cells to sense and integrate chemical, cellular, and ECM cues. By stimulating GTPase or RTK transactivation, they can also modulate the modality of cell migration. Also, they can help to upregulate MMPs, which can mediate tumor cell invasion and transcription. GPCRs also can regulate cell survival. The primary mechanism is through AKT (phosphorylate and inactivate BAD to prevent apoptosis [18]) and NFκB activation (alter the transcription of apoptotic gene products to promote cell survival [19]).

CD44 transmembrane glycoproteins belong to the families of adhesion molecules that contribute to cancer cell confined migration[20]. As one of the receptors anchored to the actin cytoskeleton, CD44 can rapidly relay mechanical stimuli (including confinement). The mechanisms include releasing of actin-bound transcription factors and directly coupling to the nuclear membrane. CD44 also involves upregulating GBM resistance to chemotherapy by increasing and stabilizing MDR1 expression which will regulate drug efflux and promote cancer cells surviving during chemotherapy[21, 22]. Besides, it can upregulate PI3K-AKT and MAPK-ERK1/2 signaling pathways to increase apoptotic resistance and migratory capacity by interacting with surrounding

microenvironment[22, 23]. Pietras et al. pointed out that CD44 can promote the GBM stem-like phenotype and contribute to radiation resistance[24].

Therefore, changes in the tumor microenvironment caused by the treatment or natural cancer progress may prompt resistance and metastasis as secondary events [25, 26]. For example, after radiation, the resistant cell populations show increased invasion capability [4, 27]. At the same time, promigratory pathways can implicate resistance induction in invading tumor cells [28]. Still use GBMs as an example. Local recurrence after radiation is prevalent and even more chance find diffused ones as invading to brain parenchyma [29]. It is consistent with signaling crosstalk between cell migration and survival programs. Hence, it is meaningful to consider metastasis and resistance as a tight-linked combination.

Lack of technologies that are precise to separate physiological migrating cells and/or monitor the invasion state is another main reason for separating the study of resistance and invasion. During a long period, in vitro migration study has been mainly performed on unconfined two-dimensional (2D) surface [30]. However, compared to a natural condition, 2D culturing system miss some important key elements and can not mimic real physiological condition [30]. As well-known, the first step of cancer metastasis is migration and invasion into adjacent tissues [31]. Interestingly, cancer cells preferent to transmit through pre-existing tissue tracks [32]. Recent intravital microscopy studies reveal that those in vivo tissue tracks have consistently narrow dimensions: vary from <3um to ~30μm in width and 100-600μm in length [33, 34]. All those pre-existing tracks can be considered as two principal types of interstitial tissues: 1) collagen-rich interstitial connective tissue, and 2) the interstitium of the brain [32]. An interesting point is that during cancer cells migrating inside those interstitial tissues there are no significant changes in track width[35]. Hence,

it is believed that, under in vivo condition, tumor cells can change their shape to fit into narrow space in vivo without tissue remodeling or degradation and can migrating following those pre-existing tracks[25, 36]. Then the question arises: whether those cells migrating under 2D condition will be different from those migrating through confined spaces? Recent cell motility studies have proved cells show different migration strategies in physiologically confined three-dimensional (3D) space compared to two-dimensional (2D) culture system [37, 38]. For example, under natural conditions, GBMs or breast tumors, most of those migrating cells often move linearly along extracellular matrix fibers with an amoeboid morphology which is totally different from petri dish cultured one [39, 40]. Therefore, controlled physical topography and confinement are necessary to induce a response of cells that is similar to the real microenvironment. That is the reason why scratch assay has been considered a lack of authenticity for cell migration study in recent years. *In vivo* models are not widely used in cancer cell confined migration studies because of its low throughput. The complexity of performing the experiments will cause reproducibility issues and prohibitive cost. Hence, multiple engineered in vitro 3D models (Table 1) have been designed to carry out GBM confined migration study and evaluate the therapeutic efficacy of potential clinical treatments. To varying degrees, they all can mimic the physical and chemical aspects of the native GBM microenvironment. Those biomaterial systems are more reproducible and can avoid the uncontrollability from animal models. Also, because of avoiding the introduction of nonhuman components, they are considered as more accurate assays. Furthermore, individual microenvironmental parameters' effects can be studied in a controlled context by using that engineered ex *vivo* platforms (by changing devices' size, shape, or coating material). They provide an opportunity for personalized medicine. Several different types of devices have been used in GBM confined migration studies. Two important standards have been used to evaluate each model:

1) the capacity to mimic aspects of the GBM microenvironment; and 2) the capability to dictate tumor progression and treatment resistance.

Microcontact-printed and micropatterned "1 D" lines or groove devices (Table 1) are widely used to constrain cells on a 2D substrate. They can be created by laser irradiation or soft lithography molding of poly-dimethylsiloxane (PDMS) directly on a silicon base or PDMS/polystyrene surface. The printed stripes will guide the GBM cell's movement. The depth of each line (groove) can range from hundreds of nanometers to tens of micrometers [41]. Depends on the size (width and depth) and gap space between each printed strip, those seeded cells will display different movements. When the gap between printed pattern is less than the cell body, the cell will adherent on grooved substrates and have a guided migration pattern with the controlled available spreading area. The resulting migration mode is known as "one-dimensional (1D)" migration. Because only the basal surface of the cell adhering to the printed pattern will receive topographical cues. However, when the gap space is larger enough for cells to get in, the cell will migrate between grooves by adherent on one or two sides of the wall [41]. Obviously, in these assays, cells are not fully compressed because confinement is only imposed by adhesions formed part. Therefore, cells' behavior can not reflect real *in vivo* situations.

Boyden chamber (transmembrane assay, Table 1) is one of the most common devices used to study the migratory response of cells to inducers or inhibitors. In this assay, a membrane that contains randomly distributed pores through which the cells migrate will provide vertical confinement to seeded cells. The most obvious advantage of this assay is it can separate migrating and non-migrating cells into two compartments and offer the advantage of analyzing migration in response to a chemotactic gradient. Since the guided patter is vertical so it can be used with both adherent

and non-adherent cell lines. However, due to the limitation of current available fabricating techniques, the thickness of the membrane still within several tens micrometers which may not enough to observe some long-term confinement triggered cellular changes. Other drawbacks include the technical challenges for a chamber set up and difficulties in visualizing the cells' behaviors during the experiments.

Microchannel/microfluidic devices (Table 1) fabricated by micro/nano techniques have straight or shaft-like spaces with rectangular cross-sections. Microchannels can be made by poly-dimethylsiloxane (PDMS), collagen, or polyacrylamide. Currently, the majority of devices are constructed via photolithography combined with soft lithography because of the special characteristics of this material: high optical transparency, high oxygen diffusing rate, and low thickness[30, 42]. The pre-defined cell migratory path within micro-sized channels is aimed to mimic the *in vivo* brain tissue conditions, for example, the in perivascular and white matter tracks in the brain[30]. The typical size of the microchannel is between 3 μm and 50 μm (widths and heights). Depending on the microchannel dimensions, the cells' migration modes will be different. When the channel size is smaller than the cell body, they may be laterally confined by all four microchannel walls. The migration direction is along the channel wall. Cells only have the freedom to move forwards and backward. To the contrary, when the channel size is big enough, cells may only attach to one or two channel walls (similar as groove device)[43]. Combined with time-lapse imaging techniques, it allows for the examination and tracking of glioma cells' motility and directionality under the confined condition similar to in vivo glioma cells following the path of white matter tracks or other heterogeneous structures[44, 45]. Besides, coating and filling the microchannel with different ECM proteins can allow them to mimic different microenvironmental

components within the brain. This can help to illustrate the selectivity of cancer cell migration on distinct ECM.
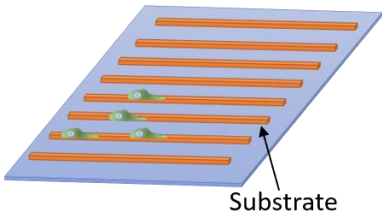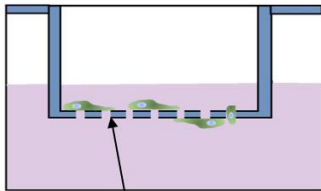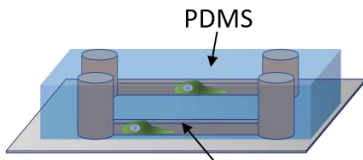
	Microprinted 1D lines	Boyden chamber	Microfluidic channels
Advantages	• Simple fabrication • Guided "1 D migration"	• Suitable for adding surface coating • Provide 3D physical confinement	• Suitable for adding surface coating • Single-cell-level observation • Track cell morphological change during movement • Provide 3D physical confinement
Limitations	• Cells are not fully compressed	• Difficult to observe cell movement and morphology change • Thickness limits the confined-time	• Stringent material choosing • Extra cell culture time
Diagram	Substrate	Membrane with nanometer- to micrometer- sized pores	PDMS Micrometer- sized channel

Table 1. *In vitro* **cell-based assays have been used to explore physical confinement affecting cell properties.**

On top of this, PDMS-based microchannel devices have been a kind of common tools for migratory study due to their novel properties. It has relevant stiffness as those in vivo micro-tracks such as muscle and nerve fibers [46, 47]. What's more, it is easy to add multi-function, including physical cures (e.g., space structure or topography) and biochemical cures (e.g., surface modification), to one single microchannel device via well-developed fabrication technologies [48, 49]. Besides, as a product of nano- or microtechnology, the small size of PDMS-based microchannel devices makes them more suitable for the high-throughput manner which becomes the preferred method due to its high efficiency and low energy cost [50, 51]. Therefore, the microfabrication techniques have been more widely used to simulate 3D micro-tracks in vitro for cancer invasion study.

In this presented study, we choose PDMS-based multifunctional microchannel devices cells which we believe are closer to physical confined-migration microenvironment to generate and separate confined-migrating cells as the potential source of therapeutic resistant cells. Conclusively, the purpose of this present study is to use a bio-engineered PDMS-based microchannel device as a tool to separate/generate sufficient confined-migrating/migrated cancer cells for study. By indicating the cause-consequence relationship between confined-migration and resistance, we attempt to indicate the potential application of bioengineered microchannel devices in producing therapeutic resistant cancer cells for anticancer study. Besides, we tried to combine microchannel technology with a high-throughput screening method together to carry out a single-cell-level study. This attempt of our mHTS platform revealed the possibility of combing single-cell-level study and high-throughput screening to address influence from the heterogeneous nature of cancer cells in cancer cell migration study. This technique can provide a new efficient method to find effective combinations of molecular targeting to improve therapy strategies and indicate appropriate formulation and scheduling of drug delivery.

Reference

1. H. Läubli and L. Borsig Selectins promote tumor metastasis *Elsevier* **20** 169-177
2. D. F. Quail and J. A. Joyce 2013 Microenvironmental regulation of tumor progression and metastasis *Nature Publishing Group* **19** 1423
3. E. W. Thompson and J. T. Price 2002 Mechanisms of tumour invasion and metastasis: emerging targets for therapy *Taylor & Francis* **6** 217-233
4. S. Alexander and P. Friedl 2012 Cancer invasion and resistance: interconnected processes of disease progression and therapy failure *Elsevier* **18** 13-26
5. T. C. A. Johannessen, J. Wang, K. O. Skaftnesmo, P. Ø. Sakariassen, P. Ø. Enger, K. Petersen, A. M. Øyan, K. H. Kalland, R. Bjerkvig and B. B. Tysnes 2008 Highly infiltrative brain tumours show reduced chemosensitivity associated with a stem cell-like phenotype *Wiley Online Library* no-no
6. T. A. Martin, L. Ye, A. J. Sanders, J. Lane and W. G. Jiang 2013 Cancer invasion and metastasis: molecular and cellular perspective *Landes Bioscience*

7. A. Omuro and L. M. DeAngelis 2013 Glioblastoma and other malignant gliomas: a clinical review *American Medical Association* **310** 1842-1850

8. M. Pàez-Ribes, E. Allen, J. Hudock, T. Takeda, H. Okuyama, F. Viñals, M. Inoue, G. Bergers, D. Hanahan and O. Casanovas 2009 Antiangiogenic therapy elicits malignant progression of tumors to increased local invasion and distant metastasis *Elsevier* **15** 220-231

9. P. De Bonis, C. Anile, A. Pompucci, A. Fiorentino, M. Balducci, S. Chiesa, L. Lauriola, G. Maira and A. Mangiola 2013 The influence of surgery on recurrence pattern of glioblastoma *Elsevier* **115** 37-43

10. Y. Piao, J. Liang, L. Holmes, A. J. Zurita, V. Henry, J. V. Heymach and J. F. de Groot 2012 Glioblastoma resistance to anti-VEGF therapy is associated with myeloid cell infiltration, stem cell accumulation, and a mesenchymal phenotype *Oxford University Press* **14** 1379-1392

11. E. K. Rofstad 2000 Microenvironment-induced cancer metastasis *Taylor & Francis* **76** 589-605

12. M. M. Gottesman 2002 Mechanisms of cancer drug resistance *Annual Reviews 4139 El Camino Way, PO Box 10139, Palo Alto, CA 94303-0139, USA* **53** 615-627

13. J. M. Croop, P. Gros and D. E. Housman 1988 Genetics of multidrug resistance *Am Soc Clin Investig* **81** 1303-1309

14. C. E. Chan and D. J. Odde 2008 Traction dynamics of filopodia on compliant substrates *American Association for the Advancement of Science* **322** 1687-1691

15. B. L. Bangasser, S. S. Rosenfeld and D. J. Odde 2013 Determinants of maximal force transmission in a motor-clutch model of cell traction in a compliant microenvironment *Elsevier* **105** 581-592

16. M. Rubashkin 2016 Extracellular cues drive integrin mediated signaling to drive cancer cell invasion *University of California, San Francisco*

17. W. Xiao 2019 Brain-Mimetic Hydrogel Platform for Investigation of Glioblastoma Drug Resistance *UCLA*

18. J.-i. Sakamaki, H. Daitoku, K. Ueno, A. Hagiwara, K. Yamagata and A. Fukamizu 2011 Arginine methylation of BCL-2 antagonist of cell death (BAD) counteracts its phosphorylation and inactivation by Akt *National Acad Sciences* **108** 6085-6090

19. F. Liu, K. Bardhan, D. Yang, M. Thangaraju, V. Ganapathy, J. L. Waller, G. B. Liles, J. R. Lee and K. Liu 2012 NF-κB directly regulates Fas transcription to modulate Fas-mediated apoptosis and tumor suppression *ASBMB* **287** 25530-25540

20. R. Marhaba and M. Zöller 2004 CD44 in cancer progression: adhesion, migration and growth regulation *Springer* **35** 211-231

21. J. Hao, H. Chen, M. C. Madigan, P. J. Cozzi, J. Beretov, W. Xiao, W. J. Delprado, P. J. Russell and Y. Li 2010 Co-expression of CD147 (EMMPRIN), CD44v3-10, MDR1 and monocarboxylate transporters is associated with prostate cancer drug resistance and progression *Nature Publishing Group* **103** 1008-1018

22. S. Misra, V. C. Hascall, R. R. Markwald and S. Ghatak 2015 Interactions between hyaluronan and its receptors (CD44, RHAMM) regulate the activities of inflammation and cancer *Frontiers* **6** 201

23. M. Wiranowska, N. Tresser and S. Saporta 1998 The effect of interferon and anti-CD44 antibody on mouse glioma invasiveness in vitro **18** 3331-3338

24. A. Pietras, A. M. Katz, E. J. Ekström, B. Wee, J. J. Halliday, K. L. Pitter, J. L. Werbeck, N. M. Amankulor, J. T. Huse and E. C. Holland 2014 Osteopontin-CD44 signaling in the glioma perivascular niche enhances cancer stem cell phenotypes and promotes aggressive tumor growth *Elsevier* **14** 357-369

25. P. Friedl and S. Alexander 2011 Cancer invasion and the microenvironment: plasticity and reciprocity *Elsevier* **147** 992-1009

26. L. W. K. Chung, A. Baseman, V. Assikis and H. E. Zhau 2005 Molecular insights into prostate cancer progression: the missing link of tumor microenvironment *Elsevier* **173** 10-20

27. L.-W. Qian, K. Mizumoto, T. Urashima, E. Nagai, N. Maehara, N. Sato, M. Nakajima and M. Tanaka 2002 Radiation-induced increase in invasive potential of human pancreatic cancer cells and its blockade by a matrix metalloproteinase inhibitor, CGS27023 *AACR* **8** 1223-1227

28. Z. Su, G. Li, C. Liu, S. Ren, Y. Tian, Y. Liu and Y. Qiu 2016 Ionizing radiation promotes advanced malignant traits in nasopharyngeal carcinoma via activation of epithelial-mesenchymal transition and the cancer stem cell phenotype *Spandidos Publications* **36** 72-78

29. T. P. Kegelman, B. Wu, S. K. Das, S. Talukdar, J. M. Beckta, B. Hu, L. Emdad, K. Valerie, D. Sarkar and F. B. Furnari 2017 Inhibition of radiation-induced glioblastoma invasion by genetic and pharmacological targeting of MDA-9/Syntenin *National Acad Sciences* **114** 370-375

30. C. D. Paul, W.-C. Hung, D. Wirtz and K. Konstantopoulos 2016 Engineered models of confined cell migration *Annual Reviews* **18** 159-180

31. L. A. Liotta 1992 Cancer cell invasion and metastasis *JSTOR* **266** 54-63

32. P. G. Gritsenko, O. Ilina and P. Friedl 2012 Interstitial guidance of cancer invasion *Wiley Online Library* **226** 185-199

33. C. D. Paul, P. Mistriotis and K. Konstantopoulos 2017 Cancer cell motility: lessons from migration in confined spaces *Nature Publishing Group* **17** 131

34. K. Konstantopoulos, P.-H. Wu and D. Wirtz 2013 Dimensional control of cancer cell migration *The Biophysical Society* **104** 279

35. K. M. Stroka, Z. Gu, S. X. Sun and K. Konstantopoulos 2014 Bioengineering paradigms for cell migration in confined microenvironments *Elsevier* **30** 41-50

36. M. Krause and K. Wolf 2015 Cancer cell migration in 3D tissue: Negotiating space by proteolysis and nuclear deformability *Taylor & Francis* **9** 357-366

37. M. Zimmermann, C. Box and S. A. Eccles 2013 Two-dimensional vs. three-dimensional in vitro tumor migration and invasion assays *Springer* 227-252

38. C. Wang, Z. Tang, Y. Zhao, R. Yao, L. Li and W. Sun 2014 Three-dimensional in vitro cancer models: a short review *IOP Publishing* **6** 022001

39. T. A. Ulrich, E. M. de Juan Pardo and S. Kumar 2009 The mechanical rigidity of the extracellular matrix regulates the structure, motility, and proliferation of glioma cells *AACR* **69** 4167-4174

40. N. V. Krakhmal, M. V. Zavyalova, E. V. Denisov, S. V. Vtorushin and V. M. Perelmuter 2015 Cancer invasion: patterns and mechanisms *Общество с ограниченной ответственностью Парк-медиа* **7**

41. D. Gallego-Perez, N. Higuita-Castro, L. Denning, J. DeJesus, K. Dahl, A. Sarkar and D. J. Hansford 2012 Microfabricated mimics of in vivo structural cues for the study of guided tumor cell migration *Royal Society of Chemistry* **12** 4424-4432
42. J. C. McDonald and G. M. Whitesides 2002 Poly (dimethylsiloxane) as a material for fabricating microfluidic devices *ACS Publications* **35** 491-499
43. Y.-J. Liu, M. Le Berre, F. Lautenschlaeger, P. Maiuri, A. Callan-Jones, M. Heuzé, T. Takaki, R. Voituriez and M. Piel 2015 Confinement and low adhesion induce fast amoeboid migration of slow mesenchymal cells *Elsevier* **160** 659-672
44. A. F. Christ, K. Franze, H. Gautier, P. Moshayedi, J. Fawcett, R. J. M. Franklin, R. T. Karadottir and J. Guck 2010 Mechanical difference between white and gray matter in the rat cerebellum measured by scanning force microscopy *Elsevier* **43** 2986-2992
45. Q. Shen, H. Niederstrasser, R. Barakat, Z. Haddadin, S. R. Miller, B. Posner and Y.-T. Kim 2020 Single-cell-level screening method for migratory cancer cells and its potential feasibility in high-throughput manner *IOP Publishing* **12** 035019
46. X. Q. Brown, K. Ookawa and J. Y. Wong 2005 Evaluation of polydimethylsiloxane scaffolds with physiologically-relevant elastic moduli: interplay of substrate mechanics and surface chemistry effects on vascular smooth muscle cell response *Elsevier* **26** 3123-3129
47. R. N. Palchesko, L. Zhang, Y. Sun and A. W. Feinberg 2012 Development of polydimethylsiloxane substrates with tunable elastic modulus to study cell mechanobiology in muscle and nerve *Public Library of Science* **7** e51499
48. L. W. Fisher 2010 Single-and multi-functional arrayed microchannel fluidic devices
49. B.-B. Xu, Y.-L. Zhang, H. Xia, W.-F. Dong, H. Ding and H.-B. Sun 2013 Fabrication and multifunction integration of microfluidic chips by femtosecond laser direct writing *Royal Society of Chemistry* **13** 1677-1690
50. E. Berthier, E. W. K. Young and D. Beebe 2012 Engineers are from PDMS-land, Biologists are from Polystyrenia *Royal Society of Chemistry* **12** 1224-1237
51. D. J. Beebe, G. A. Mensing and G. M. Walker 2002 Physics and applications of microfluidics in biology *Annual Reviews 4139 El Camino Way, PO Box 10139, Palo Alto, CA 94303-0139, USA* **4** 261-286

Contents

Chapter 1. Physical Confinement During Cancer Cell Migration Triggers Therapeutic Resistance and Cancer Stem Cell-like Behavior

Qionghua Shen[1], Tamara Hill[1], Xue Cai[2], Loan Bui[3], Rami Barakat[1], Emily Hills[1], Turki Almugaiteeb[4], Anish Babu[5], Patrick H Mckernan[5], Michelle Zalles[6], James D Battiste[5*] and Young-Tae Kim[1,7*]

[1]Neuroengineering Lab, Department of Bioengineering, University of Texas at Arlington, TX

[2]Department of Neurosurgery, University of Oklahoma Health Sciences Center, OK

[3] Department of Aerospace & Mechanical Engineering, University of Notre Dame, IN

[4]RPD Innovations, Riyadh, Saudi Arabia

[5] Department of Neurology, University of Oklahoma Health Sciences Center, OK

[6] Oklahoma Medical Research Foundation, OK

[7]Department of Urology, UT Southwestern Medical Center, TX

*Corresponding authors:

Young-Tae Kim, Ph.D.
Department of Bioengineering
500 UTA Blvd ERB244
University of Texas at Arlington
Arlington, TX 76010
E-mail: ykim@uta.edu
Fax: 817-272-2251
Phone: 817-272-5023

James D. Battiste, MD, Ph.D.
Department of Neurology
920 Stanton L. Young Blvd, Suite 2040
University of Oklahoma Health Science Center
Oklahoma City, OK 73104
E-mail: James-Battiste@ouhsc.edu
Fax: 405-271-5723
Phone: 405-271-4113

Abstract

Metastasized cancer cells have an increased resistance to therapies leading to a drastic decrease in patient survival rates. However, understanding of the underlying cause for this enhanced resistance is lacking. Our microchannel technology allowed us to successfully produce therapeutic resistant confined-migrating cells in multiple cancer types. The heightened resistance correlated with up-regulation in efflux proteins (ABCG2, NUP62, and MDR1) and the expression of cancer stem cell related marker (CD133 and ALDH). Moreover, the re-localization of Yes-associated protein (YAP) to the cell nucleus indicated an elevated level of cytoskeletal tension. The increased cytoskeletal tension suggested that mechanical interactions between cancer cells and tight surroundings during metastasis is one of the factors that contributes to therapeutic resistance and acquisition of cancer stem cell (CSC) like features. With these findings and our technology, we are able to provide therapeutic resistant and CSC like cells to be utilized in developing new strategies for the treatment of metastatic cancer.

Introduction

More than 90% of mortality caused by cancer is attributable to metastases [1, 2]. Due to its unique systemic nature and resistance to existing therapeutic agents, metastatic cancer is largely incurable with current common treatments [1,3].

Cell migration is a key element of the invasion-metastasis cascade; the extraordinary motility and deformability of escaped migrating cells allow them to easily creep under physical confinement [4,5]. During this process, cells undergo a resistant change known as metastatic resistance [6]. Although the major mechanisms of resistance have been widely investigated, studies which reveal the relationship between migration in physical confinement and the procurement of therapeutic resistance are still not well-researched. In addition, a rare population of tumor cells with stem cell-like properties, named cancer stem cells (CSCs), plays a distinct role in driving metastasis. CSCs are very difficult to focus studies on because of their minimal presentation within the tumor population; however, previous works have suggested that CSC initiation and maintenance may be related to physical inputs including extracellular matrix stiffness within the local microenvironments [7,8]. Hence, mechanical inputs such as interstitial pressure from the microenvironment, might greatly affect the CSC-like behaviors of cancer cells and drive metastatic invasion. To generate appropriate tools with physical inputs to induce or enrich treatment resistant cancer cells is a critical step for a better understanding of the mechanisms underlying treatment resistance.

In this study, we i). produced a group of confined-migrating cancer cells by allowing them to creep under certain physical confinement (i.e., microchannel width that is smaller than cell size); and ii). carried out detailed molecular analyses on those confined-migrating cancer cells to uncover the

relationship between mechanical interaction and acquired therapeutic resistance. Focusing on G55 glioblastoma and MDA-MB-231 breast cancer cell lines, this study aimed to confirm that physical confinement induces chemotherapeutic and radio-therapeutic resistance. Western blot analyses were conducted to determine which molecules are potential key players for physical confinement induced therapeutic resistance. Immunostaining and hypoxic analysis further allowed us to peer into the relationship between cytoskeletal pressure, CSC-like properties and physical confinement induced therapeutic resistance. We also found the similar phenomenon (i.e., physical confinement induces therapeutic resistance) from lung, prostate, and patient-derived GBM. Thus, we believe this physical confinement induced therapeutic resistance is a universal trait in various cancer types.

Material and Methods

Fabrication of Microchannel Device

Two different styles of microchannel devices described in our previous studies were used for this study (demonstrated in supplemental information Fig. S1. A and B) [46]. Combined utilization of standard negative photolithography and soft lithography was the core of our microchannel device fabrication, with recessed features fabricated on a silicon wafer coated with SU-8 photoresist (Microchem Corp, Newton, MA). The thickness of coating was controlled by spin speed which determined the microchannels' height. A mixture of polydimethylsiloxane (PDMS) (Sylgard 184 Silicone Elastomer Base, Dow Corning) and curing agent (Sylgard 184 Silicone Elastomer Curing Agent, Dow Corning) in a ratio of 10:1 (v/v) was poured over the completed master and pre-baked for 2 min at 75°C, then solidified for 5 min at 150°C. Subsequently the peeled PDMS devices with the designed microchannels were carefully cut, decontaminated with 70% ethanol, and assembled.

Cell Culture

The human glioblastoma cell line G55 was provided by The University of Oklahoma Health Sciences Center. The cells were cultured in a serum-free DMEM/F-12 medium supplemented with 1x B-27 (Invitrogen), 1x Insulin-Transferrin-Selenium-X (Invitrogen), and mouse EGF (epidermal growth factor, 20ng/ml, PeproTech). MDA-MB-231 human breast carcinoma cells were provided by The University of Texas at the Southwestern Medical Center in Dallas. The cells were cultured in DMEM/F-12 medium (Corning/Cellgro) supplemented with 10% fetal bovine serum (FBS).

Migrating Cell Initiating and Cell Harvesting

For G55 cells, 25 x 10^3 cells were introduced at each side entrances of the microchannel device (totally 50 x 10^3 cells per device). All devices were maintained in 10% serum medium to facilitate the initiation of migration via confinements. For MDA-MB-231 cells, before introducing the cells into the microchannel devices, 6-well plates (n=3) containing microchannel devices were coated with collagen type I (Corning, REF 354236) overnight, then rinsed three times for neutralization. 100 x 10^3 cells were seeded into each well and cultured in 10% serum supplemented media for up to 7 days to allow from ample cells to migrate through the microchannels. The culture medium was abandoned, and the cells were washed twice with PBS. Then all devices were incubated with Trypsin-EDTA for 5 min, with later addition of an equal volume of medium, to halt trypsin. Quickly, the bottom of the well was scraped with Costar® 3008 Cell Lifter (Corning Inc) to remove 2D cells and verified under the microscope to make sure there were no remaining 2D cells. The PDMS device was peeled to expose the migrating cells. Once more, the wells were incubated with Trypsin-EDTA for 5 min and migrating cells were collected from 18 devices (total cell number was estimated to be 60 x 10^3 (Fig. S3)). For the control group, channel-less PDMS pieces were disassembled and cells were collected from one well after a 5 min incubation with Trypsin-EDTA. Cells from both groups were centrifuged for 5 min at 4000rmp. The supernatant was discarded and the cell pellet was harvested.

Western Blot

Total cell lysates were obtained by adding RIPA buffer (R0728, Sigma-Aldrich) and protease inhibitor cocktail (P2714, Sigma-Aldrich). Equilibrated protein samples were loaded into a 10% SDS-Page gel, electrophoresed and then electro-transferred to a PVDF membrane (Bio-Rad). Transferred membranes were blocked with a blocking buffer containing 5% non-fat milk

(Labscientific, M0841). The following monoclonal antibodies were used: Nanog (Cell Signaling, D73G4), CD133 (Cell Signaling, D2V8Q), CD44 (Cell Signaling, 8E2), ALDH1/2 (Santa Cruz, sc-166362), ALDH1 (Cell Signaling, D9J7R), MDR1/ABCB1 (Cell Signaling, E1Y7B), HIF1-α (Cell Signaling, D5F3M), ABCG2 (Cell Signaling, D5V2K), nucleoporin-62 (Santa Cruz, sc-48373), EpCAM (Cell Signaling, VU1D9) and EPAS-1 (Santa Cruz, 190B). Target proteins were visualized with IgG secondary mouse or rabbit antibodies and a chemiluminescent substrate (Santa Cruz, sc-2048). All Western blot results were normalized by total protein (Fig. S4).

3D Reconstruction of Migrating Cells

Microchannel devices with migrated cells were fixed using 4% paraformaldehyde for 10 min and perfused with washing solution (0.5% triton in 1xPBS) for 1 hour. Samples were stained with 2hour of Actin-stain^{TM} 488 (3:500, #PHDG1, Cytoskeleton) and 15min of PI (Propidium iodide, 500nM, MP, 195458) at room temperature. Images were scanned using a z-step size of 0.5 µm. 3D reconstruction was carried out by MATLAB and ImageJ.

Immunostaining

Microchannel devices with a sufficient number of migrated cells were fixed using 4% paraformaldehyde for 10 min and washed with PBS. After blocking with 4% goat serum in washing solution(0.5% triton in 1xPBS) for 1 hour, samples were stained with either ABCG2 (1:500, Santa Cruz, sc-377176), nucleoporin P62 (1:500, ThermoFisher, PA5-21882) or YAP (1: 500, Santa Cruz, sc-271134) antibody at 4°C overnight. After washing 3 times with washing solution, samples were incubated with Alexa Fluor® AffiniPure Goat Anti-Rabbit IgG (1:200, Jackson ImmunoResearch Laboratories) for 2 hours at room temperature. Signal visualization and

image capture were performed using a ZEISS LSM 800 fluorescence microscopy. Fluorescence intensities were quantified by ImageJ. The ratio of YAP intensity between the cytoplasm and the nucleus was taken as an indicator of mechanical pressure to the cells when they traveled through the microchannels.

Drug Accumulation Test

Devices with 5 x 5 µm microchannels was used to maintain cells. 20×10^3 cells were seeded to the central reservoir of each device and cultured for up to 6 days. All devices were treated with 0.01 mg/ml (17µM) Doxorubicin (Dox, Sigma-Aldrich, St. Louis) for 4 hours, and. then cells were washed with live cell image medium (#1582202, Life Technologies) and kept in the image medium for the first time point for imaging. All samples were imaged by a ZEISS LSM 800 fluorescence microscopy using bright field, and Rhodamine (Dox). Cells in three different locations were imaged: central reservoir (2D control cells) and 5 x 5 reservoir (5R, cells migrated through 5 x 5 µm microchannels). The samples were kept in the image medium overnight and imaged again for the second time point. All images were quantified for fluorescence intensities by ImageJ.

Viability Analysis

GBM cells were treated with Dox (17µM) overnight or Temozolomide (TMZ, 0.25mM, 0.5mM & 1mM, T2577, Sigma) for 72 hours at 37°C. MDA-MB-231 cells were incubated with Dox (17µM) overnight or 5-Fluorouracil (5-Fu, 25µM, Sigma-Aldrich) for 72 hours. Cell viability after drug treatment was determined with the Green Live/Dead Stain (34J66, ImmunoChemistryJ66, ImmunoChemistry) with 1:1000 (v/v) in PBS.

G55 Radiation and Viability Test

G55 cells were seeded at the both sides of the entrance of the microchannels (total 50 x 10^3 cells per device) in 2ml DMEM (Corning Cellgro) media supplemented with 10% of FBS (Atlanta Biologicals) and 1% of penicillin/streptomycin (Cellgro) and incubated for 3-4 days in a culture incubator under standard conditions. The same number of cells for the 2D cell culture were seeded in plain 6-well plates in 2ml same media and cultured overnight. Then radiation of a single dose of 2Gy, 5Gy and 10Gy was performed with a high dose-rate ^{137}Cesium (Cs) unit (4.5 Gy/min) at room temperature [47,48] (Fig. 2 B). To make a condition in the 2D cell culture similar to the confined-migrating cells (inside microchannel) during radiation, a PDMS cover was put on the top of each well just before radiation, and was removed after radiation. Cell viability of both 2D and confined-migrating cells was assessed at 48 hours post radiation. For assay of 3D cell viability, Hoechst 33342 (0.5µg/ml, Thermofisher Scientific) staining overnight and then Propidium iodide (PI, 0.5µg/ml, MP Biomedicals) staining for 30min (all at 37°C) was carried out. Images were taken using a Nikon E-2000 fluorescence microscopy under 10x, and the nuclei (both total and dead) inside the channels were counted. For assay of 2D cell viability, the media in each well were collected and the cells in correspondent wells were collected after trypsin (0.25%, VWR) treatment and were added to the collected media, the total volume of each sample is 2.5ml. 10µl of each sample were mixed with 10µl of trypan blue stain 0.4% (Invitrogen), and 10µl of that was used to determine the cell viability using a cell counter according to the manufacture's protocol (Invitrogen).

Immunohistochemistry

Mouse xenograft models were established using the G55 cell line (glioblastoma) that was stereotactically implanted into the striatum of a mouse brain guided by Bregma coordinates. The

brain was harvested after allowing time for tumor growth and then fixed with formalin and paraffin embedded (FFPE). The IHC was performed on Leica Bond RXM platform using Polymer Refine Detection system (DS9800). FFPE tissues were sectioned at 4 µm thickness and mounted on positively charged slides. The slides were dried overnight at room temperature and incubated at 60°C for 45 minutes. Slides were transferred to the Leica Bond RXM for dewax and then treated for target retrieval at 100°C for 20 minutes in a retrieval solution, either at pH 6.0 . The sections were incubated with 5% goat serum (01-6201, ThermoFisher Scientific) for 30 minutes. Endogenous peroxidase was blocked using peroxidase-blocking reagent, followed by the primary antibody (ABCG2, Abcam 207732) incubation for 60 minutes. For the secondary antibody, post-primary IgG-linker and/or Poly-HRP IgG reagents was used. Detection was done using 3, 3′-diaminobenzidine tetrahydrochloride (DAB) as chromogen and counter stained with hematoxylin. Completed slides were dehydrated (Leica ST5020), and mounted (Leica MM24). Antibody specific positive control (human placenta) and negative control (omission of primary antibody) were parallel stained. Slides were imaged by light microscopy.

Hypoxia Level Test

Microchannel devices with adequate number of migrated cells were incubated with the Image-iT® Hypoxia Reagent (10µM, H10498, Life Technologies) at 37°C for 30min. Visualization and image capture were performed using a ZEISS LSM 800 fluorescence microscopy under 20X with excitation/emission of 490/610nm. Intensity in the central reservoir, inside the microchannels and the satellite reservoirs were measured by ImageJ and compared among the groups.

Reseeding Experiment

For G55, after harvesting the live cell pellet (as described previously) from 18 devices (about 54 x 10^3 cells in total), cells were reseeded in 24-well plates and re-cultured for 48 hours. Then Trypsin-EDTA treated for 5 min to collect cells from the plates and proteins were harvested. For MDA-MB-231 migrated cells, cells were re-seeded in the 2D culture environment and collected at 2 days, 3 days, 4 days, and 8 days post seeding for Western blot analysis.

Statistical Analyses

Microsoft Excel was used to calculate the averages and standard deviations (STDs). To compare the significance, a one-way ANOVA tests and Tukey post hoc tests among multiple groups and the two-tails student *t*-test were performed. A *P*-value of less than 0.05 was considered statistically significant.

Results

Confined-migrating Cancer Cells Develop Chemotherapy and Radiotherapy Resistance

The confined-migrated cells that crept through physical confinement showed characteristic resistance to chemo-therapeutic agent, Doxorubicin (Dox). Both GBM and MDA-MB-231 cancer cell lines were treated with 17µM (0.01 mg/ml) Dox for visualization of intracellular drug mobility, due to the degree of Dox autofluorescence at this concentration [9]. After 4 hours Dox incubation, samples were imaged at two different timepoints: immediately after Dox removal (4hr) and 16 hours (overnight). The autofluorescence of Dox in intracellular compartments (total cell, nucleus, and cytoplasm) was measured and compared. After drug treatment for 4 hours, Dox intensities in two locations (2D and 5R) showed no significant differences, however, Dox accumulation was highest at the nucleus due to DNA-Dox interaction (Fig. 1 A1 and B1). After overnight with Dox free medium, the cells which migrated through 5 x 5 μm (5R) microchannels had significantly lower concentration of Dox in all intracellular compartments as compared to 2D cultured cells (Fig. 1 A2 and B2). Both G55 (Fig. 1 C) and MDA-MB-231 (Fig. 1 D) cells showed obvious changes in Dox intensity under different degrees of confinement. When comparing 4hr and overnight, we observed increased Dox intensity in the nucleus of 2D cultured cells, but the confined-migrated cells showed significant decrease. For G55 cells, there was 12% increase (2D) and 41% decrease (5R) (Fig. 1 E1). For MDA-MB-231 cells, 23% increase (2D) and 43% decrease (5R) (Fig. 1 F1). The cytoplasmic Dox intensity decreased in G55 cells (-11% for 2D and -31% for 5R cells), but the intensity increased in MDA-MB-231 (+104% for 2D and +69% for 5R). Total Dox intensity changes after overnight incubation is shown in Fig1. E3 and F3. To address the implication of increased Dox efflux in the confined-migrated cells, cell viability after Dox treatment was

examined: G55 cells showed 20% higher viability in the migrated group (for 5R) as compared to 2D cells (Fig. 1 G); MDA-MB-231 2D cells showed an extremely high sensitivity to Dox (~15% viability) compared to migrated cells (~100% viability) (Fig. 1 I). These results were consistent with the pattern of Dox intensity changes under different degrees of confinement. To further confirm the confined-migration induced chemotherapeutic resistance, TMZ and 5-FU (clinically used chemotherapeutic agents) were used for G55 and MDA-MB-231, respectively. After 72 hours TMZ treatment, the viability was significantly higher for migrated cells (5R) than the 2D cells at all doses (Fig. 1 H). After 72 hours 5-FU treatment, the migrated cells showed a significantly higher (~100% in 5R) viability than 2D cells (~50%) (Fig. 1 J). Taken together, these data elucidated that the increased drug efflux of confined-migrated cells might be involved in endowing metastatic cancer cells with resistance to a variety of chemotherapies.
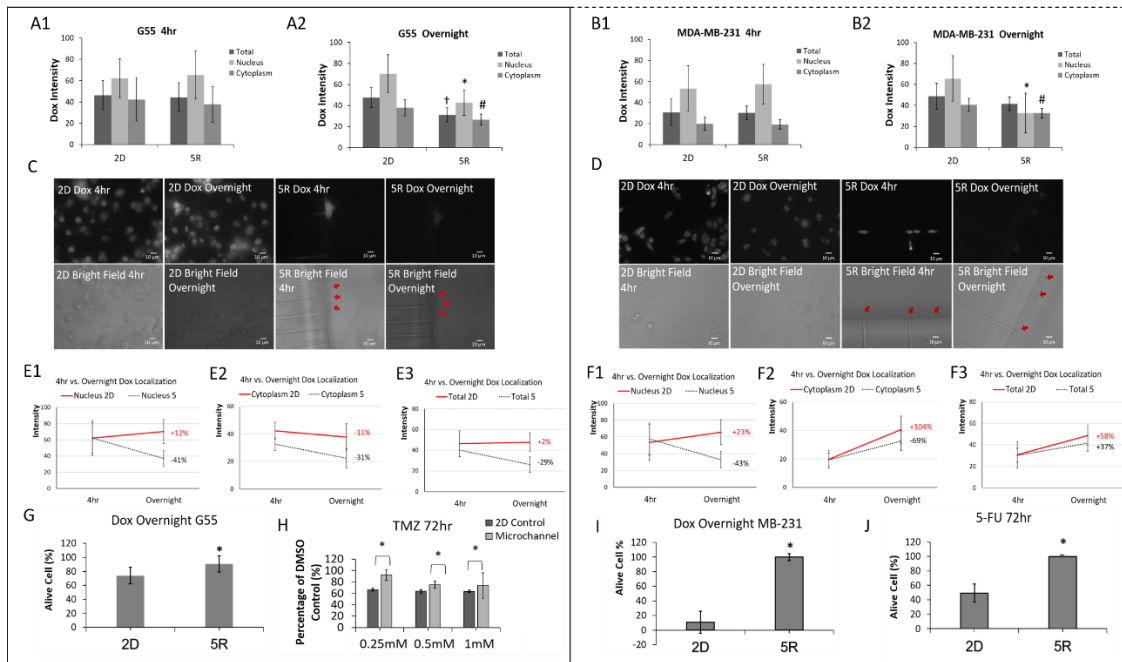

Fig. 1. Confined-migrating cancer cells develop chemotherapeutic resistance by increasing drug efflux (left panel are G55 results, right panel are MDA-MB-231 results). **A-B.** Quantitative comparison of Dox intracellular accumulation between 2D culture (2D) and cancer cells that migrated through 5 x 5 μm microchannels (5R). Dox (17μM) was introduced to all cancer cells

then removed after 4 hours and replaced with the Dox free medium. After overnight incubation with Dox free medium, Dox intensities were quantified in the nucleus, cytoplasm and whole cell (total). N>20 per group. All experiments were triplicated. †p<0.05 between 2D Total and others; *p<0.05 between 2D nucleus and others; #p<0.05 between 2D cytoplasm and others. **C-D.** Representative images of Dox accumulation in 2D culture and cells which have migrated through 5 x 5 μm microchannels. **E-F.** Changes of Dox intensity over time under different degrees of confinement. Percentage shows intensity changes between 4hr and overnight. N>20 per group. **G-I.** Viability after Dox (17μM) 4hr treatment plus overnight Dox free incubation. N>20 per group. *p<0.05 between 2D and others. **H.** G55 cell viability after Temozolomide treatment (0.25mM, 0.5mM and 1mM) for 72 hours. *p<0.05. **J.** MDA-MB-231 cell viability after 5-Fu (5μM) treatment for 72 hours. *p<0.05. Experiments were duplicated.

To determine the characteristic radiation resistance of the confined-migrating cells and 2D cells, two groups of cells were equally irradiated with doses of 2 Gray (Gy), 5Gy and 10Gy, and then cell survival rates, which were normalized to the non-irradiated group, were compared among these two groups (Fig. 2 A). The data showed that at low doses (2Gy and 5Gy), 2D cells and the confined-migrating cells showed no significant differences in radio-sensitivity, although, the cell viability was reduced with dose increasement in both groups. At the highest dose (10Gy), the confined-migrating cells showed a significantly higher survival rate over the 2D cells (Migrating: 94.8 ± 10.1 vs. 2D: 87.8 ± 4.1, P=0.0165) (Fig. 2 B). There was no significant decrease in viability of confined-migrating cell even after treatment with the highest dose (Figs. 2 B-C). These results confirm that confined-migrating cells have an increased resistance to radiation.
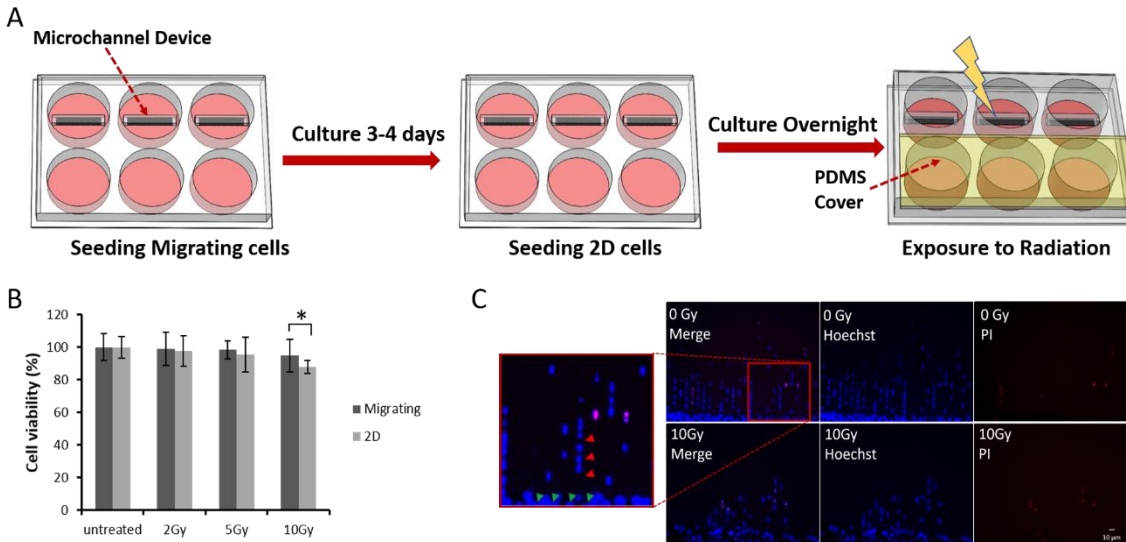
Fig. 2. Confined-migrating cells exhibit more radiation resistance than the 2D cultured cells.
A. G55 cells were seeded and allowed to migrate in 5µm width microchannel (top row of 6-well plate) and to grow in 2D (bottom row of 6-well plate); then the plate was irradiated in various doses with a PDMS cover on the top of the 2D wells to eliminate the potential effect of PDMS on viability. **B.** Quantitative comparison of cell viability between 2D and confined-migrating cells at different doses of radiation; average ± Std. *p<0.05. N>20 images from at least 3 wells for migrating cells per group; N=6 for the 2D cultured cells per group. **C.** Representative live/dead images of confined-migrating G55 cells (migrating through 5 x 5 µm microchannels) treated with 0Gy and 10Gy radiation. Images were taken 48hr post treatment. (Red arrows indicate lined confined-migrating cells inside microchannels; Green arrows indicate 2D cultured cells.)

Confined-migrating Cells Exhibit Significantly Increased Drug Efflux Proteins

In Dox accumulation studies, cells that crept through physical confinement exhibited an increased

Dox efflux as compared to 2D cultured cells. Western blot analyses revealed that the confined-

migrating cancer cells up-regulated the following drug efflux proteins: ABCG2, MDR1, and

nucleoporin-62 (NUP62) (Fig.3 A-E). In G55 cells, the confined-migrating cells expressed four-

times ABCG2 (Fumitremorgin C inhibiting experiment also proved ABCG2 increment in

confined-migrating cells (Fig. S2)); two-times MDR1; and three-times NUP62 as compared to 2D

cultured cells (Figs. 3 A-C). Similarly, both ABCG2 and MDR1 showed increased expressions in

confined-migrating MDA-MB-231 cells as 2.5 times and 29 times compared to 2D cultured cells

(Fig. 3 D and E). Additionally, immunostaining revealed a higher expression of ABCG2 and

NUP62 protein in G55 and MDA-MB-231 cell when they migrated through the microchannels, especially the 5 x 5 μm microchannels (Fig. 3 F and G). The increased drug-efflux protein expression of confined-migrating cells contribute to higher cell viabilities due to increased drug expulsion.
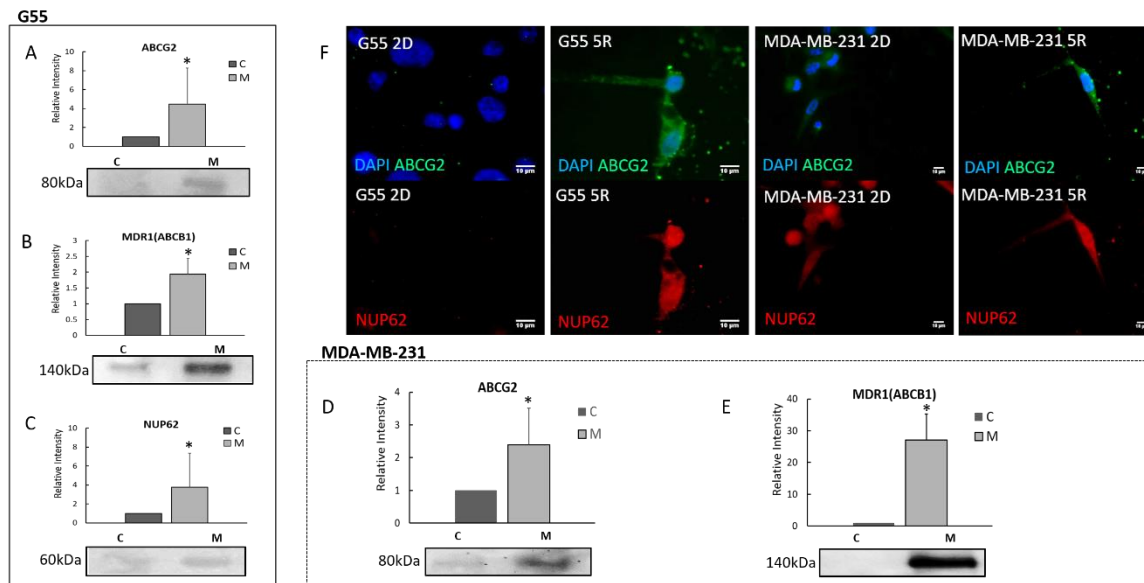
Fig. 3. Confined-migrating cells express significant increased drug efflux proteins. A-C: Quantitative comparison of drug efflux proteins (ABCG2, MDR1 and NUP62) between G55 confined-migrating cells (indicated by M) and 2D cells (indicated by C). **D-E:** Quantitative comparison of drug efflux proteins (ABCG2 and MDR-1) in MDA-MB-231 confined-migrating cells (indicated by M) and 2D cells (indicated by C). All Western blot results were normalized by the total proteins. Average ± Std. All experiments were reproduced. *P<0.05. **F-G.** Immunostaining images of NUP62 and ABCG2 for G55 and MDA-MB-231 cells in 2D culturing and after migrating through 5 x 5 μm microchannels (5R). (Blue: DAPI; Red: NUP62; Green: ABCG2)

Confined-migrating Cancer Cells Highly Up-regulate CSCs Related Biomarkers in Various Cancer Types

To further understand the increased therapeutic resistance, we examined whether the confined-migrating cancer cells exhibit cancer stem cell like properties. CD133, a biomarker for cancer stem cells (CSCs), expression in confined-migrating G55 cells was increased 50% compared to

2D control (Fig. 4 A1); while, CD44, another biomarker for CSCs, expression was reduced around 90% in the migrating group (Fig. 4 A2). This CD133-CD44 shift has been reported in a patient-derived glioma stem cell (GSC) cell line when cells were subject to hypoxia [10]. Aldehyde dehydrogenase (ALDH) is also frequently used to identify CSCs [11, 12]. In this study, the confined-migrating G55 cells expressed two times ALDH (Fig. 4 A3) and four times EPAS-1, a specific marker for GSCs (Fig. 4 A4). CD133 expression in confined-migrating MDA-MB-231 cells was significantly increased to 6.2 times (Fig. 4 B1) along with other breast CSC biomarkers: ALDH (1.7 times), EpCAM (1.3 times) and Nanog (3.2 times) (Fig. 4 B2-B4).

To find out whether such increase of CSC properties in confined-migrating cells was restricted to a certain type of cancer or is ubiquitous, several other types of cancer cells (patient-derived C25 GBM, A549 lung cancer, and PC3 prostate cancer) were tested (Fig. 4 C-E). CD133 expression in the confined-migrating cells was 16 times higher in C25 cells (Fig. 4 C), 4 times in A549 cells (Fig. 4 D), and 5 times in PC3 cells (Fig. 4 E). These results clearly indicate that the confined-migrating cancer cells exhibit cancer stem cell like properties which could be correlated to increased therapeutic resistance.
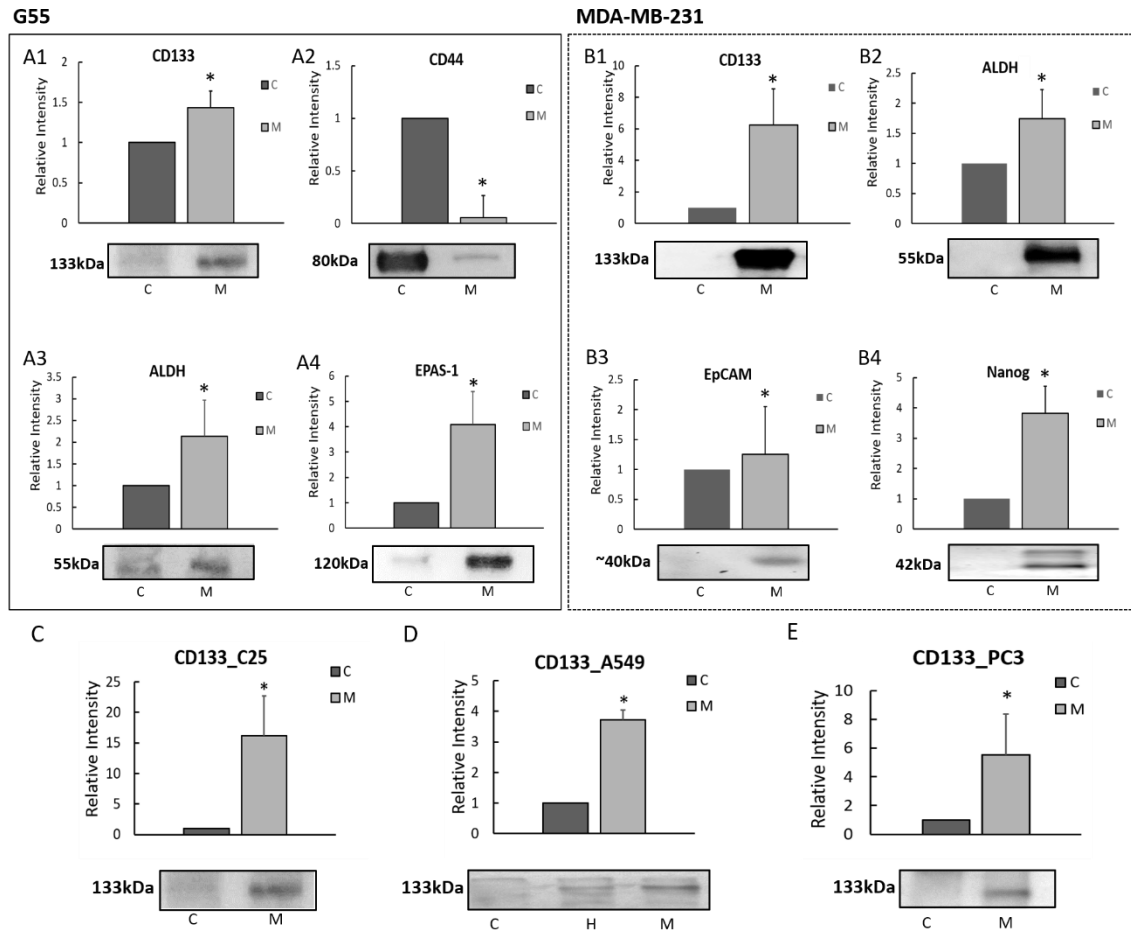
Fig. 4. Increased expression of cancer stem cell related markers in confined-migrating cancer cells. Quantitative comparison of cancer stem cell related markers using Western blot analyses between confined-migrating (M) and 2D cultured (C) cancer cells. **A1-A4**: G55 cells. **B1-B4:** MDA-MB-231cells. **C-E:** Increased expression of CD133 in different types of confined-migrating cancer cells: C25 patient derived GBM cells, A549 lung cancer cell line, and PC3 prostate cancer cell line. (H: hypoxia condition) All results were normalized as relative intensity to the expression in control group. Average ± Std. *$p<0.05$. All experiments were reproduced. Representative blot images of each marker are shown below their respective graph.

<u>Physical Confinement Increases Migrating Cancer Cells' Cytoskeleton Tension with Minimal</u>

<u>Hypoxic Stress</u>

When migrating inside and outside microchannels, cells showed different morphology due to confinement from their surroundings. Here, in order to show impacts from different degrees of confinements, we added 15 x 15 µm microchannel (Fig. 5 A1). When cancer cells migrating

through a 5 x 5 µm microchannel, their nucleus were confined by the tight space such that the nucleus turned to be a specially elongated shape. Based on 3D reconstruction model we calculated the cross-section ratio (cross section acreage of cell/cross section acreage of microchannel) for the confined-migrating cells. For 2D cells, the cross section was considered as 0. Cells inside 5 x 5 µm microchannel were exposed to significantly higher confined pressure, shown by more than 80% cell membrane clinging to microchannel walls (Fig. 5 A2). While migrating in microchannels, cells need to overcome the resistance associated with the confinement. To assess the increase in resistance in microchannels due to different channel dimensions, we borrowed the concept from hydrodynamics by expressing the resistance as a function of channel dimensions: height (h), width (w), and length (L) while the viscosity of the fluid (µ) is kept as constant:

$$R\ (Resistance) = \frac{12\mu L}{hw^3}\left[1 - \frac{192}{\pi^5}\left(\frac{w}{h}\right)\sum_{i=1,3,5}^{\infty}\frac{tanh\left(\frac{i\pi}{2}\left(\frac{h}{w}\right)\right)}{i^5}\right]^{-1}$$

To comparing the resistance, three different sized microchannels were considered (5 x 5µm, 5 x 12µm and 15 x 15µm), leading to the calculated resistances summarized in Fig. 5A3. Considering the effective hydraulic resistance associated with the 15 x 15µm (w x h) channel as the baseline, it appears that the effective resistance a cell needs to overcome to migrate in a 5 x 5µm cross-section is 81 times higher due to confinement, which suggests a much higher energetic demand from the cell to migrate through and to complete its journey. With the channel dimensions at 5 x 12µm (w x h), the resistance to overcome becomes 19.3 times higher than the baseline. The result was consistent with in vivo model. In G55 murine xenographic model of glioblastoma multiforma those elongated migrating cells within cortical white matter tracts (labeled with arrowhead) demonstrated highly ABCG2 expression (Fig. 5 A4).

YAP relocation from cytoplasm to nucleus (measured as a ratio) indicates increased cytoskeleton tension due to shear force on the cell membrane [13]. To investigate the relationship between confined-migrating, therapeutic resistance and CSC like behaviors, we examined Yes-associated protein (YAP) relocation and intracellular oxygen level in the different degrees of confinement. The YAP ratio was increased as the microchannel width decreased in both cell types (Fig. 5 B and G). In both G55 (Fig. 5 C) and MDA-MB-231(Fig. 5 H), nuclear YAP fluorescence was evidently lower than in the cytoplasm for the 2D group, and cells that migrated through physical confinement had higher YAP fluorescence inside the nucleus. YAP fluorescence nucleus localization was consistent with 3D reconstruction results (Fig. 5 A). It proved that the confined pressing force due to the tight surroundings did increase the confined-migrating cell's intracellular skeleton tension.

Hypoxia is a well-known factor that induces cancer stem cell like variation, malignant growth, and cancer metastases [14,15,16]. Hypoxia-induced factor 1-alpha (HIF-1α), a subunit of transcription factor HIF-1 which, regulates multiple cellular activities including cell survival in hypoxic conditions, and epithelial-to-mesenchymal (EMT) metastatic cascades[17, 18], was up-regulated 20 times in migrating G55 cells and 4 times in migrating MDA-MB-231 cells (Fig. 5 F and K). To determine if HIF-1α increasement was due to hypoxic condition during migration the intracellular oxygen level was measured by Image-iT® Hypoxia Reagent expression. Interestingly, cells in the central 2D area showed a higher fluorescence intensity compared to the cells around the microchannel entrance and those migrating via microchannels (Fig. 5 D and I). For G55 cells, when cells were close to the microchannel entrance the fluorescence intensity dropped to 30% of the cells in the 2D center. After migrating into 5 x 5 μm microchannels, cells exhibited the lowest hypoxia dye intensity (Fig. 5 E). For MDA-MB-231 cells, when cells were close to the microchannel entrance and inside the microchannels the hypoxic dye intensity dropped to 20% of

the 2D cells (Fig. 5 I). If we compare HIF-1α expression between hypoxia cells and confined-migrating cells, around two times higher expression was observed in confined-migrating group (supplementary data, Fig. S4). Based on these results, the increase in HIF-1α expression was not caused by a hypoxic condition during confined-migration.

A1

2D   15-15μm   5-5μm

PI   F-Actin

A2 Cross Section Ratio

A3 Hydralic Resistance

h=5, w=5
h=12, w=5
h=15, w=15

A4

Normal Mouse Brain   GBM Xenograft in Mouse Brain

ABCG2

G55

B YAP Ratio (N/P)

C 2D YAP   5R YAP

E Hypoxia Dye

D 2D Bright Field / 5*5 Entrance Bright Field / 5*5 MC Bright Field
2D Hypoxia Dye / 5*5 Entrance Hypoxia Dye / 5*5 MC Hypoxia Dye

F HIF-1α

120kDa

MDA-MB-231

G YAP Ratio (N/P)

H 2D YAP   5R YAP

I Hypoxia Dye

J 2D Bright Field / 5*5 Entrance Bright Field / 5*5 MC Bright Field
2D Hypoxia Dye / 5*5 Entrance Hypoxia Dye / 5*5 MC Hypoxia Dye
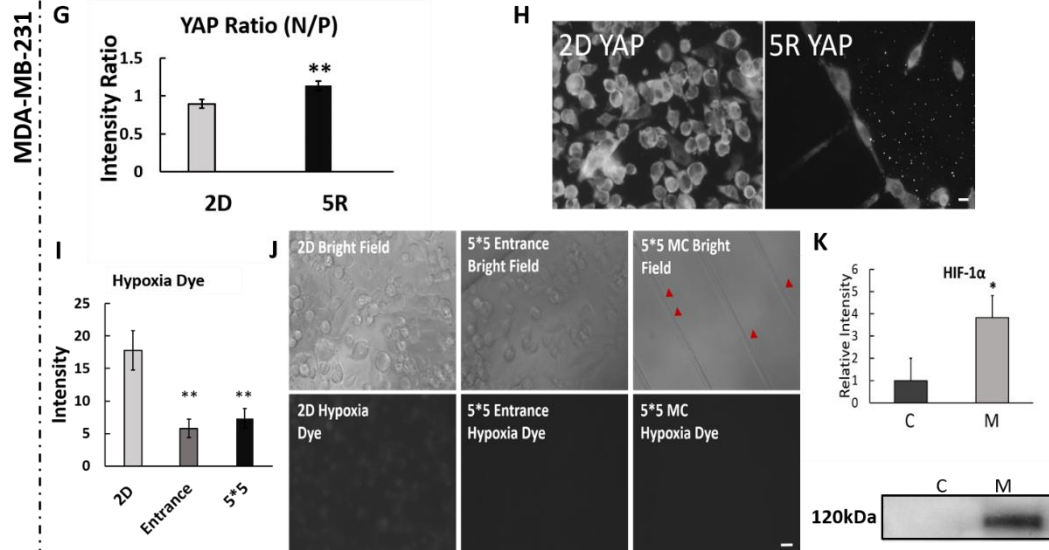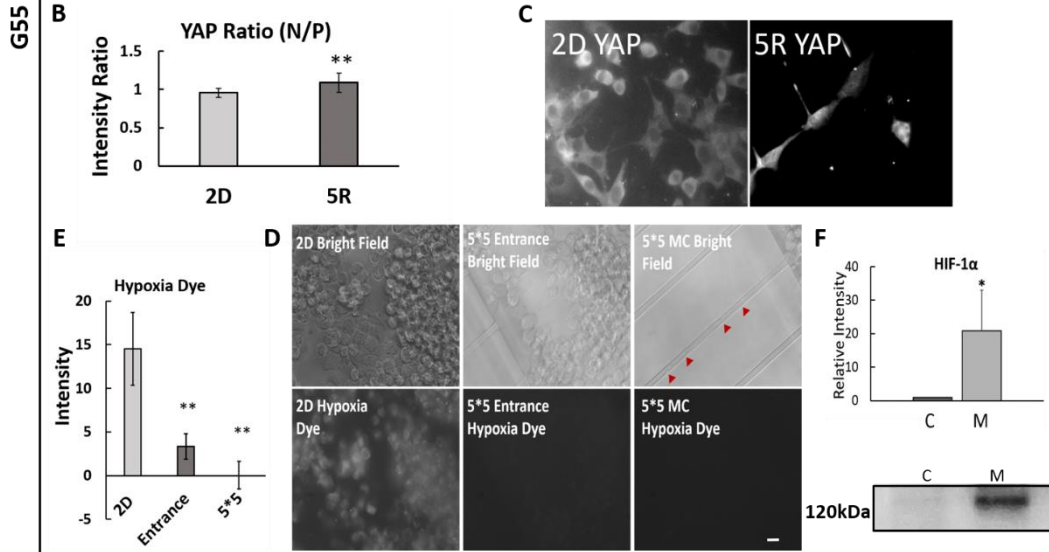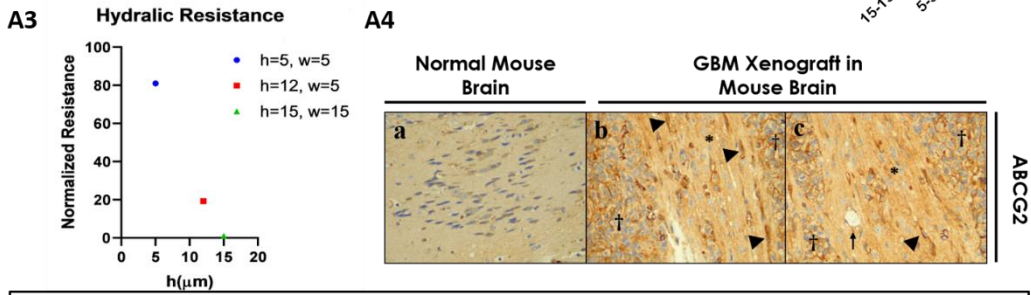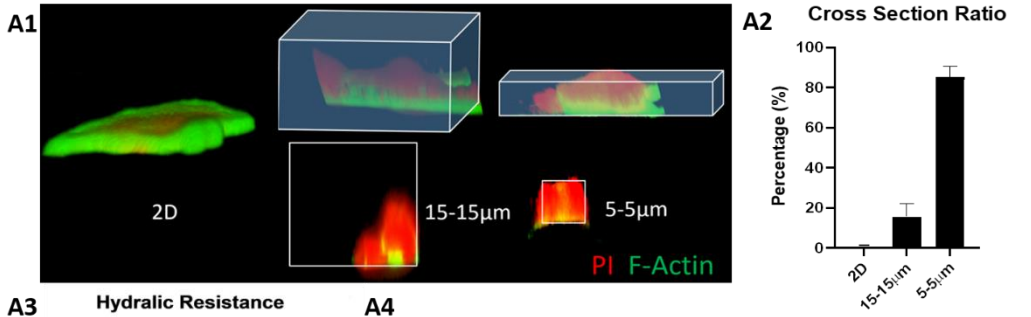
K HIF-1α

120kDa

Fig. 5. Confined-migrating cancer cells exhibit increased cytoskeleton tension with minimal hypoxic stress. A1: 3D reconstruction model for MDA-MB-231 cells under different degrees of confinement (Red: PI; Green: F-actin). **A2**: Cross section ratio of MDA-MB-231 cells inside microchannel. Average ± Std, n=4. *p<0.05 (cross section ratio = cross section acreage of cell/cross section acreage of microchannel) **A3:** Hydraulic resistance inside microchannels with different dimensions. h: height; w: width. Results are normalized by the lowest resistance number. **A4:** Immunohistochemical staining for ABCG2 in the G55 murine xerographic model of glioblastoma multiforme demonstrated highly ABCG2 expression in migrating tumor cells within cortical white matter tracts. a: health mouse brain tissue (noncancerous). b-c: In areas bordering G55 tumors (labeled with †), elevated ABCG2 expression can be observed in migrating tumor cells within cortical white matter tracts (labeled with*). Arrow: blood vessel. Arrowhead: tumor cells highly expressing ABCG2 in a whole cell pattern. **B** and **G:** Quantitative comparison of YAP expression (N/P; nucleus/cytoplasm) between 2D cultured and confined-migrating cells. 5R: cells migrated through 5 x 5 µm microchannel. **C** and **H:** Representative YAP fluorescence images of G55 (**C**) and MDA-MB-231 (**H**) cells. **D** and **I**: Representative hypoxia dye fluorescence images of cells in the central reservoir (2D), 5 x 5 µm entrance and inside 5 x 5 µm microchannels (MC). Red arrows indicate the cells confined inside the microchannels. **E** and **J**: Comparison of hypoxia dye intensity of the cells in different locations. **F** and **K**: Western blot HIF-1α relative intensity. C: 2D cultured cells, M: cells migrated through 5 x 12 µm microchannels. All results were normalized to the total proteins. Average ± Std. *p<0.05, **p<0.01 between 2D and others. Scale bar: 5 µm. All experiments were reproduced.

Protein Expression Changes Induced by Confined-migration Persist After Removal From Physical

Confinement

To determine if the protein changes induced by confined-migration remained permanently, migrating cancer cells were collected and re-cultured on the 2D environment over different time periods. In G55 cells, expression levels of selected proteins (ABCG2, ALDH and CD44) were assessed by western blots and compared among 2D control cells, migrating cells, and 2-day re-cultured cells. There was no significant difference in these proteins between the migrating group and the re-cultured group, but both were significantly different from 2D cultured cells (Fig. 6 A-C). Likewise, confined-migrating MDA-MB-231 cells were collected and re-cultured for 2, 3, 4 and 8 days. Western blot results showed that cells could maintain the altered protein expression levels up to 4 days whereas, at day 8 of re-culture, all protein levels finally returned to the original

baseline (Fig. 6 D-F). Although protein changes induced by confined-migration are not permanent, the changes persist for certain time frame.
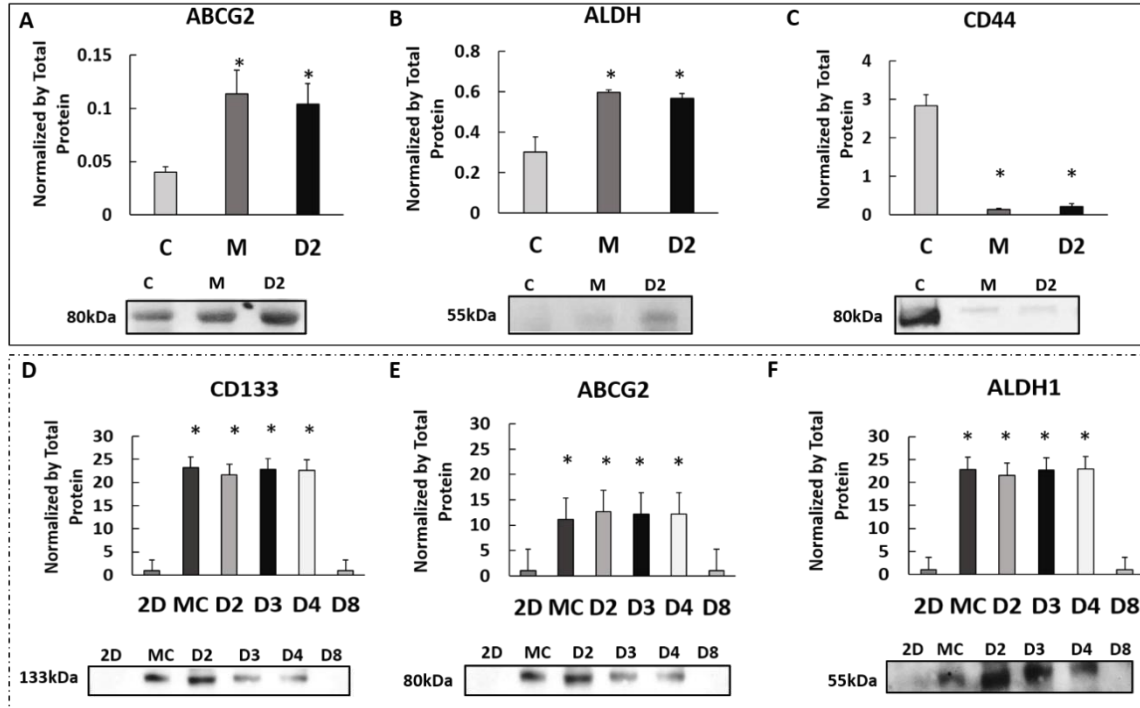
Fig 6. Protein expression changes induced by confined-migration persist after removal from physical confinement. **A-C:** Comparison of selected proteins (ABCG2, ALDH and CD44) expression in G55 cells between 2D culture (2D), confined-migrating (M), and 2 days after reseeding confined-migrating cells (D2). **D-F:** Comparison expressions of selected proteins (CD133, ABCG2 and ALDH1) in MDA-MB-231 cells between 2D culture (2D), confined-migrating (M), and 2, 3, 4, and 8 days after reseeding confined-migrating cells (D2, D3, D4, and D8). Representative blot images of each marker are shown below their respective graphs. All results were normalized to the total proteins. Average ± Std. *p<0.05. All experiments were reproduced.

Discussion and Conclusion

Currently, treatment with radiation and chemotherapy after surgical resection to remove tumors is the standard-of-care for cancer patients [19,20]. However, the highly therapeutic resistant nature of metastatic cancer cells tends to limit the efficacy of current cancer treatments. A better understanding of what triggers confined-migration induced resistance is important for improving anticancer strategies, specifically for metastatic cancer. In this study, we successfully isolated and examined therapeutically resistant confined-migrating cancer cells; we uncovered that mechanical stimulation caused by physical confinement could be one of the factors that leads to increased resistance in migratory cells. This is accomplished by cells adjusting their membrane protein channels and up-regulating CSCs related biomarkers.

Viability studies after certain chemotherapy or radiation treatments showed confined-migrating/migrated cells to have significantly higher survival rates than 2D cultured cells. Based on these results, we confirmed cells which experience confined-migration fall under the resistant category. Our drug efflux experiment supported the increased viability; confined-migrated cells have lower drug accumulation compared to the control group for both cancer types due to increased efflux. It is well-established that cancer cells under the resistance category can change the activity and/or structure of the cell membrane in order to regulate chemical transportation [21, 22]. On the cell membrane, this is mostly controlled by the ATP-binding cassette (ABC) transporter proteins including P-glycoprotein (ABCB1), the multidrug resistance-associated protein 1 (MRP1), MRP2 and ABCG2 [23, 24]; on the cell nucleus, resistance could be controlled by nucleoporins as the gateway that regulates the molecular exchange between the cell nucleus and the cytoplasm [25,26]. Western blot data, showing increased expressions of ABCG2 and MDR1 on the cell membrane

and NUP62 on the nuclear envelope (G55 cells in particular), were consistent with viability and drug efflux studies. These data provide evidence that confined-migration is tightly linked to up-regulation of multidrug resistance associated proteins, leading to drug resistance. Furthermore, the proliferation-inhibiting effect during confined-migration is responsible for increased radiation resistance (data was not shown).

Besides the prominence up-regulated therapeutic resistance, we also observed some interesting molecular alterations on confined-migrating cells. Transmembrane glycoprotein CD133 and aldehyde dehydrogenase (ALDH) are the foremost markers used in isolating stem cells from various tissues, including CSCs [27]. When in a confined-migrating state, both GBM and breast cancer cells showed increased CD133 and ALDH expression, indicating the acquisition of cancer stem cell-like features results from migration through physical confinement. Changes in other CSC related markers, CD44, EPAS-1 (for GBM), EpCAM, and Nanog (for breast cancer) further confirm that CSC like features can be acquired during confined-migration. Additionally, we observed increased expression of CD133 in several other cancer cells (A549 lung cancer, PC3 prostate cancer, and C25 patient-derived GBM), suggesting that induction of CSC-like behaviors is not just limited to a specific cancer cell type, but possibly a feature in all migrating cancer cells. Among the changes of confined-migration induced CSCs biomarkers, we observed that CD44 and CD133 expression is inversely related in GBM: increased CD133 and decreased CD44. The expression shift between CD44 and CD133 is known to be influenced by environmental factors, such as hypoxia or chemo-radiotherapy [10]. The observed shift can be attributed to the confined environment experienced by migrating cells. Also, a boosted resistance to radiation therapy can be another kind of evidence of confined-migrating cells' CSC-like properties [28]. Taken together, we

believe that physical confinement during migration can guide activation of specific intracellular cascades that induce CSC-like behaviors.

Understanding the factor(s) which trigger confined-migration induced therapeutic resistance and CSC-like behavior is critical to develop therapeutic strategies for metastatic cancer treatment. In our study, the major difference between a confined migrating cell and a 2D cultured cell is degree of physical confinement: cells migrating via physical confinement where cells' proliferation is restricted and there is inherently more contact with surrounding; versus cells in 2D where cells can freely grow, proliferate, or migrate without any physical constraint. In order to ascertain which factor(s) trigger therapeutic resistance and cancer stem cell like behavior during confined-migration, we investigated if the cells were experiencing hypoxia and/or shear force by interaction with their tight surroundings. HIF-1α, a well-known intracellular indicator of developmental response to hypoxia, showed an increasement in confined-migrating cells. However, our hypoxic data demonstrated that cells inside the microchannels were subjected to only minimal or no hypoxic ($< 5\%$ atm O_2) conditions. HIF-1α is not only up-regulated in hypoxic conditions, it can also be activated through an oxygen-independent manner by various cytokines through the PI3K-AKT-mTOR pathway [29], which is known to increase survival under various stress conditions [30, 31]. These results suggest that the lack of oxygen is not the major factor triggering therapeutic resistance in cancer cells during confined-migration. Therefore, we assert the observed treatment resistance with increased efflux proteins and up-regulation of HIF-1α and other CSC related markers, could be induced by mechanical interaction between cells and their surroundings rather than oxygen deficit. To further elucidate the role of mechanical interaction, Yes-associated protein (Yorkie-homologues YAP) whose nuclear localization property is accompanied with cells' response to a narrow ECM passageway [13], was used as a tool to demonstrate the intracellular

skeletal tension caused by mechanical interaction during migration through physical confinement. YAP nuclear localization indicated that cellular skeletal tension was increased during confined-migration. Also, immunohistochemical staining of ABCG2 in glioblastoma multiforme xenographic model showed when G55 stocked in white matter track would turned to elongated shape and demonstrated higher ABCG2 expression. This phenomenon was consistent with acquisition of drug resistance and increase in CSC related biomarker expression. Hence, we conclude that confined pressure from the surrounding environment during migration has a profound impact on cell behaviors [32, 33] and leads to up-regulated therapeutic resistance and procurement of CSC like features. These features acquired during confined-migration were maintained at least for 48 hours when removed from confinement. Therefore, performing physical confinement to migrating cells provides a potentially new avenue for obtaining multifactorial therapeutic resistant cancer cells (having increased drug efflux and CSC like behavior) which can be used in the development of new anticancer treatments, specifically targeting metastatic cancer.

Acknowledgments

Author Contributions

Y.T.K. and J.D.B. were the principal investigators and conceived the idea. Q.S., T.H. and X.C. wrote the paper. Q.S. and T.H. developed the idea and designed the experiments. Y.T.K. and L.B. designed the microchannel devices. Q.S. provided all G55 data. T.H. provided all MDA-MB-231 data. X.C. and J.D.B. carried out all radiation experiments. P.M. and M.Z. did immunohistochemistry. R.B. provided A549 data and E.H. provided PC3 data. All authors reviewed the manuscript and declared no competing financial interests.

References

1 Valastyan, S. & Weinberg, R. A. J. C. *Tumor metastasis: molecular insights and evolving paradigms*. *cell* **147**, 275-292 (2011).

2 Gupta, G. P. & Massagué, J. J. C. Cancer metastasis: building a framework. *cell* **127**, 679-695 (2006).

3 Lambert, A. W., Diwakar R. Pattabiraman, and Robert A. Weinberg. . Emerging biological principles of metastasis. *Cell* **168.4** 670-691 (2017).

4 Friedl, P. & Wolf, K. J. N. r. c. Tumour-cell invasion and migration: diversity and escape mechanisms. **3**, 362 (2003).

5 M., M. Cellular mechanobiology and cancer metastasis *Birth Defects Research Part C: Embryo Today: Reviews* **81**, 329-343 (2007).

6 J., M. D. Mechanics & Malignancy: Physical cues and changes that drive tumor progression. *Georgia Institute of Technology* (2015).

7 Sneddon, J. B. & Werb, Z. Location, location, location: the cancer stem cell niche. *Cell stem cell* **1**, 607-611 (2007).

8 Yu, H., Mouw, J. K. & Weaver, V. M. Forcing form and function: biomechanical regulation of tumor evolution. *Trends in cell biology* **21**, 47-56 (2011).

9 Li, D. *et al.* Cancer therapy and fluorescence imaging using the active release of doxorubicin from MSPs/Ni-LDH folate targeting nanoparticles. *Biomaterials* **34**, 7913-7922 (2013).

10 Brown, D. V. *et al.* Expression of CD133 and CD44 in glioblastoma stem cells correlates with cell proliferation, phenotype stability and intra-tumor heterogeneity. *PLoS One* **12**, e0172791, doi:10.1371/journal.pone.0172791 (2017).

11 Visvader, J. E. & Lindeman, G. J. Cancer stem cells in solid tumours: accumulating evidence and unresolved questions. *Nat Rev Cancer* **8**, 755-768, doi:10.1038/nrc2499 (2008).

12 Liu, S. *et al.* Breast cancer stem cells transition between epithelial and mesenchymal states reflective of their normal counterparts. *Stem cell reports* **2**, 78-91 (2014).

13 Li, Z. *et al.* Hypoxia-inducible factors regulate tumorigenic capacity of glioma stem cells. *Cancer cell* **15**, 501-513 (2009).

14 Zhong, H. *et al.* Overexpression of hypoxia-inducible factor 1α in common human cancers and their metastases. *Cancer research* **59**, 5830-5835 (1999).

15 Rofstad, E. K. Microenvironment-induced cancer metastasis. *International journal of radiation biology* **76**, 589-605 (2000).

16 Kim, J.-w., Tchernyshyov, I., Semenza, G. L. & Dang, C. V. HIF-1-mediated expression of pyruvate dehydrogenase kinase: a metabolic switch required for cellular adaptation to hypoxia. *Cell metabolism* **3**, 177-185 (2006).

17 Tsai, J. H. & Yang, J. Epithelial–mesenchymal plasticity in carcinoma metastasis. *Genes & development* **27**, 2192-2206 (2013).

18 Turner, J. G. & Sullivan, D. M. CRM1-mediated nuclear export of proteins and drug resistance in cancer. *Current medicinal chemistry* **15**, 2648-2655 (2008).

19 Henry-Mowatt, J., Dive, C., Martinou, J.-C. & James, D. Role of mitochondrial membrane permeabilization in apoptosis and cancer. *Oncogene* **23**, 2850 (2004).

20 Doyle L A, R. D. D. Multidrug resistance mediated by the breast cancer resistance protein BCRP (ABCG2). *Oncogene* **22**, 7340 (2003).

21   Dean, M. ABC transporters, drug resistance, and cancer stem cells. *Journal of mammary gland biology and neoplasia* **14**, 3-9 (2009).

22   Bleau, A. M., Huse, J. T. & Holland, E. C. The ABCG2 resistance network of glioblastoma. *Cell Cycle* **8**, 2936-2944 (2009).

23   Eramo, A. *et al.* Chemotherapy resistance of glioblastoma stem cells. *Cell death and differentiation* **13**, 1238 (2006).

24   Stupp, R. *et al.* Effects of radiotherapy with concomitant and adjuvant temozolomide versus radiotherapy alone on survival in glioblastoma in a randomised phase III study: 5-year analysis of the EORTC-NCIC trial. *Lancet Oncol* **10**, 459-466, doi:10.1016/S1470-2045(09)70025-7 (2009).

25   Stupp, R. *et al.* Neoadjuvant chemotherapy and radiotherapy followed by surgery in selected patients with stage IIIB non-small-cell lung cancer: a multicentre phase II trial. *Lancet Oncol* **10**, 785-793, doi:10.1016/S1470-2045(09)70172-X (2009).

26   Cai, X. & Sughrue, M. E. Glioblastoma: new therapeutic strategies to address cellular and genomic complexity. *Oncotarget* **9**, 9540-9554, doi:10.18632/oncotarget.23476 (2018).

27   Chun, Y.-S., Kim, M.-S. & Park, J.-W. Oxygen-dependent and-independent regulation of HIF-1alpha. *Journal of Korean medical science* **17**, 581 (2002).

28   Le Belle, J. E. *et al.* Proliferative neural stem cells have high endogenous ROS levels that regulate self-renewal and neurogenesis in a PI3K/Akt-dependant manner. *Cell stem cell* **8**, 59-71 (2011).

29   Kim, S. M. *et al.* Brassinin induces apoptosis in PC-3 human prostate cancer cells through the suppression of PI3K/Akt/mTOR/S6K1 signaling cascades. *Phytotherapy research* **28**, 423-431 (2014).

30   Gattazzo, F., Urciuolo, A. & Bonaldo, P. Extracellular matrix: a dynamic microenvironment for stem cell niche. *Biochimica et Biophysica Acta (BBA)-General Subjects* **1840**, 2506-2519 (2014).

31   Fletcher, D. A. & Mullins, D. Cell mechanics and the cytoskeleton. *Nature* **463**, 485-492, doi:10.1038/nature08908 (2010).

32   Pathak, A. & Kumar, S. Independent regulation of tumor cell migration by matrix stiffness and confinement. *Proceedings of the National Academy of Sciences* **109**, 10334-10339 (2012).

33   Dupont, S. *et al.* Role of YAP/TAZ in mechanotransduction. *Nature* **474**, 179 (2011).

34   Luna, J. I., Grossenbacher, S. K., Murphy, W. J. & Canter, R. J. Targeting cancer stem cells with natural killer cell immunotherapy. *Expert opinion on biological therapy* **17**, 313-324 (2017).

35   Pietras, A. *et al.* Osteopontin-CD44 signaling in the glioma perivascular niche enhances cancer stem cell phenotypes and promotes aggressive tumor growth. *Cell stem cell* **14**, 357-369 (2014).

36   Kopfstein, L. & Christofori, G. Metastasis: cell-autonomous mechanisms versus contributions by the tumor microenvironment. *Cellular and Molecular Life Sciences CMLS* **63**, 449-468 (2006).

37   Rudrabhatla, S. R., Mahaffey, C. L. & Mummert, M. E. Tumor microenvironment modulates hyaluronan expression: the lactate effect. *Journal of investigative dermatology* **126**, 1378-1387 (2006).

38   Marcato, P. *et al.* Aldehyde dehydrogenase activity of breast cancer stem cells is primarily due to isoform ALDH1A3 and its expression is predictive of metastasis. *Stem cells* **29**, 32-45 (2011).

39   Lugli, A. *et al.* Prognostic impact of the expression of putative cancer stem cell markers CD133, CD166, CD44s, EpCAM, and ALDH1 in colorectal cancer. *British journal of cancer* **103**, 382 (2010).

40   Lassen, N., Black, W. J., Estey, T. & Vasiliou, V. The role of corneal crystallins in the cellular defense mechanisms against oxidative stress. *Seminars in cell & developmental biology* **19**, 100-112.

41   Talks, K. L. *et al.* The expression and distribution of the hypoxia-inducible factors HIF-1α and HIF-2α in normal human tissues, cancers, and tumor-associated macrophages. *The American journal of pathology* **157**, 411-421 (2000).

42   Terris, B., Cavard, C. & Perret, C. EpCAM, a new marker for cancer stem cells in hepatocellular carcinoma. *Journal of hepatology* **52**, 280-281 (2010).

43   Cimino, A. *et al.* Epithelial cell adhesion molecule (EpCAM) is overexpressed in breast cancer metastases. *Breast Cancer Res Tr* **123**, 701-708 (2010).

44   Lu, X., Mazur, S. J., Lin, T., Appella, E. & Xu, Y. The pluripotency factor nanog promotes breast cancer tumorigenesis and metastasis. *Oncogene* **33**, 2655-2664, doi:10.1038/onc.2013.209 (2014).

45   Trerotola, M., et al. . CD133, Trop-2 and α2β1 integrin surface receptors as markers of putative human prostate cancer stem cells. *American journal of translational research* **2.2**, 135 (2010).

46   Bui L, S. Q., Hill T, et al. . Microchannel Device for Proteomic Analysis of Migrating Cancer Cells. *Biomedical Physics & Engineering Express* (2018).

47   Mehta, M. *et al.* HuR silencing elicits oxidative stress and DNA damage and sensitizes human triple-negative breast cancer cells to radiotherapy. *Oncotarget* **7**, 64820-64835, doi:10.18632/oncotarget.11706 (2016).

48   Munshi, A., Hobbs, M. & Meyn, R. E. Clonogenic cell survival assay. *Methods Mol Med* **110**, 21-28, doi:10.1385/1-59259-869-2:021 (2005).

Supplementary Material

Supplementary Methods

Microchannel Device Design

An engineered combination of PDMS devices were collected and applied to our study [1]. PDMS devices were fabricated by negative photolithography combined with soft lithography. The flower device contains 5µm x 5µm microchannels. Six independent reservoirs can separate and collect cells that migrated through physical confinements (Fig. S1. A). Satellite reservoirs were individually connected to a central reservoir to guarantee the purity for each cell group but control the cells under the same testing condition. The long device contains 600 microchannels with a dimension of 5µm x12µm (length x width). The total length of a single microchannel is around 5mm which could hold enough cells inside for protein collection (Fig. S1. B). Cells outside microchannel were considered as 2D cultured cells; cells migrating inside microchannel were considered as migrating cells and collected for Western blot analysis; cells that crept throughout the microchannel were considered to be migrated cells and used for drug studies and immunostaining (Fig. S1. C). Fig. S1. B demonstrated protein collecting process.
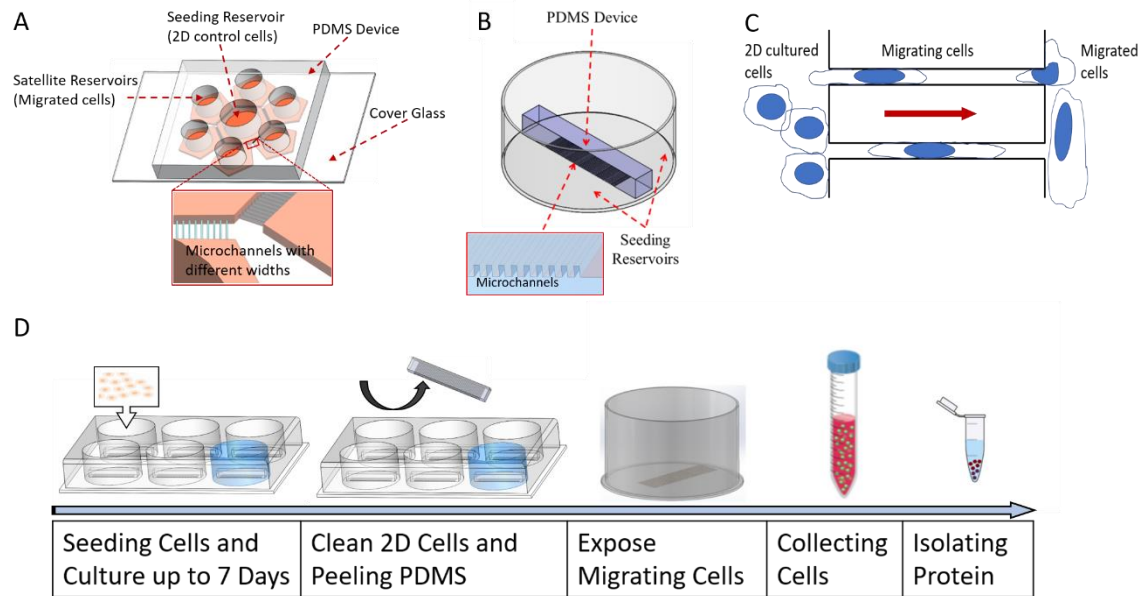
Fig. S1. A: A flower device equipped with different dimensioned microchannels for drug testing and immunostaining. **B:** A long device equipped with extensive microchannels for migrating cells collection. **C:** Demonstrational image of 2D cultured cells, migrating cells and migrated cells. (Red arrow indicated cell migrating direction) **D:** Procedures for migrating cell and protein collection.

ABCG2 Inhibition Test

Three groups of flower devices with enough migrating G55 cells were treated with either 17µM Dox or 5µM Fumitremorgin C (FTC) or 17µM Dox + 5µM FTC for 4 hours at 37°C. Autofluorescence images were taken for Dox, FTC and Dox + FTC groups after the addition of a fresh image medium. Samples were kept in the image medium overnight, and then were stained with the Live/Dead staining for 10min at room temperature. Again, respective images were obtained. Dox autofluorescence was quantified by ImageJ and the cell viability was calculated based on the Live/Dead staining signals.

Quantification of Collected Migrating Cells

Hoechst33342 (Invitrogen) staining of the nuclei was used to count total cell numbers. G55 cells were cultured in the long devices (n=3) for 5 days to initiate migrating cells. After 2D cells were removed by Trypsin-EDTA, devices were stained with Hoechst33342 for 1 hour and FDA-PI (for live and dead cell counting, respectively) for 20min at 37°C. PDMS microchannel devices were peeled to expose migrating cells. Hoechst33342 signals of the entire microchannel device were recorded by video. Fluorescent images for Hoechst/FDA/PI signals were taken at 3 randomly picked sites from each device under 20x (Fig. S3 B).

Hypoxia Culture

A hypoxia chamber constructed from a polycarbonate, air-tight container. A mixture of 90% nitrogen, 5% Carbon dioxide and 5% oxygen was used to purge the chamber. Cells were cultured in hypoxic condition (<5% oxygen) for 72 hours, the chamber was purged once a day at 24-hour intervals. Hypoxia Incubator Chamber (27310 Stem Cell Technologies) was used to collect initial data.

Total Protein Quantification

Total protein samples with equal amount (24µl) were loaded into two pieces of 10% SDS-page gels for all western blot tests samples. One gel was electro-transferred to a PVDF membrane for further western blot study. The other was stained by the Brilliant Blue to visualize total protein bands. Quantification of the intensities of the bands was performed by ImageJ. The transferred PVDF membrane was detected by GAPDH antibody (1:5000, HRP-60004, Proteintech) to indicate the protein loading amount.

Results and Discussion

FTC ABCG2 Inhibition

FTC is a well-known and widely used ABCG2 inhibitor [2]. In this study, the changes of Dox intensities were shown as overnight intensity minus 4-hour intensity. Here FTC data were not shown in Fig. S2. A, because FTC doesn't have auto fluorescence, but we did use it as a background control for signal quantification in Dox+FTC group. In G55 2D group, nuclear Dox intensities were increased in both Dox (about 4 units) and Dox + FTC (about 6 units) groups with slightly higher in the Dox + FTC group. In the 5*5 microchannel groups, an overnight intensity decrease was significantly bigger in Dox groups than in Dox + FTC groups, in which the intensity dropped in Dox groups was around 27 units and the intensity dropped in Dox+FTC groups was 3.4 units, indicating an obvious pumping out inhibition (Fig. S2. A). We believed that after cells migrated through such 3D confined spaces more ABCG2 proteins would be acquired in the cell membrane because higher influence was shown in migrated groups. Correspondingly, in microchannel groups, overnight viability in Dox + FTC treated groups was about 10% lower compared to Dox treated ones, especially in the 5*5 group. No significant killing effect was seen in FTC groups (Fig. S2. B).
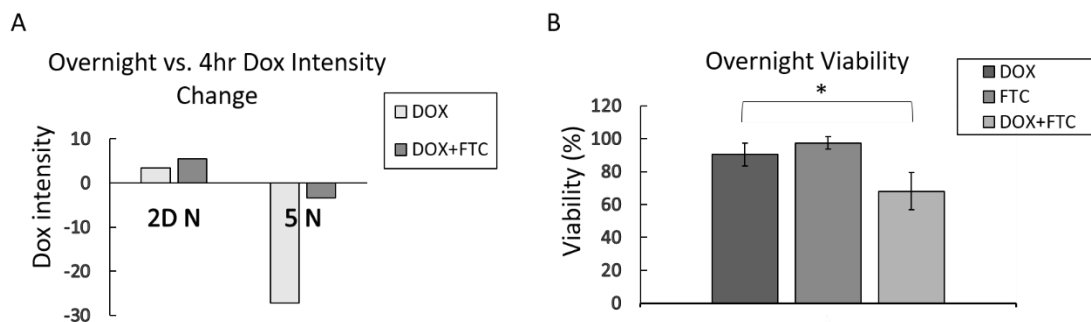
Fig. S2. A: Dox intensity changes between 4hr and overnight incubation. Data was presented as overnight intensities minus 4hr intensities. (2D N: nucleus intensity in central area; 5 N: nucleus intensity in cells migrated through 5*5 microchannels). N≥25 cells. **B:** Overnight viability of cells migrated through microchannels. Cell viability was analyzed by a Live/Dead Stain. N≥65, * P<0.05.

Quantification of Collected Migrating Cells

About 3356 ± 68 G55 cells were collected from each long device with our collecting method. This

equated to almost 60 x 10^3 cells that were collected from 18 devices totally for protein analysis

study (Fig. S3. A left side) with an almost 94% cell viability (Fig. S3. A right side). Representative

fluorescent images showed consistent results of the viability (Fig. S3. B).
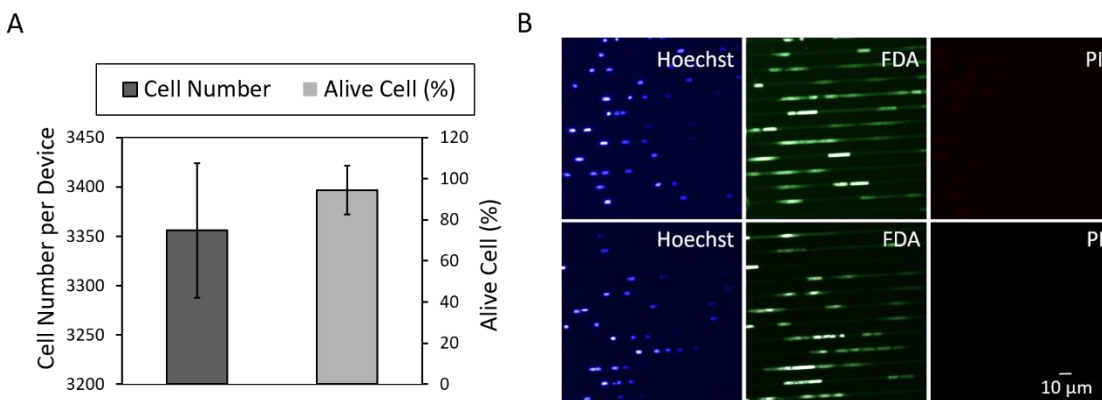

Fig. S3. A: G55 cell number (left) and cell viability (right) from each long device after peeling. Cell viability was calculated by Hoechst33342 and PI staining. **B:** Representative images of G55 cells inside the long device. Blue: Hoechst33342 (total cells); Green: FDA (live cells); Red: PI (dead cells).

Hypoxia-induced factor Compariation

2D cells cultured under hypoxia condition and confined-migrating cells were collected and protein analysis was carried out. Results showed almost two times HIF-1α expression (Fig. S4 right). This indicated that HIF-1α can also be triggered by confined-migration rather only by hypoxia condition.
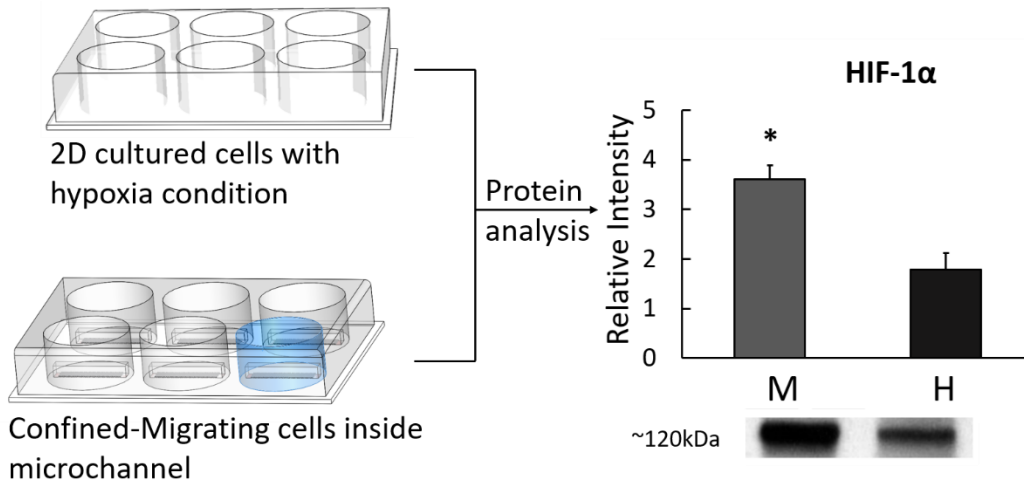
Fig. S4. HIF-1α elevated expression in a confined-migrating group rather than a hypoxia group. G55 Western blot results are shown as average ± Std. Representative blot images of each marker are shown below their respective graphs. All results were normalized to the total proteins. *p<0.05. All experiments were reproduced.

Total Protein Quantification

For both cell lines (G55 and MDA-MB-231), although we attempted to load an equal amount of proteins based on the protein concentration, the gel staining showed inequality (Fig. S5. A and C). GAPDH bands turned to be inconsistent with total gel staining. It has been pointed out that GAPDH [3] or β-actin [] signal could be affected by hypoxia and/or migration for certain cancer types. Therefore, we decided to utilize the results of total proteins from gel staining for normalization and for accurate results.
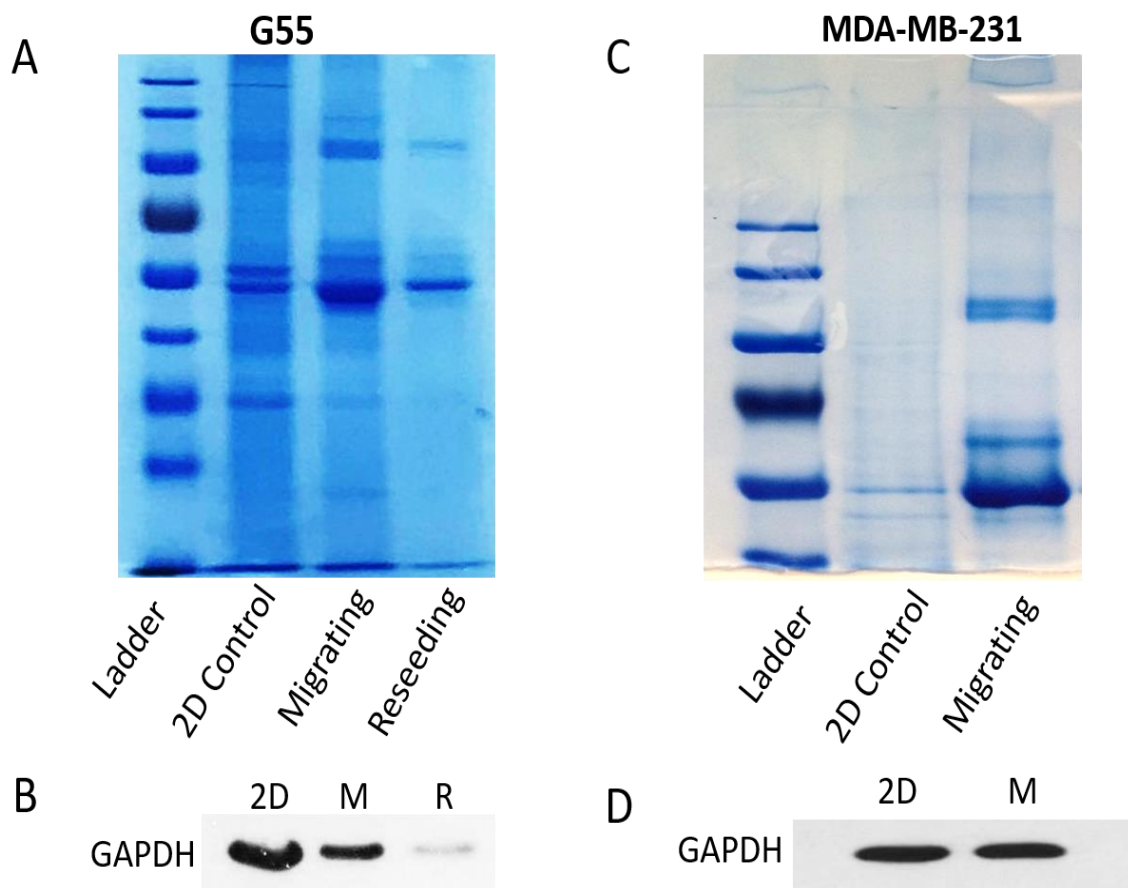
Fig. S5. Gel staining for total proteins and western blot for detecting GAPDH. G55 (**A**) and MDA-MB-231 (**C**) gels with Brilliant Blue staining for total protein analysis, and corresponding western blots of GAPDH (B and D). (2D: Non-migrating cells; M: migrating cells; R: reseeded migrating cells).

References

1. Bui L, S. Q., Hill T, et al. . Microchannel Device for Proteomic Analysis of Migrating Cancer Cells. *Biomedical Physics & Engineering Express* (2018).
2. Rabindran, Sridhar K., et al. *Fumitremorgin C reverses multidrug resistance in cells transfected with the breast cancer resistance protein. Cancer research* **60.1**, 47-50 (2000).
3. Lee, Hyon Jae, et al. *Methylglyoxal can modify GAPDH activity and structure. Annals of the New York Academy of Sciences* **1043.1**, 135-145 (2005).
4. Dittmer, Angela, and Jürgen Dittmer. *β-Actin is not a reliable loading control in Western blot analysis. Electrophoresis* **27.14**, 2844-2845 (2006).

Chapter 2. Migration and Physical Confinement are Two Indispensable Elements in Upregulating GBM's Chemotherapeutic Resistance

Qionghua Shen[1], Adam Adrien Germain[1] and Young-Tae Kim, PhD[1,2] *

[1]Department of Bioengineering, University of Texas at Arlington, TX

[2]Department of Urology, University of Texas Southwestern Medical Center, Dallas, TX

*Corresponding author:
Young-Tae Kim, Ph.D.
Department of Bioengineering
500 UTA Blvd ERB244
University of Texas at Arlington
Arlington, TX 76010

E-mail : ykim@uta.edu
Fax: 817-272-2251
Phone: 817-272-5023

Keywords: GBM, migration, physical confinement, chemotherapeutic resistance

Abstract

Metastatic glioblastoma multiform (GBM) has a low survival rate due to a single cell spreading into adjacent brain tissue and along the white matter tract. Also, those spreading cells usually show upregulated therapeutic resistance. Therefore, it is interesting to study the relationship between migration, confinement, and resistance. In this presented study, we used G55, a typical migratory glioblastoma cell as a model and created three different cell populations: 1) migrating without confined impute; 2) receiving confined impute but with very limited migrating space; 3) migrating under confinement via different *in vitro* migration study methods (scratch assay, trans-well assay, and microchannel assay). Comparison among those three groups of cells in both protein expression and chemotherapy sensitivity proves that migration and physical confinement together is the key to increase interstitial invasive cancer cells' (e.g., G55) chemotherapeutic resistance and is indispensable. Hence, the microchannel device as a kind of platform that can welly provide physical confinement and allow cells to migrate a certain distance is a better method for metastatic cancer study at least for metastatic triggered therapeutic resistance study.

Introduction

Glioblastoma multiforme (GBM) has a low survival rate due to the diffuse and invasive behavior of GBM cells[1]. Unlike other aggressive malignancies, GBM's invasion patterns are within adjacent brain tissue. Instead of intravasation distant tissues, it commonly spread by direct extension and infiltration into adjacent brain tissue and along with the white matter tract[1-3]. More and more clinical evidence reveals that those diffused GBM cells have highly chemotherapeutic resistance and it is the major reason for poor treatment effect[4]. Therefore, it is critical to understand the invasion behavior of GBM and its link to increased chemoresistance.

The pre-existing tissue track within the brain like the interstitial system (ISS) always guides GBM migration[5]. ISS is a kind of interstitial tissue including the subpial space, white matter tracts, and vascular beds[6,7]. Having consistently narrow dimensions (3-30um in width and 100-600um in length) is one major characteristic of those brain tissue tracks[7]. It is noteworthy that GBM cells can travel through narrow tracks with the least resistance and no significant changes in track width during or after the migration [8]. Therefore, it proves GBM cells not only preferentially follow those pre-existing tracks but also have the capacity to adapt their shape to those confined space. It suggests that topographies of ECM structures may play a critical role in tumor metastasis and influence metastatic cancer cell's cellular function. Hence, as one of the most important biophysical cues of brain ISS, confinement could be one of the main elements causing cellular functional change of metastatic GBM during metastasis.

Modern anticancer therapy is challenged by two key functions of cancer progression: invasion and survival (resistance to therapy). Through pathways controlling cancer invasion and resistance to therapy have been considered separately, recent indirect evidence suggests that signaling networks

underlying both cancer invasion and resistance overlap and provide biologically relevant synergism[9,10]. Especially for reactive resistance, which is required during tumor progression as an adaptive response to microenvironmental signals, can be adjusted by a space-dependent manner. It has been discovered when cells inside narrow tracks (eg. cells migrate inside microchannel device), cell proliferation will be downregulated, and expression of proteins associated with multidrug resistance, such as P-gp[11]. Therefore, it could be an interesting question, if without biophysical cues, like confinement, from microenvironment will those migrating or invasive cancer cells (GBM in particular) still show similar upregulated resistance? Or simply put biophysical cues (eg. physical confinement) without or with very limited movement is enough for cancer cells to generate the same properties?

In this presented study, we used G55, the most common migratory cancer cells with the capability of adapting to confined space, as a testing model to explore the relationship between migration, confinement, and resistance, particularly chemotherapeutic resistance. Three major in vitro migration study methods have been used to create different cell populations: 1) migrating without confined impute (scratch assay); 2) receiving confined impute but with very limited migrating space (trans-well assay); 3) migrating under confinement (microchannel device). We compared those three groups of cells in both protein expression and chemotherapy sensitivity parts to verify our hypothesis that migration and physical confinement together is the key element that can increase interstitial invasive cancer cell's chemotherapeutic resistance and is indispensable.

Material and method

Cell Culture

The human glioblastoma cell line G55 was provided by The University of Oklahoma Health Sciences Center. The cells were cultured in a serum-free DMEM/F-12 medium supplemented with 1x B-27 (Invitrogen), 1x Insulin-Transferrin-Selenium-X (Invitrogen), and mouse EGF (epidermal growth factor, 20ng/ml, PeproTech).

Produce Different Conditional Cells

For generating migrating G55 cells, the scratch assay was used. 50 x 10^3 cells were seeded to each well of a 6-well plate with 10% serum medium. After 3 days of culture, a consistent scratch would be created by scratcher (Fig1. A). Cells would be maintained for another 2 days to generate migrating cells.

Confined G55 cells were produced by a trans-well membrane with 8µm pore size and 10µm thickness (Fig1. B). 600µl DMEM with 10% serum medium was added into the lower compartment. Insert the upper compartment and let the membrane prewet for 1min. Add 15 x 10^3 G55 cells in 200µl 2% serum medium was into the upper compartment. Keep the trans-well plate at 37◦C and 5% CO_2 overnight to produce confined cells with limited migration distance.

To generate a confined-migrating, microchannel device with 5mm long channel was used (Fig1. C). The cross-section of the microchannel is 5 x 5µm. 10 x 10^3 G55 cells were introduced at each side entrances of the microchannel device (total 20 x 10^3 cells per device, for immunostaining cells were only dropped to one side of the device). All devices were maintained in 10% serum medium for 5 days to facilitate the initiation of migration via confinements.
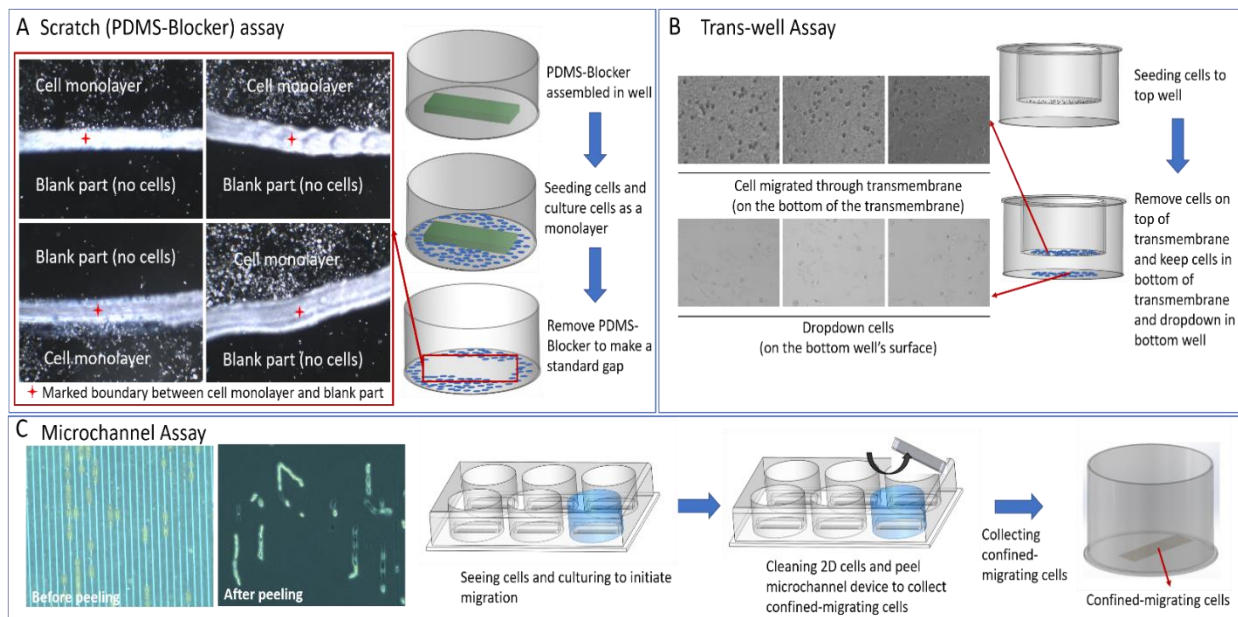
Figure 1. Schematic diagram of collecting three different conditional cells. A. Use PDMS-Blocker to create a uniform scratch for collecting 2D migrating cells. The left part shows the uniform scratch gap created by removing PDMS-Blocker after 3 day's culture. **B.** Trans-well assay is used to generate confined cells with minimal migration distance. The left part shows transmembrane with 8µm pore size and cells migrated through the filter membrane. Those cells on the bottom side of the filter membrane and drop down into the lower compartment were considered as confined cells. **C.** Microchannel devices with 5 x 5µm (h x w) sized microchannels are assembled to 6-well plates to facilitate confined-migrating cells. Left images show confined-migrating cells within microchannel and exposed after peeling devices.

Chemo-sensitivity Study

To collect confined-migrating cells from the microchannel device, Trypsin-EDTA and Costar® 3008 Cell Lifter (Corning Inc) were used to clean outside 2D cells. The PDMS device was peeled to expose the confined-migrating cells. Confined-migrating cells from 18 devices (total cell number was estimated to be 60 x 10^3) inside microchannels were be collected by additional trypsinization step. Cells from both the bottom side of the trans-well membrane and lower well were considered as confined cells. Cells on the top side of the trans-well membrane were cleaned by a cotton swab. Added 500µl Trypsin-EDTA to each well to detach confined cells from filter membrane bottom and lower well. 2D migrating cells were collected from the blocker area. Right

before peeling the PDMS-Blocker, the boundary was labeled by the maker. After 2 days' culture, only cells migrated into the labeled area remained as others would be cleaned by cell lifter. Trypsinization step was used to collect the remaining 2D migrating cells. Cells cultured in a normal petri dish were considered as a 2D control group.

Anti-cancer drug Temozolomide (TMZ, 500nM, T2577, Sigma) was used to exam different conditional cells' responses to chemotherapy. All groups of cells were collected and reseeded to 96 well plates and pre-culture overnight to allow cells to re-attach to surface. 500nM TMZ was added to all groups of cells and cells were maintained under consistent condition. 0.1% DMSO was used as a negative control. Cell viability was examined by MTS Assay (CellTiter 96$^{\circledR}$ AQueous Non-Radioactive cell proliferation assay, Promega). Results were normalized as a percentage of DMSO control for all groups.

Actinomycin D Transcription Inhibition

8nM of actinomycin D was chose to inhibit new protein production (FigS2). For 2D migrating cells (scratch assay), all devices were incubated with 8nM actinomycin D for 48hrs after scratch made. For confined cells (trans-well assay), cells were pre-treated with 8nM actinomycin D in 2% serum medium for 24hrs before adding cell solution into trans-well devices. Images were taken after 24hrs AD incubation. For confined-migrating cells (microchannel assay), all devices were maintained normally until cells moved close to microchannel opening (but not start to migrate into microchannel). Then all devices were incubated with 8nM actinomycin D solution for 48hrs before image taking. 0.1% DMSO was used as control condition for all tested groups.

Immunostaining

All three conditional cells were fixed with 4% paraformaldehyde consistently. Samples were blocked in 4% goat serum in washing solution (0.5% triton in 1X PBS) for 1 hour at room temperature. Samples were incubated with primary antibodies including CD133 (Cell Signaling, D2V8Q) and ABCG2 (Cell Signaling, D5V2K) at 4°C overnight. Secondary antibodies including Goat anti-migG1 Dylight 594 (1:250, Jackson Immuno Research) and Goat anti-mIgG2b Alexa Fluor 488 (1:250, Jackson Immuno Research) were prepared in the washing solution. Secondary incubation was conducted at room temperature for 2 hours followed by DAPI staining for the nuclei for 20 minutes. All signals were picked from the individual cell (n≥20 cells) at 20X and quantified using Image J.

Western Blot

Cells from all groups were centrifuged for 5 min at 4000rmp. The supernatant was discarded and the cell pellet was harvested.Total cell lysates were obtained by adding RIPA buffer (R0728, Sigma-Aldrich) and protease inhibitor cocktail (P2714, Sigma-Aldrich). Equilibrated protein samples were loaded into a 10% SDS-Page gel, electrophoresed, and then electro-transferred to a PVDF membrane (Bio-Rad). Transferred membranes were blocked with a blocking buffer contained 5% non-fat milk (Labscientific, M0841). CD133 (Cell Signaling, D2V8Q) and ABCG2 (Cell Signaling, D5V2K) were used as the primary antibodies. Target proteins were visualized with IgG secondary mouse or rabbit antibodies and a chemiluminescent substrate (Santa Cruz, sc-2048). All Western blot results were normalized by loading protein.

Statistical Analysis

GraphPad was used to make all graphs and generate statistical analysis. One-way ANOVA and Tukey post hoc test was used to compare the significance among multiple groups. A *p*-value of less than 0.05 was considered statistically significant.

Results

Confined-migrating cells show increased resistance to chemotherapeutic reagent

Anticancer reagent Temozolomide was chosen to test those conditional cells' chemo-sensitivity. After being collected through a different method, all cells were re-seed to 96-well plate and pre-culture overnight to let cells attach. 500nM TMZ was used for the test. After 48hrs' treatment, confined-migrating cells (MC group in Fig2) displayed significantly higher viability (almost 90% alive) compared to other groups (Fig2). However, confined cells (TW group in Fig2) from trans-well assay and 2D migrating cells (SC group in Fig2) from scratch assay showed a similar survival rate compared to normal cultured cells (2D group in Fig2).
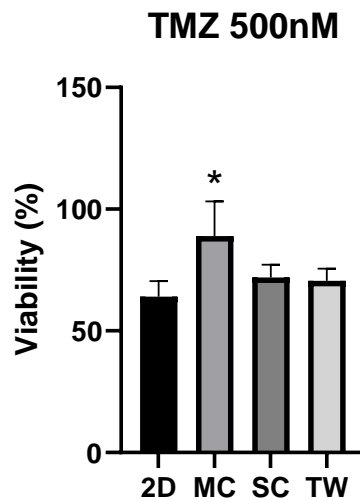
TMZ 500nM

Figure 2. Higher TMZ resistance was observed in confined-migrating cells. All groups of cells were incubated with 500nM TMZ for 48hrs. The DMSO group was used as control. 2D: normal

culturing cells; M: confined-migrating cells; SC: 2D migrating cells collected via scratch assay; TW: confined cells collected via trans-well assay. All results were normalized to DMSO control and shown as mean + Std. *p<0.05 between confined-migrating group (MC) and other groups.

Confined-migrating action need newly produced proteins

To assess the difference between confined-migrating, confined, and 2D migrating cells, we utilized

Actinomycin D (AD) to inhibit new protein production. Actinomycin D as a traditional anti-cancer

chemotherapy medication can inhibit transcription[12]. Therefore, it also has been widely used to

prevent new protein production for research. Here we chose 8nM actinomycin D, which is lower

than its IC50 to inhibit new protein production (FigS2). For microchannel devices, after 48hrs of

AD incubation, no cell got into 5 x 5µm microchannels (Fig3. A). Whereas the control group had

a lot of cells migrated within microchannel (Fig3. A red arrows). Hence, AD treatment did

influence confined-migration. But it had no obvious influence on 2D migration. As observed in

Figure3. B, no significant difference in 2D migration behavior between the control group and AD

incubated group. Trans-well assay experiment proved its inhibition on cells' shape adapting when

facing to confinement. Compared to the control group, AD treated groups had significant lesser

cells migrating through the trans-well membrane (Fig3. C1). The quantitative result showed almost

20 times more cells trans through the trans-well membrane in the control group (Fig3. C2).

Therefore, AD treatment's confined-migrating inhibition is mainly due to influence of
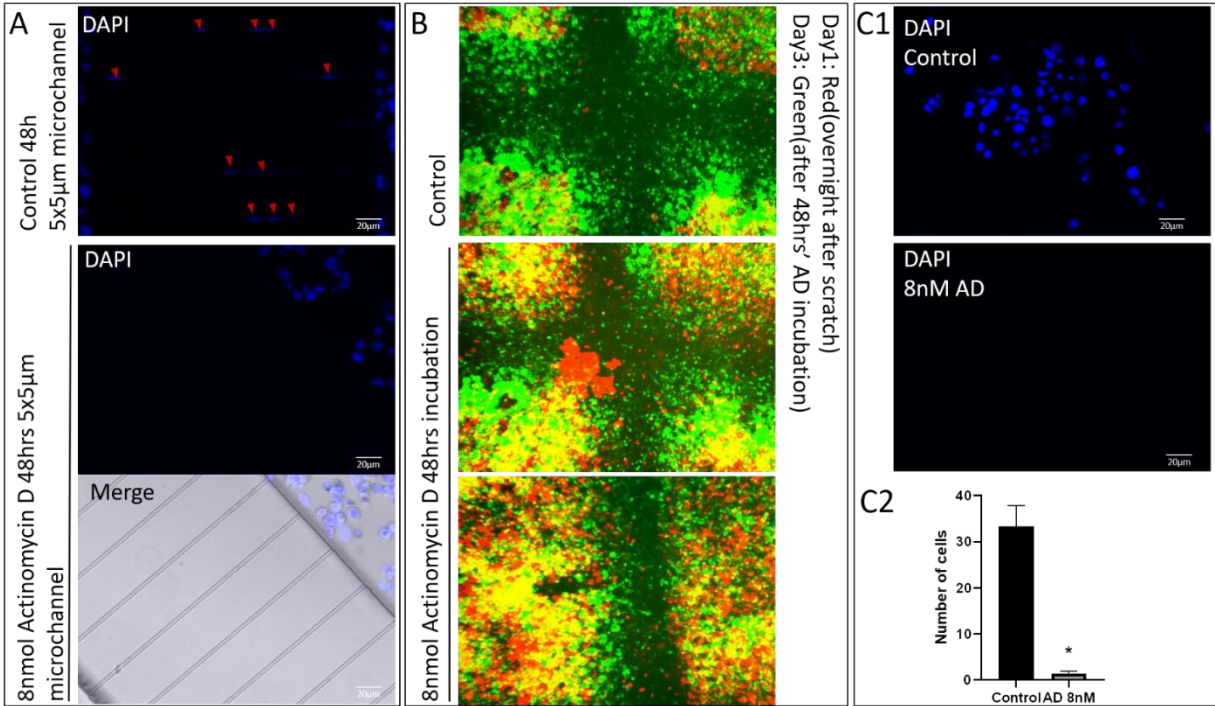
confinement adaption.

Figure 3. Actinomycin D influences confined-migrating. A. Devices were incubated with 8nM actinomycin for 48hrs after cells get close to microchannel opening. Red arrows indicate confined-migrating cells within microchannels. Cells were stained with DAPI after fixation. **B.** Cells were incubated with 8nM actinomycin D after making a scratch. Pseudo colors were added to images that were taken at different time points. Red: overnight after scratch. Green: after 48hrs' AD incubation. **C1.** Cells migrated through 10µm trans-well membrane with 8µm pore. Images were taken after 48hrs incubated 8nM AD. Cells were stained with DAPI after fixation. **C2.** Quantitative comparison of migrated cell numbers between control group and 8nM AD group. *p<0.05. Mean + Std. Control: 0.1% DMSO. 8nM AD: 8nM actinomycin D.

Confined-migrating cells display upregulated therapeutic resistance-related proteins

To assess why those confined-migrating cells had a higher survival rate differed from other cells we examined the expression of some therapeutic resistance-related proteins (CD133 and ABCG2) among those conditional cells through immunostaining and Western blot analysis. According to immunostaining, no cells from the 2D migrating group (SC) or confined cells (TW) showed CD133/ABCG2 positive (Fig4. A&B). While CD133/ABCG2 positive cells were only detected from the confined-migrating (MC) group (Fig4. C). A more detailed protein analysis was carried out via Western blot. Figure4. D1 showed the highest (3 times as high as 2D control) CD133

expression was detected from confined-migrating cells. While the 2D migrating cells generated by scratch assay showed a similar amount of CD133 as normal cultured cells (Fig4. D1). Though confined cells produced by trans-well assay displayed twice the amount of CD133 compared to normal cultured cells, its CD133 amount was still significantly lower than confined-migrating cells separated from microchannel devices (Fig4. D1). For ABCG2, confined-migrating cells (MC) showed more than 2 times expression compared to normal cultured cells, whereas confined cells' (TW) and 2D migrating cells' (SC) ABCG2 expression showed no significant difference compared to normal cultured cells (Fig4. D2).
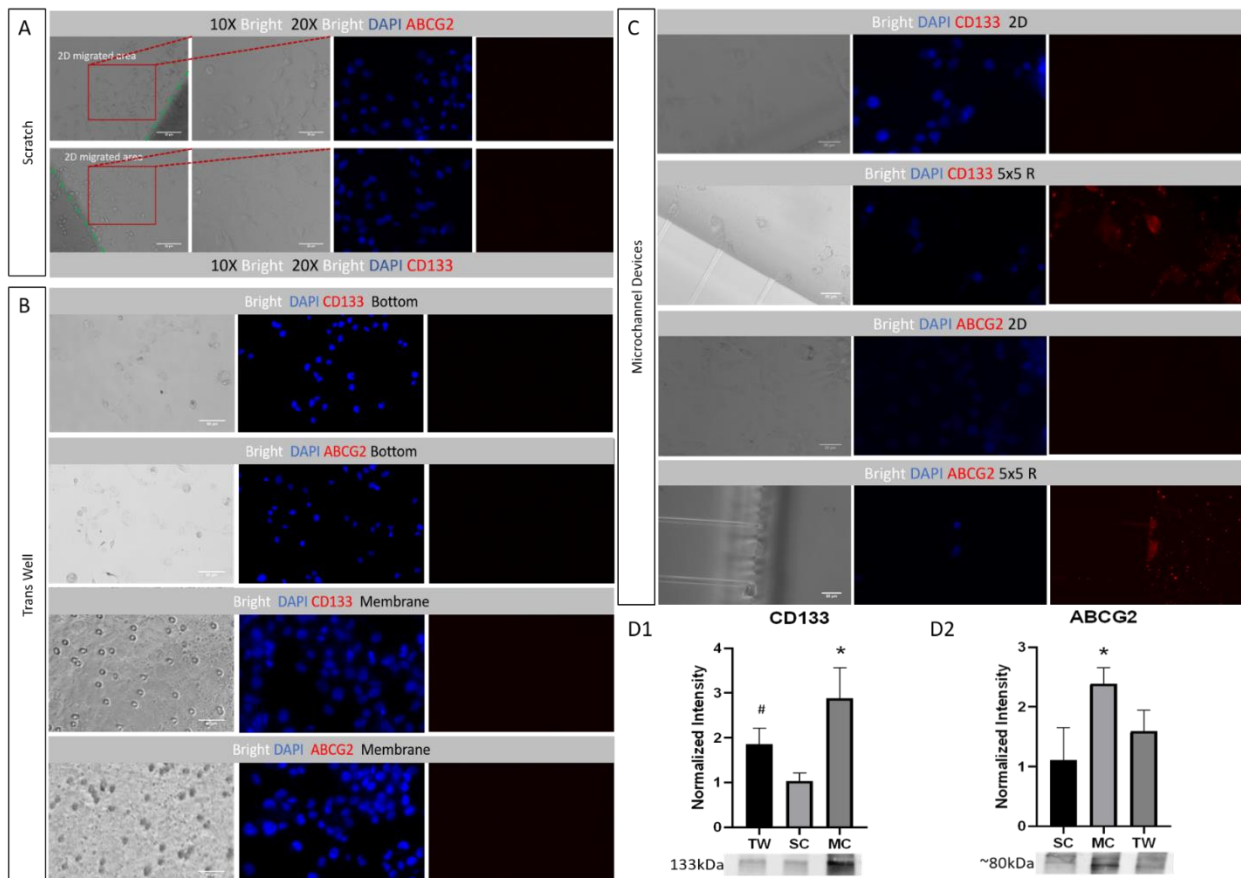

Figure 4. Upregulated therapeutic resistance-related proteins are detected from confined-migrating cells. A. CD133 and ABCG2 immunostaining images for 2D migrating cells from the scratch assay. Green dashed line labeled the boundary of scratch-made by PDMS-Blocker. 2D

migrating cells area is indicated in the image. Second column images are zoom in part for red window labeled area within first column images. **B.** CD133 and ABCG2 immunostaining images for confined cells from the trans-well assay. Images were taken from both dropped cells in the lower compartment (labeled as Bottom) and cells migrated across the filter membrane (labeled as membrane). **C.** CD133 and ABCG2 immunostaining images for confined-migrating cells from the microchannel device. Blue: DAPI; Red: CD133/ABCG2. **D1&D2.** Quantitative CD133 and ABCG2 expression for three conditional cells via Western blot. All data showed as normalized to normal cultured cells. TW: confined cells from trans-well assay; SC: 2D migrating cells from scratch assay; MC: confined-migrating cells through microchannel device. *$p<0.05$ between the MC group and others. #$p<0.05$ between the TW group and SC group. Mean + Std. All experiments were reproduced.

Discussion

Invasion and resistance are two major challenges of recent cancer treatment. Most metastatic cancers, glioma, in particular, have the capability to acquire increased resistance to chemo- or/and radiotherapies after migrating to adjacent or distal organs, for example, gliomas[13-15]. Seeking valid strategies to inhibit invasion and/or resistance is one of the major goals of modern anti-cancer therapy to achieve. Therefore, choosing a suitable platform to facilitate research is important. The primary step for it is to understand the link between metastasis and therapeutic resistance.

Adapting to physical confinement and migrating a certain distance are two important components of metastasis[16,17]. Understanding which one is more important in metastasis-related therapeutic resistance is necessary. Therefore, we designed some simple experiments to help us understand this questionable relationship. We utilized three widely used cancer metastasis study platforms: scratch assay, trans-well assay, and microchannel device, to create three conditional cells: 2D migrating, confined, and confined-migrating. By comparing their response to chemotherapy and different protein expression we were able to undiscover the causality between confined, migration, and resistance. Also, it can give us some idea of how to choose a suitable research platform.

TMZ sensitivity results showed confined-migrating cells induced by microchannel devices had a significantly higher survival rate compared to normal cultured cells (Fig2). However, 2D migrating and confined cells from scratch assay and trans-well assay were not different from normal cultured cells. This finding indicated that confined-migrating cells in a microchannel device had increased resistance compared to cells produced by other culture systems. It is an interesting observation since it is well known that an *in vivo* environment differs from traditional culture condition[18-20]. The complicated ECM farm work *in vivo* can not only guide cell movement but also provide certain physical confinement to those moving cells[21,22]. Because of this difference, it is difficult to applicate *in vitro* study results *in vivo*. In another word, only confined or 2D migrating cells are different from those confined-migrating ones at least in the chemosensitivity part. Besides, we utilized Actinomycin D's transcription inhibition[23] proved newly produced proteins are necessary to facilitate confined-migrating especially in adapting to physical confinement (Fig3. A&C). However, new protein production is not required for 2D migrating (Fig3. B). What's more, immunostaining and western blot results indicated there are several survival-related proteins increased in the confined-migrating group. CD133, a cancer stem cell marker, is related to cancer cell survival and metastasis. It is significantly upregulated in confined (trans-well) and confined-migrating (microchannel) cells with much higher incrassation in confined-migrating cells (Fig4. D1). ABCG2, a drug efflux protein, also upregulated in confined-migrating cells (Fig4. D2). It plays a role in increase chemotherapeutic resistance in several cancer types including G55. The above results confirmed confined-migrating cells produce by microchannel devices are different from normal cultured cells with increased resistance at least chemotherapeutic resistance. Besides, the comparison between confined-migrating cells from microchannel, confined cells from trans-

well assay, and 2D migrating cells from scratch assay demonstrated that confinement and migrating are indispensable in upregulating cancer cells' resistance during metastasis.

In summary, this study proves to provide physical confinement and maintain a certain distance of migration are two indispensable steps to demonstrate metastatic cancer's upregulated therapeutic resistance. Therefore, simply based on whether welly mimic physical confinement triggered the therapeutic resistance process, the microchannel device has its unique superiority. It could be a better *in vitro* method to produce metastatic gliomas for anti-cancer study, for example, drug screening.

Reference:

1   Holland, E. C. Glioblastoma multiforme: the terminator. *Proceedings of the National Academy of Sciences* **97**, 6242-6244 (2000).
2   Manini, I. *et al.* Role of microenvironment in glioma invasion: what we learned from in vitro models. *International journal of molecular sciences* **19**, 147 (2018).
3   Viapiano, M. S. & Lawler, S. E. in *CNS Cancer*   1219-1252 (Springer, 2009).
4   Giese, A., Bjerkvig, R., Berens, M. E. & Westphal, M. Cost of migration: invasion of malignant gliomas and implications for treatment. *Journal of clinical oncology* **21**, 1624-1636 (2003).
5   Claes, A., Idema, A. J. & Wesseling, P. Diffuse glioma growth: a guerilla war. *Acta neuropathologica* **114**, 443-458 (2007).
6   Brightman, M. W. & Kaya, M. Permeable endothelium and the interstitial space of brain. *Cellular and molecular neurobiology* **20**, 111-130 (2000).
7   Pizzo, M. E. & Thorne, R. G. in *Brain edema*   105-127 (Elsevier, 2017).
8   G. Gritsenko, P., Ilina, O. & Friedl, P. Interstitial guidance of cancer invasion. *The Journal of pathology* **226**, 185-199 (2012).
9   Al Saleh, S., Sharaf, L. H. & Luqmani, Y. A. Signalling pathways involved in endocrine resistance in breast cancer and associations with epithelial to mesenchymal transition. *Int J Oncol* **38**, 1197-1217 (2011).
10   Furnari, F. B. *et al.* Malignant astrocytic glioma: genetics, biology, and paths to treatment. *Genes & development* **21**, 2683-2710 (2007).
11   Nunes, A. S., Barros, A. S., Costa, E. C., Moreira, A. F. & Correia, I. J. 3D tumor spheroids as in vitro models to mimic in vivo human solid tumors resistance to therapeutic drugs. *Biotechnology and bioengineering* **116**, 206-226 (2019).

12   Perry, R. P. & Kelley, D. E. Inhibition of RNA synthesis by actinomycin D: characteristic dose‑response of different RNA species. *Journal of cellular physiology* **76**, 127-139 (1970).

13   Boudadi, K. & Antonarakis, E. S. Resistance to novel antiandrogen therapies in metastatic castration-resistant prostate cancer. *Clinical Medicine Insights: Oncology* **10**, CMO-Ss34534 (2016).

14   Ramirez, Y. P., Weatherbee, J. L., Wheelhouse, R. T. & Ross, A. H. Glioblastoma multiforme therapy and mechanisms of resistance. *Pharmaceuticals* **6**, 1475-1506 (2013).

15   Yu, F. *et al.* SPOCK1 is upregulated in recurrent glioblastoma and contributes to metastasis and Temozolomide resistance. *Cell Proliferation* **49**, 195-206 (2016).

16   Wirtz, D., Konstantopoulos, K. & Searson, P. C. The physics of cancer: the role of physical interactions and mechanical forces in metastasis. *Nature Reviews Cancer* **11**, 512-522 (2011).

17   Charras, G. & Sahai, E. Physical influences of the extracellular environment on cell migration. *Nature reviews Molecular cell biology* **15**, 813-824 (2014).

18   Baker, B. M. & Chen, C. S. Deconstructing the third dimension–how 3D culture microenvironments alter cellular cues. *Journal of cell science* **125**, 3015-3024 (2012).

19   Edmondson, R., Broglie, J. J., Adcock, A. F. & Yang, L. Three-dimensional cell culture systems and their applications in drug discovery and cell-based biosensors. *Assay and drug development technologies* **12**, 207-218 (2014).

20   Antoni, D., Burckel, H., Josset, E. & Noel, G. Three-dimensional cell culture: a breakthrough in vivo. *International journal of molecular sciences* **16**, 5517-5527 (2015).

21   Kraning-Rush, C. M. & Reinhart-King, C. A. Controlling matrix stiffness and topography for the study of tumor cell migration. *Cell adhesion & migration* **6**, 274-279 (2012).

22   Friedl, P. Dynamic imaging of cellular interactions with extracellular matrix. *Histochemistry and cell biology* **122**, 183-190 (2004).

23   Cassé, C., Giannoni, F., Dubois, M.-F. & Bensaude, O. The transcriptional inhibitors, actinomycin D and α-amanitin, activate the HIV-1 promoter and favor phosphorylation of the RNA polymerase II C-terminal domain. *Journal of Biological Chemistry* **274**, 16097-16106 (1999).

Supplementary materials and methods

Quantification of Total Protein

24µl of protein samples of each conditional cells were loaded into two pieces of 10% SDS-page gels equally. Brilliant Blue staining was conducted to one gel for visualization of total protein bands. The other gel was electro-transferred to a PVDF membrane for further Western blot study.

The intensities of the total protein band were quantified via ImageJ. The transferred PVDF membrane was detected by the GAPDH antibody (1:5,000, HRP-60004, Proteintech) to indicate the protein loading amount.

Actinomycin D 48hrs Incubation Viability Test

For the IC50 test, 5000 G55 cells were seeded to each well of 96-well plate. Cells were maintained at 37°C, 5% CO2 overnight. Plates were treated with Actinomycin D (AD, 0nM, 12nM, 24nM,56nM, 120nM in 0.1% DMSO) for 30 minutes. Cells' viabilities were checked by MTS assay. IC50 was calculated by GraphPad.

Results and Discussion

Total Protein Quantification

Although we attempted to load an equal amount of proteins based on the protein concentration, the gel staining and GAPDH bands showed inequality (Fig. S1). Therefore, in order to maintain the accuracy of protein analysis, all Western blot results were normalized to the total protein amount.
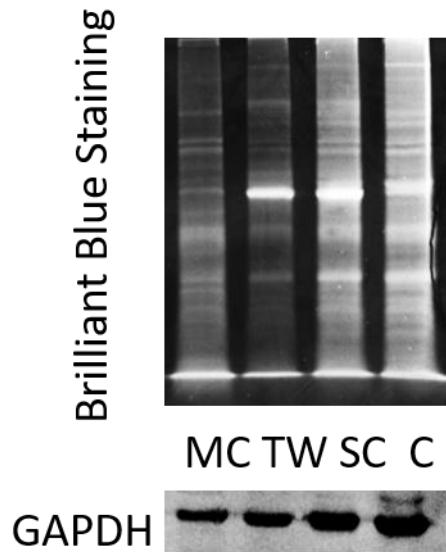
Figure S1. Gel staining for total proteins and Western blot for detecting GAPDH. G55 gels with Brilliant Blue staining for total protein analysis, and corresponding Western blots of GAPDH (lower image). (MC: confined-migrating cells produced by microchannel assay; TW: confined cells induced by trans-well assay; SC: 2D migrating cells produced by scratch assay and C: control cells cultured on normal culture dish).

IC50 of 48hrs Actinomycin D Treatment

Actinomycin D 48hrs incubation's IC50 for G55 was tested by MTS assay. For G55 cells IC50 was around 8.69nM (FigS2).

G55 Actinomycin D 48hrs

IC50   8.69
R squared0.9657
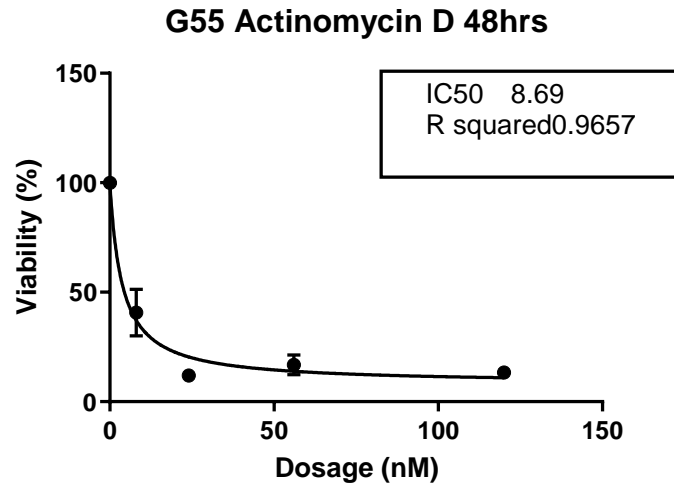
FigS2. IC50 for Actinomycin D 48hrs Incubation. G55 cells treated for various doses of Actinomycin D for 48hrs and IC50 was around 8.69nM. 0.1%DMSO was used as control group. Average ± standard deviation. N=3 per group.

Chapter 3. Single-cell-level Screening Method for Migratory Cancer Cells and Its Potential Feasibility in High-throughput Manner

Qionghua Shen[1], Hanspeter Niederstrasser, PhD[2], Rami Barakat[1], Zaid Haddadin[1], Sandra Rose Miller[1], Bruce Posner, PhD[2] and Young-Tae Kim, PhD[1,3] *

1Department of Bioengineering, University of Texas at Arlington, TX

2Department of Biochemistry, University of Texas Southwestern Medical Center, Dallas, TX

3Department of Urology, University of Texas Southwestern Medical Center, Dallas, TX

*Corresponding author:
Young-Tae Kim, Ph.D.
Department of Bioengineering
500 UTA Blvd ERB244
University of Texas at Arlington
Arlington, TX 76010

E-mail: ykim@uta.edu
Fax: 817-272-2251
Phone: 817-272-5023

Keywords: Single-cell-level, High-throughput, Microchannel device, Migratory cancer

Abstract

High-throughput screening (HTS) is a well-established approach for tumor-specific drug development because of its high efficiency and customizable selection of antineoplastic drugs. However, there is still a lack of an appropriate cell-based HTS specific for migratory cancer cells. In the study presented here, we created a novel assay (mHTS): a single-cell-level screening method targeting migratory cancer cells and can be applied in a high-throughput manner. This mHTS platform is based on microchannel devices (providing physical confinement during cell migration and limit migrating cells' proliferation rate) assembled 96-well plate (fitting to HTS manner). To determine the feasibility of this assay, we quantified the anti-migratory and anti-viability effects of several molecules (Cytochalasin D, Doxorubicin, and AZD-6244) on migrating (creeping inside microchannel) glioblastoma multiforme (GBM) cells. After analyzing migration screening data that was collected on a single-cell-level, we were able to compare those drug's effects on cancer cells' migration velocity and uncovered the migration inhibiting potential of AZD (500nM and 1000nM). Viability data based on single-cell-level screening also allowed us to further understand the same drug's different lethality toward migrating and normal 2D cultured cancer cells. The Pre-classification of subpopulations enables us to study the heterogeneity of cancer and ensures our method's feasibility for a high-throughput manner. All these results proved our mHTS platform is suitable for single-cell-level anti-migration drug screening and has potential feasibility in promoting the development of anti-migratory-cancer-drug in a high-throughput manner.

Introduction

Multimodal treatments of tumors, involving surgery followed by radio- and/or chemotherapy, have considerable improvements. Nevertheless, patients with migratory cancer (highly infiltrative cancer type) have extremely low survival rates (e.g. less than 5% of 5-year survival rates in glioblastoma multiforme (GBM)[1]). The poor prognosis arises from metastasizing cells' increased resistance, known as metastatic resistance, after migrating among the tissue.[2] It is well documented that the cancer cell's migration is the key element of the invasion-metastasis cascade.[3] Thus, developing novel drug(s) to inhibit cancer cell migration and/or overcome metastasis derived therapeutic resistance has become a hot topic in anti-cancer research, especially for those migratory cancer types.

With the advent of automated high-throughput screening (HTS) and drug loading system, it is possible to develop an innovative assay to identify therapeutic molecule(s) which effectively block cancer cell migration, resulting in the transformation of a fatal diffuse tumor into a local aggregated tumor and/or eradicate the treatment-resistant migrating cancer cells. HTS comprises a new line of research into the discovery of new molecules targeting migratory cancer cells because of its ability to utilize low volume but a high density of assay format to evaluate large compound libraries on migratory cancer cells via rapid screening.[4] There are several migratory cancer cell-based platforms suitable for HTS manner: Scratch assay[5], Cell exclusion zone assay[6], and Transmembrane assay[7]. Scratch and cell exclusion zone assay create a cell-free zone across the middle area of cell confluent monolayer and allow cells to migrate toward the cell-free zone. Migrating cells' viability and/or migratory velocity are quantified under various targeting molecules. However, both assays cannot provide physical confinement during cell migration. It

is well documented that when cells migrating in a 3D environment the surrounding matrix will provide additional friction forces that are raised from physical confinement (steric hindrance)[8]. The varying geometric confinement will influence cell morphology and motility[9]. A recent study also finds that physical confinement is the key element to address metastasis resistance.[6, 7] In this situation, Transmembrane assay would be a better assay since it allows cells to migrate through a dense extracellular matrix (ECM) and narrow (5-8µm) pores under the influence of a chemoattractant gradient. Cell viability and/or percentage of cells crossing membrane under various targeting molecules are quantified to investigate the therapeutic effect of the target molecule(s). However, difficulties in tracking the migratory cells in narrow vertical pores don't allow quantifying migration speed reduction under targeting molecules.[10] Furthermore, the single-cell-level analysis is important for discovering cancer drugs due to cancer cell's heterogeneity. However, these assays are limited to detect the average profile of the whole population rather than single-cell-level so that they fail to characterize complex cancer microenvironment.[11] Therefore, it is necessary to develop a new migratory cancer cell-based platform, which is suitable for HTS with the capability to provide physical confinement during cell migration and can carry out single-cell-level screening, for anti-metastatic cancer research.

To address this urgent need, we utilized microchannel technology to develop a single-cell-level mHTS platform that can monitor in real-time how cancer cells migrate through the spatially restricted space and how migratory inhibitors affect cancer cell's migration/viability. Currently, a microchannel device has been widely used in cancer invasion study due to its capability to present the physical interactions of cancer cells with surrounding physically complex environments.[9,12] What's more, the microchannel device provides a better way to carry out single-cell-level study since it can easily separate and control individual cell's movement and tracing cell's behavior[12].

For example, using a periodic dimensionally confined microchannel to mimic the heterogeneous microenvironment in tumor stroma can successfully simulate individual cell's motility and morphology dynamics[13]. It is also helpful to understand cancer tissue's heterogeneity via providing varying geometric confinement to separating subpopulation[9].

In this mHTS platform, we designed a new double-arced microchannel device that can provide physical confinement with migrating cancer cells and assemble into a 96-well plate. Over 100 microchannels/devices, high content imaging system and automated quantification software track the migration speed and monitor the viability of over 20,000 migrating cells/96-well plate at a single-cell-level. Glioblastoma multiforme (GBM), a common and aggressive brain tumor with rapid growth and highly diffusive infiltration, has been chosen to demonstrate the feasibility of the single-cell-level migratory HTS (mHTS) platform for determining how migratory inhibitors affect cancer cell's migration/viability. For migrating inhibition study, we chose Cytochalasin D (CytoD), a cell-permeable migration-suppressor by inhibiting actin polymerization. [14] For viability study, we chose Doxorubicin (Dox) and AZD-6244 (AZD), which are commonly used anti-cancer drugs for breast[15, 16], bladder [17, 18], and lymphocytic leukemia[19, 20].

Material and Methods

Device Design and Principle

The microfluidic device was designed to fit the wells of a 96-well plate (Falcon, EI Paso County, Co) (Fig1. A), which is an acceptable plate for the IN Cell Analyzer 6000 microscope (GE Healthcare, Pittsburgh). The outside arc of each device had a radius of 3mm, and the first microchannel was 910 µm away from the device's two edges in longitude (Fig1. B&FigS1). The extruded blank parts provided extra attachment for consolidating assimilability. Each microchannel device contained 110 channels separated 30 µm from one another. Each microchannel has designed dimensions of 8x12 µm to provide similar physical confinement as in vivo tissue tracks. Those tracks have consistently narrow dimensions (3~30µm in width)[21] (width x height) and also to minimize the influence on molecular diffusion(Fig1.C). Long channels (2.5 mm in length) (FigS1) are specifically designed to maintain a high number of migrating cells. The total thickness of each device was 2mm ± 0.5mm (Fig1.C), allowing the device to be covered by 100 µl of cell culture medium.
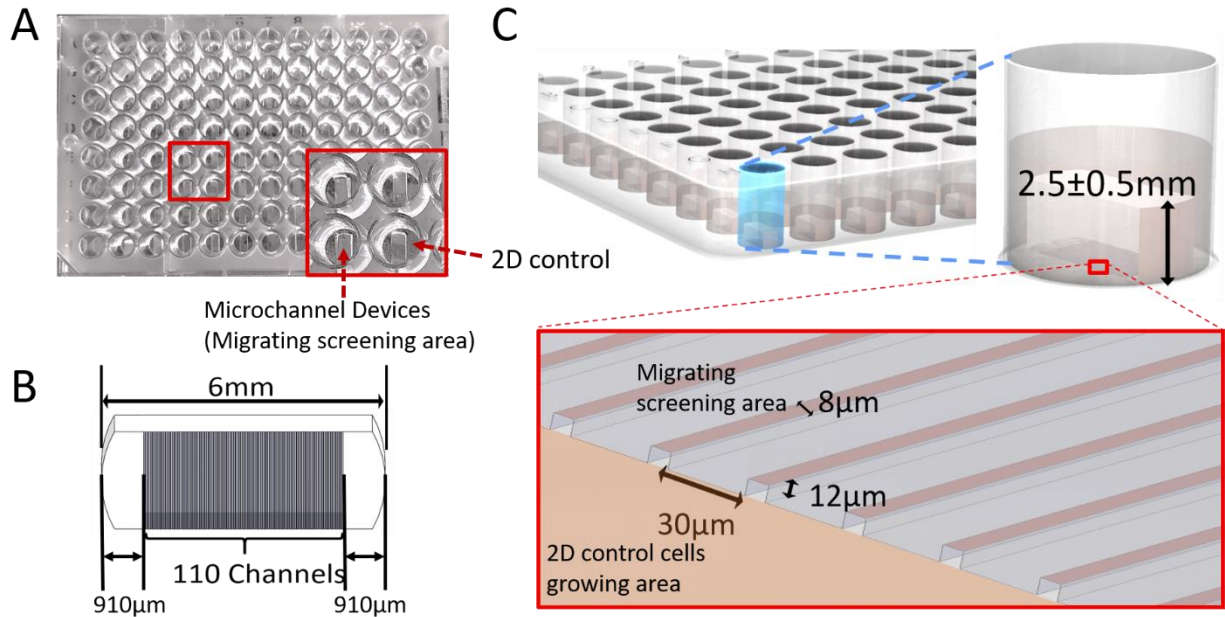
Figure 1. Screening plate with microchannel device A. Photo of a 96-well plate with microchannel devices assembled inside. The red window at the bottom is the zoom-in image. Red arrows indicate the microchannel device and the 2D control area. **B.** PDMS microchannel device. The length for each device is 6mm. The length of each channel area is 2.5 mm. Each microchannel device contains 110 separated channels and the microchannel area is 910µm from the two edges of the device. **C.** Microchannel devices were assembled to a 96-well plate with the channel side face-down. The thickness of each device is 2.5±0.5mm with 8 µm in width, 12 µm in height and the distance between every two microchannels is 30 µm (as shown in the red window). The orange part shows the 2D control cells growing area and the gray part indicates the migrating cell area.

Fabrication of Microchannel Devices

Here we used photolithography combined with soft lithography to make microchannel platforms.

Silicon wafer molds were designed by standard photolithography. First, SU8-5 (Microchem Corp, Newton, MA) was used to create photo-patterned microchannel layers with a thickness of 12 µm.

The half-round reservoir layer, 100 µm thick, was created by SU8-50 (Microchem Corp, Newton, MA) and was aligned to the microchannel layer and solidified by photo-patterning. To make the devices, polydimethylsiloxane (PDMS) (Dow Corning, Sylgard 184) was mixed with a curing agent at a ratio of 10:1 [v/v]. The mixture was then poured onto the designed wafer until the

thickness reached 2.5 ± 0.5mm. Once the PDMS solidified, the rudimentary parts of the device were punched out by a number 6 puncher (Integra, York, PA). Two half-circle reservoirs were cut along a parallel line from the channel openings to create a sizeable opening for cell seeding and drug treating. To assemble the microchannel device tightly onto the bottom of each well plate, we carried out oxygen plasma treatment to modify the surface. All devices' attaching quality was checked and controlled using a microscope before adding cells.

Cell line and Culturing

Human glioblastoma cell line G55 was provided by the University of Oklahoma and D54-EGFR was provided by the University of Texas Southwestern Medical Center at Dallas with the approval of the institutional review board. Before seeding, all cells were maintained in serum-free Dulbecco's Modified Eagle's Medium/F-12 Medium (DMEM/F-12) with 2% B-27 (Invitrogen), 0.25% Insulin-transferrin-selenium-X (Invitrogen), 25 µg/ml gentamicin, 20ng/ml human basic fibroblast growth factor (bFGF), and 20 ng/ml mouse EGFx at 37°C, 5% CO_2.

Cells were dropped to both sides of the microchannel device with a number of 15k per 10µl (equal to 1,500,000 cell/mL) in each well (5µl contains 7.5K cells dropped close to each side's opening of microchannel device) in DMEM-F12 medium with 10% fetal bovine serum [v/v] for enhancing cells' attachment to the plate bottom. Cells were put close to the channels' opening to ensure that enough cells migrated, the channels' opening in the devices (8 x 12 µm) were small enough to keep cells from traveling through while being added.

Quantification Cell Migration Speed

Cells were maintained for four days to initiate enough migrating cells. Once a high number of cells (with around 200 per device) migrated inside the microchannels, drugs or therapeutic molecules were added (Fig2). To test for the variation of migration velocity, all cells were incubated for 48h at 37°C, 5% CO_2. 2.5 µg/mL Hoechst33342, with a dilution ratio of 1:4000, was used to stain the cells' nuclei before taking images. Plates were imaged under an IN Cell Analyzer 6000 microscope (GE Healthcare, Pittsburgh) using a Nikon 20X/0.45 objective. The dye was excited with a 405nm laser. Cells were imaged every 30 minutes for 4 hours, alive while maintained at 37°C, 5% CO_2. GE Developer Toolbox 1.9.3 software was used to track nuclei. Briefly, individual nuclei were segmented and their XY positions were tracked at each time point. Pipeline Pilot 9.5 (Biovia, San Diego) was used to collate and transform the nuclear Cartesian coordinates into individual cell velocity and distances traveled, generate per well mean velocities, and classify nuclei into separate velocity subgroups for histogram calculations.
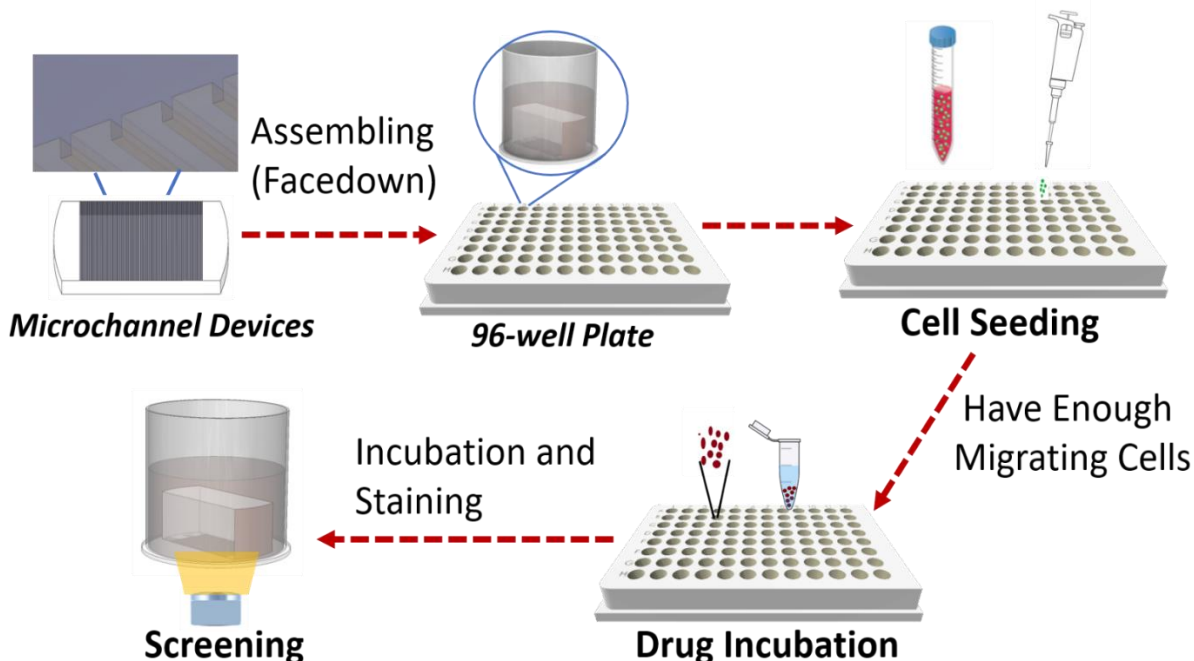
Figure 2. The single-cell-level mHTS platform for drug screening. Miniaturized microchannel units (with 8µm x 12µm; 110 microchannels) are placed on a 96-well plate. GBM cells are seeded and either grown on the 2D surface (non-migrating GBMs) or migrating via microchannels (migrating GBMs). Anti-cancer molecules non-migrating and migrating GBM cells via ECHO liquid handler. The synergistic effect of small molecules/drugs on cancer cell migration and viability is quantified by In Cell Analyzer and Cell Profiler. Hoechst stains both migrating (via microchannels) and non-migrating GBM cells.

Cell Viability Assay

Here, we compared the viability rates between non-migrating cells and migrating cells. Two 96-well plates were prepared, one with microchannel devices, one without microchannels (blank control). Four days before chemotherapeutic treatment, cells were seeded to each plate, while maintaining the same seeding number of 15k per well (1,500,000 cell/mL). After 72h of exposure to chemotherapeutic molecules, the control plate's viability rate was determined by optical density measurements at 490 nm with CellTiter 96 MTS assay (Promega, Madison, WI). Propidium iodide (PI) / Hoechst 33342 double staining was used to quantify the migrating cells' viability. The

migrating cells were stained by Hoechst 33342 (overnight) and PI (30min). Six fields of view covering the entire microchannel area were imaged using 405 nm (Hoechst 33342) and 488 (PI) lasers. Using CellProfiler 2.2.0 (Carpenter Lab, Broad Institute of Harvard and MIT), the cell number in each condition was collected and the viability rate was calculated. In both groups, 0.1% DMSO was used as the negative control. By dividing by the DMSO rate, the relative percent viability was calculated for each tested condition (3 replicated wells for each condition).

Statistical Analysis

Two groups of Z' and CV were calculated to reflect and compare robustness (bulk level Z' and CV: based on average and standard deviation from each well; single-cell-level Z' and CV: based on individual data within each subgroup). All results reported were demonstrated as mean ± standard deviation. Single-factor ANOVA was performed for multi-group comparison. The statistical difference between migrating and normal 2D culturing cells were compared by the student t-test. $p < 0.05$ was considered significantly different. Excel and GraphPad Prism 8.0.2 were used as essential tools to obtain all calculations and graphs.

Results

Screening area and collecting individually tracked migrating cell's information

To track the individual cell's migrating speed, the cell's nucleus was stained with Hoechst 33342 overnight after observing enough migrating cells (at least 3 cells in each microchannel). Using IN Cell Analyzer 6000 microscope, we took a group of 6-sites images that can cover the whole microchannel area for each screened device (Fig3.A). For anti-migration screening, images for each position were recorded every 30min for 4 hours to monitor the cell's migration behavior after incubation with different therapeutic reagents for a certain period (48hrs/72hrs, Fig3.B). By tracking stained nuclei using GE Developer Toolbox 1.9.3 software, we obtained all the segmented individual nucleus' XY position at each time point. Each cell's position at a specific time point is defined as $(X_n, Y_n)\_N$, where the time point is denoted by subscript "n", the cell number is labeled by "N" (Fig3.C). Based on coordinates change that collected within the recording period in every 30min, each cell's moved distances between two-time points is calculated as "$\sqrt{((X_{n+1}, N - X_n, N)^2 + (Y_{n+1}, N - Y_n, N)^2)}$". A sample cell's movement during certain tracking period was listed in the table (Fig3. D). Based on collected movement information we calculated two migration speed metrics (for certain cell denoted as "N"): Net migration speed (MS_{net}) = (distance $(X_{first}, Y_{first})\_N$ to $(X_{last}, Y_{last})\_N$) / ($Time_{last}$ - $Time_{first}$) ; and Total migration speed(MS_{total}) = Sum (distance $((X_1, Y_1)\_N$ to $(X_2, Y_2)\_N)$ + distance $((X_2, Y_2)\_N$ to $(X_3, Y_3)\_N)$ +...)/ ($Time_{last}$ - $Time_{first}$). The total number of the tracked individual cell for each device could up to 300 with an average of around 230.
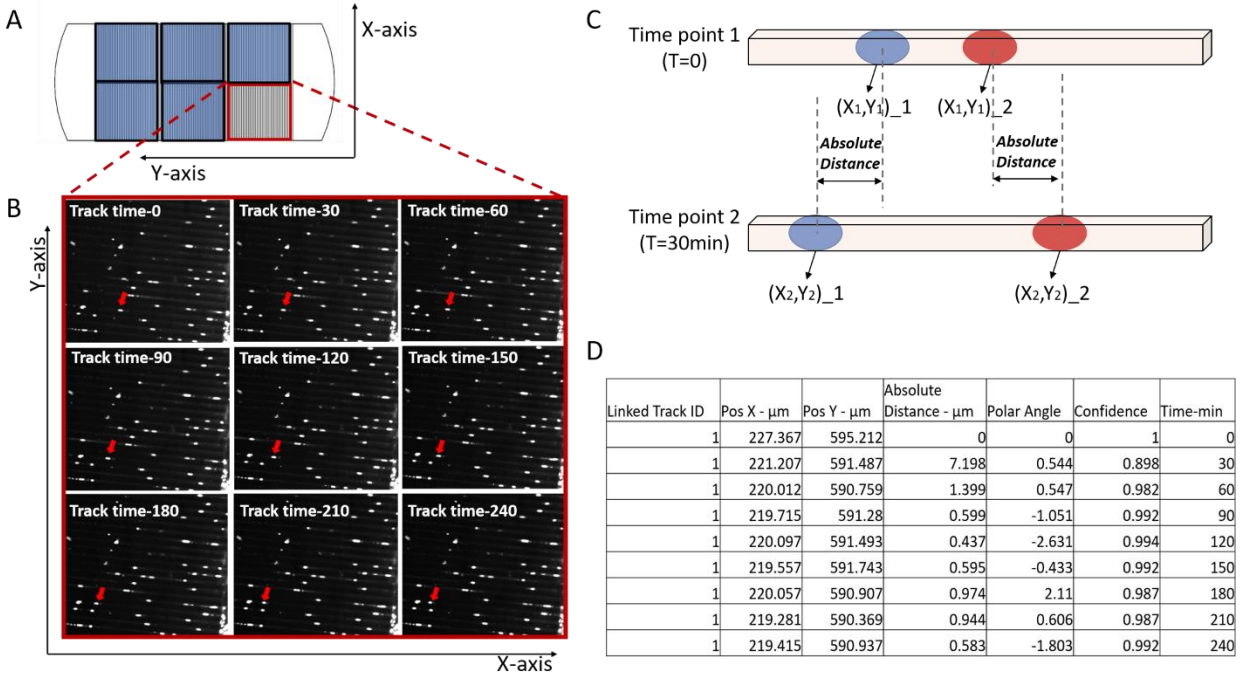
Figure 3. Single-cell-level quantification of cancer cell migration. A. A group of 6-sites images (covered the whole microchannel area) were taken each well. X- and Y-axis as labeled. **B.** Hoechst 33342 stained cells were imaged every 30 minutes for 4 hours. One of the migrating cancer cells is labeled by the red arrow. X- and Y-axis as labeled. **C.** Individual nuclei were segmented and their XY positions were tracked at each time point. The position of each tracked cell at a certain time point "n" was defined as (Xn, Yn)_N, N: tracked cell's ID. Cell moved distance was reported based on cell nuclei's coordinates. **D.** One sample cell's coordinate for once tracking period is showed in the table. Absolute distance is calculated based coordinate of a cell. The polar angle shows a cell's moving direction. Confidence number (range 0~1, highest number = 1) indicates the accuracy level of the tracking system.

Migrating inhibition related drug screening and different sensitive populations' separation

Hoechst labeled migrating G55 cells were incubated with various doses of Cytochalasin D (CytoD, 0.095μM, 0.3μM, 0.95μM, and 3μM in 0.1% DMSO, 2D cultured G55's IC50, and in-channel viability were represented in supplementary data FigS3) for 30 minutes before the screening. The drug medium was replaced by fresh cell culture medium right before tracing. Recording to the coordinating information we can easily get the cell's MS_{total} and MS_{net}. Though with some variation among individual cells, due to G55 cells' heterogeneity, both MS_{total} and MS_{net} showed a

correlative relationship with CytoD dosages (Fig4.A). Cytochalasin D, as an actin polymerization disturber, is believed to damage actin by binding to F-actin polymer and preventing the polymerization of actin monomers.[10] From our previous study, actin activity was associated with cancer cell migration and this activity was significantly increased in migrating cancer cell groups.[22] The decreasing velocity associating with increasing the CytoD concentration proved our prior observations and proved the accuracy of our screening system in an mHTS manner.

For the trial operation of migration inhibition screening, two commercialized anti-cancer drugs, Doxorubicin (Dox) and AZD-6244 (AZD), with different dosages were chosen as examples. The MS_{net} results indicated that the high dosage of AZD (500nM & 1000nM) significantly reduced G55 cell migration velocity compared to the DMSO control group (Fig4.B). To further compare drugs' effects, we grouped the MS_{total} of individual cells into 3 cohorts ('slow'≤0.2µm/min, 'fast'≥0.6µm/min, and 'medium' in between) based on cells' MS_{total} distribution. There were more slow and medium movers in 500nM (70%) and 1000nM AZD (73%) groups compared to the DMSO group and a lower percentage (only 0.6%) of fast movers were in 1000nM AZD group (Fig4.C). However, Dox showed no migration inhibition, but rather a slightly increased migration speed. When combined Dox 100nM with CytoD (300nM), G55 cell migration speed was only 63.4% of the just Dox group (Fig4.B). A low percentage of the slow mover and a high percentage of medium and fast mover was in Dox treated group. Especially in the 100nM Dox group, the percentage of fast mover was almost doubled compared to the control group (Fig4.D). Though the migration speed had a significant difference in migration speed between the Dox group and Dox + CytoD group, there was no significant difference in movers' fraction within those two groups.
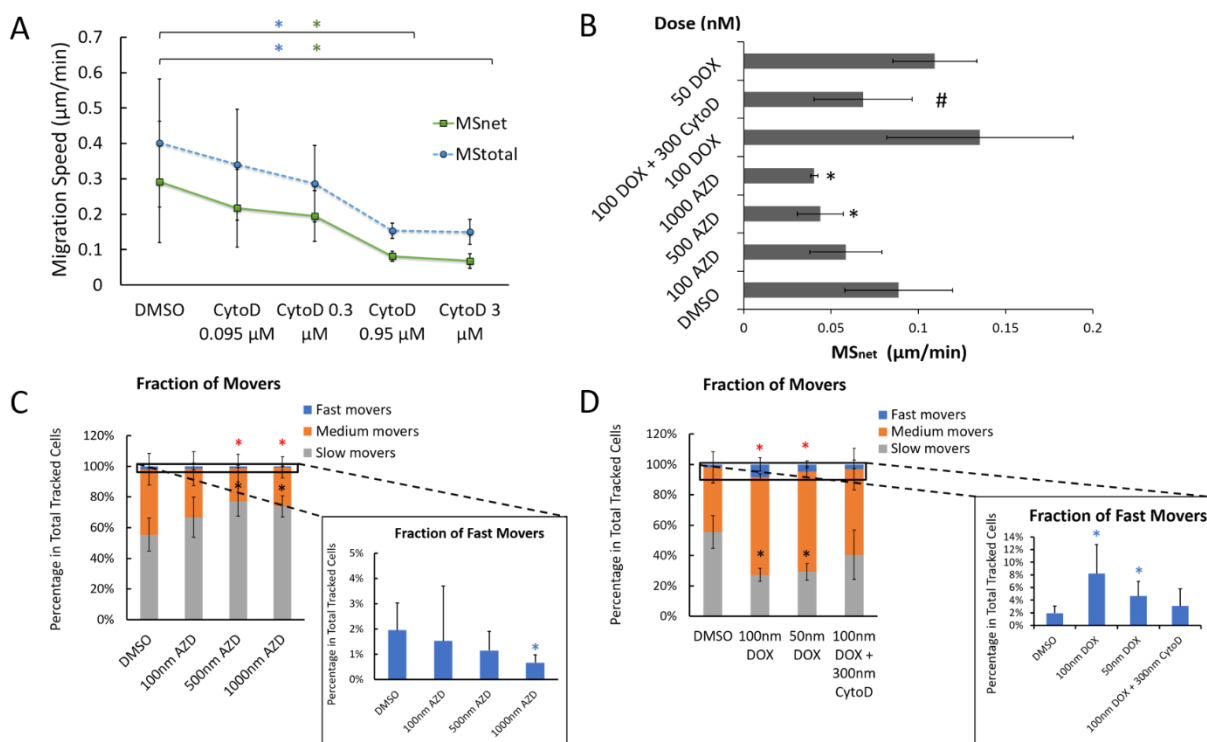
Figure 4. Quantification of the migratory inhibiting effect of drugs in a high-throughput manner. A. Cells' net migration speed (MS_{net}) and total migration speed (MS_{total}) were tracked after 30min incubation with various dosages of CytoD (0.095μM, 0.3μM, 0.95μM, and 3μM). The average MS_{net} and MS_{total} were calculated and compared with the DMSO control group (*p< 0.05). **B.** MS_{net} was compared between different drug-treated groups. Results showed as average ± SD (based on the bulk average value from each well). Total tracked cell number n≥226/each condition. *p<0.05 between DMSO control group and others; #p<0.05 between 100nM Dox and 100nM Dox+300nM CytoD group. **C.** The fraction of fast, medium and slow movers for the AZD treated group. */*/* p<0.05 between DMSO control group and others. **D.** The fraction of fast, medium and slow movers for Dox treated group. */*/* p<0.05 between DMSO control group and others.

Comparing 2D cultured and migrating cells' drug susceptivity by viability screening

Plates with/without microchannel devices with sufficient migrating/2D G55 cells were treated with DMSO (0.1%), Dox (500nM, 250nM, and 100nM) in 0.1% DMSO, and AZD (1000nM, 500nM, and 250nM) in 0.1% DMSO for 72 hours (drug uptake would not be affected by cellular morphometry in/outside microchannel based on our previous study[23]. Then live/dead staining images were taken for each device by utilizing Hoechst33342 and PI staining. Figure 5A revealed

the live/dead image for inside the microchannels and in the 2D reservoir (2D control) view. The

Dox treated 2D group had almost 20% more PI stained cells in comparison to the DMSO control

group. To quantify the viability, MTS assay and PI/Hoechst double staining screening-counting

methods were used, respectively, for the 2D control group and the migrating group. Only a high

dosage of Dox (500nM) and AZD (1000nM & 500nM) displayed similar lethality for both 2D and

migrating groups (Fig5.B). Otherwise, migrating cells inside the microchannel appeared to exhibit

significantly higher viability (20% in 250nM AZD, 30% in 250nM Dox, and 23% in 100nM Dox)

compared to 2D cells outside the microchannel. The minimal killing effects exhibited in the

migrating group for both drugs which indicated their increased resistance to chemo-treatment.
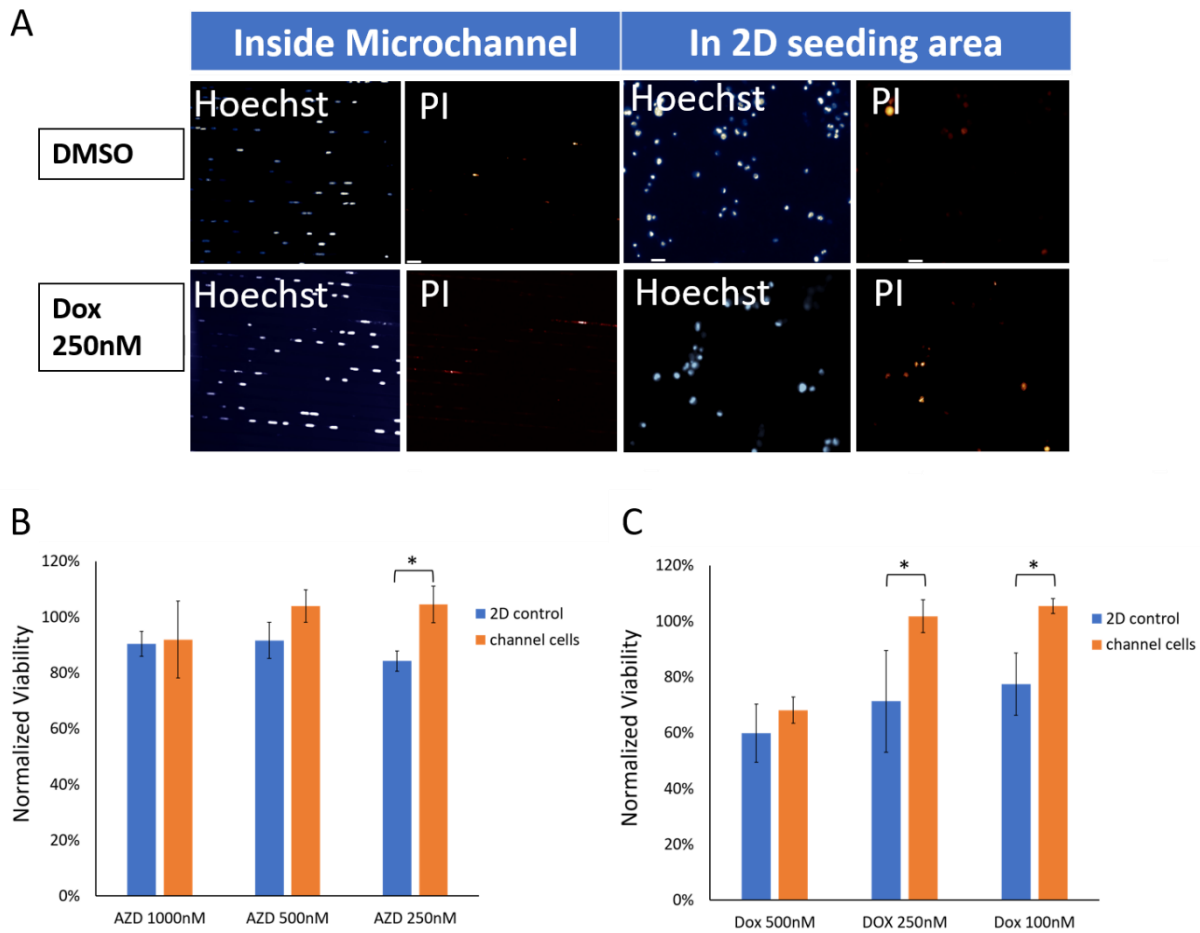
Figure 5. Viability screening was carried out to compare drug sensitivity differences between 2D cultured cells and migrating cells. A. Representative Hoechst 33342 and Propidium iodide (PI) staining images for both cells inside microchannel and 2D cells after treatment (DMSO or Dox 250nM/0.1% DMSO). Blue: Hoechst. Red: PI. Scar bar: 15μm. **B &C.** Viability rates of 2D cultured cells and confined-migrating cells after 72hours incubation with two drugs (DOX/0.1% DMSO and AZD/0.1% DMSO). PI / Hoechst 33342 double staining was used to quantify cell viability in the microchannel group and MTS quantification was used for the 2D group. In all groups, 0.1% DMSO was used as background control. Final results provided as the relative percentage by dividing the DMSO number. Results showed as average ± SD (based on the bulk average value from each well). *p<0.05.

Comparing bulk level data and subpopulation-classified single-cell-level data's performance

in heterogeneous cancer cells' HTS

Traditionally the number of Z-prime (Z', the acceptable range is 0~1) combined with the coefficient of variation (CV, the receivable number is < 20%) is used to judge whether a particular assay is suitable for a full-scale high-throughput screen.[24, 25] Z' (Eq.1) measures the statistical effect size. The CV (Eq.2) can express the precision and repeatability of an assay.[26]

$$Z' = 1 - \frac{3*(Rs+Rc)}{|\mu s - \mu c|} \quad 1$$

R_s and R_c are the standard deviations of the sample (i.e., drug-treated group) and the control (i.e., DMSO treated group). μ_s and μ_c are the means of the sample and control.

$$CV = \frac{SD_{signal}}{Mean_{signal}} \times 100 \quad 2$$

SD_{signal} is the standard deviation of the sample and $Mean_{signal}$ is the mean of the sample.

However, due to cancer cells' high heterogeneity, commonly used bulk level Z' (quantified based upon bulk measurement) might be not suitable for cancer tissue HTS. Because it is easily being influenced by cell type (heterogeneous cell line has worse Z' compared to homogenous one). Thus, firstly, to evaluate bulk level Z's reliability for cancer cells HTS, we chose the highly heterogeneous cell line G55 and more homogenous cell line D54-EGFR (based on nucleus size and drug response Fig6A-C) as two models to study the effect of cell type on Z'. Two screening plates containing the two cell lines were incubated with CytoD for 30 minutes before the screening (IC50 for both cell lines are represented in supplementary data FigS2). The mean MStotal of every well was calculated based on all tracked cells (N>60). Relative cell movements were calculated as

the percentage of DMSO control (Fig.6A&B). Three replicated wells' values were used to analyze Z' (all mean and standard deviations came from bulk average value from each well). Calculated Z' was shown in the table of Fig6D. The heterogeneous G55 group revealed a large absolute number of Z' and a significant variation of CV (0-48%). While, as expected more homogenous D54-EGFR group returned a Z' close to 0 and dosage variability CV < 20%. This is because Z' is a function of standard deviations that is sensitive to outliers. When the tested sample has high heterogeneity a large number of 'outliners' will be presented and cause the problem of Z'. In this presented study, G55, as a classic heterogeneous cell line, too many outliers in either the positive or negative group could adversely affect the Z'. However, for D54-EGFR, as more closing to homogenous, Z' was increased. All these indicated that bulk level Z' would partly depend on the cell type. So, it might be inequitable to judge this mHTS method only based on bulk level Z' and CV. Some additional simple analytic measurements that focus on heterogeneity and can be applied in a high-throughput manner are needed.

Clearly, the poor Z' showed above was mostly because of using bulk average value (Fig.6D). While if simply calculate the Z' and CV based on single-cell-level data, as expected, the Z' and CV would be even worse because of enlarging the influence caused by heterogeneity. Therefore, to meet the requirement of HTS purpose, additional pre-management for single-cell-level data is necessary. Thus, we tried to draw on the successful experience by classifying the whole cell population into several small cohorts. We repeatedly studied G55 cells' MS_{total} distribution under DMSO treatment (control condition) and separated all tracked cells into 3 different groups (slow, fast, and medium). Interestingly, we found that the percentage ratio for each subgroup almost remained the same (70% for slow movers, 25% for medium movers and 5% for fast movers), although the baseline changed a little bit. We classified Cyto D treated groups following the same

percentage ratio (top 5% as fast movers, bottom 70% as slow movers and medium movers in between) and calculated mean and standard deviation based on individual cell's MS_{total} within each subgroup (Fig.6F~H). Then we calculated Z' for each subgroup. As shown in Fig6E, Z' and CV were significantly improved for fast mover and medium mover (most Z' were >0 and all CV were <20) compared to negative Z' from the bulk average (Fig.6D). However, slow mover group's Z' were still slight negative (>-1) because the mean showed no difference from the control group. The possible reason is that the slow movers showed less sensitivity to treatment since the baseline was already too low (those cells don't move a lot natively). It needs to be pointed is that subclassification needs to be based on cell type.
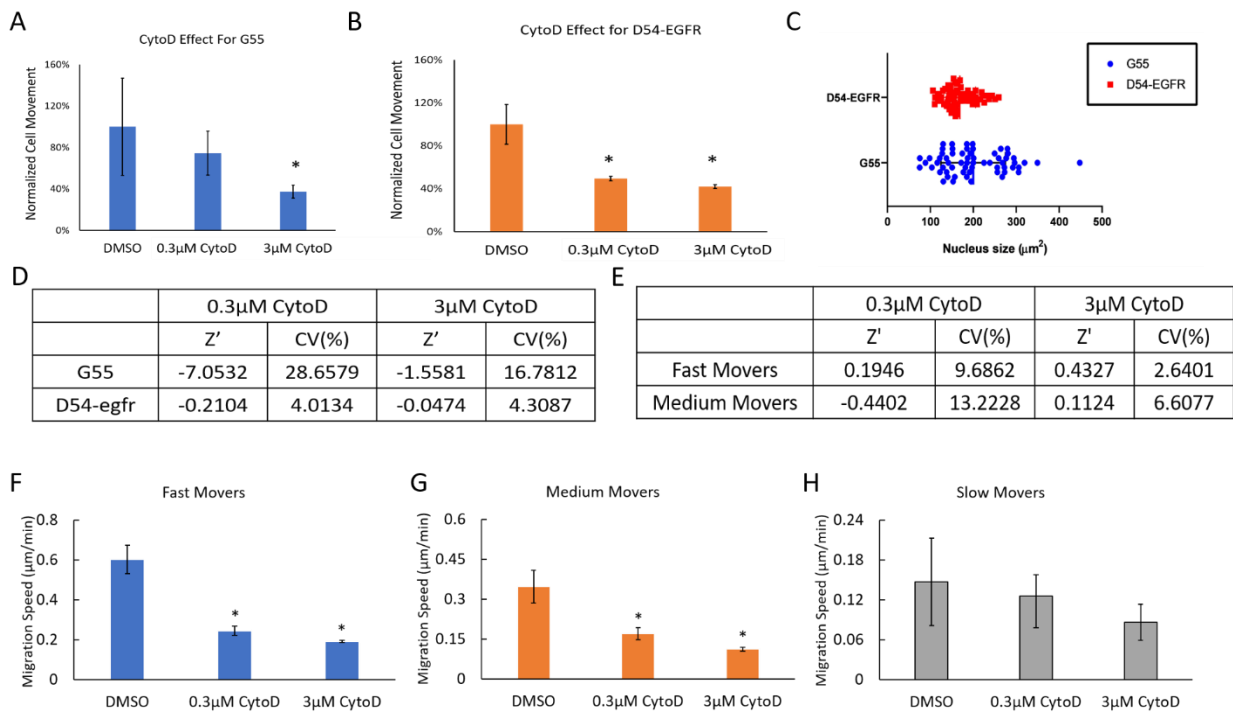
Figure 6. Subgroups pre-classification for single-cell-level data can improve mHTS's application in heterogeneous cancer cells. A.B CytoD migration inhibition for G55 and D54-EGFR. (* p<0.05 between DMSO control group and others) **C.** Nucleus size distribution for G55 and D54-EGFR. (p<0.001, n=65) **D.** Bulk level Z' and CV for migration with different drug treatments. Z' and CV were calculated based on bulk measurement for each cell line under different drug conditions and listed in the table. **E.** Single-cell-level Z' and CV for migration speed under different drug treatments. Z' factor and CV were calculated based on individual data for each

subgroup. **F~H.** Fast, medium and slow movers' MS_{total} for CytoD treated G55 cells. Results showed as average $\pm$ SD (based on single-cell-level data under each condition). (* $p<0.05$ between DMSO control group and others, n>30 for all subgroups)

Discussion

GBM invasion is characterized by rapid proliferation and the ability to migrate as individual cells.[27, 28] For the past decades, research on mechanisms of GBM migration and invasion have relied on the use of the standard in vitro cell migration assays (i.e., Scratch and Boyden chamber assays).[29] Whereas, mechanistic insights from these studies are limited. None of these models can accurately represent the locomotion of cancer cells through the brain parenchyma under physical confinement, which is believed to increase cancer cell's therapeutic resistance, let alone combine with high-throughput screening. Hence, our group developed a novel ex vivo, integrated microchannel platform that is suitable for a single-cell-level mHTS. This method is based on automated high content imaging and drug loading system. With the help of this system, we aim to develop an innovative assay to identify therapeutic molecules that effectively block cancer cell migration, resulting in the transformation of a diffusive tumor into a local aggregated tumor and/or eradicate the treatment-resistant migrating GBM cells.

First, we reported the design detail of our novel microchannel platform and its capability of holding sufficient migrating cells. The overall size of the PDMS device was designed to fit a 96-well plate which is the most commonly used platform for HTS. The extra attachment area and the homogenous length of the microchannels were successfully standardized. 110 2.5mm long microchannels are capable to maintain a high number of migrating cells (around 250/device) under physical confinement. 2mm thickness of the device allows it to be loaded with the drug by ECHO

automatically. Then, using Hoechst 33342 staining we were able to locate individual cells. Combined utilization of IN Cell Analyzer 6000 microscope and GE Developer Toolbox 1.9.3 software helped us to track every single cell's XY position at each time point and generated migration speed data according to position change during the screening period. Here, with our tracking system, we can not only generate net migration speed (MS_{net} = (distance (X_{first},Yfirst)_N to (X_{last}, Y_{last})_N) / ($Time_{last}$-$Time_{first}$)) but also generate total migration speed (MS_{total} = Sum (distance ((X_1,Y_1)_N to (X_2,Y_2)_N) + distance ((X_2,Y_2)_N to (X_3,Y_3)_N) +...)/ ($Time_{last}$ - $Time_{first}$)). For those commonly used migration analysis techniques, though with help of well-developed computer tracing software, it is still difficult to monitor cells' MStotal, which indicates the real migrating activity, due to the cell's random motion trails.[30] However, our microchannel system limits the cell's motion trails (almost fixed Y position) while providing suitable physical confinement during migrating. It will reduce tracking difficulty and computation. The CytoD migration inhibition results provided evidence of the feasibility of this semi-automatic system. Besides, with the help of Pipeline Pilot 9.5, we collated the nuclear Cartesian coordinates per cell velocity and was able to classify cells into separate velocity subgroups for histogram calculations. There is increasing evidence that cancer tissue has its heterogeneity with distinct genotypes and phenotypes of cells having divergent biological behaviors.[31] Separating cells into subgroups based on cells' migration activity and studying their different responses to treatment will give us a better understanding of tumor heterogeneity and its relevance to cancer therapeutic resistance.[31, 32] In this presented study, we utilized Dox[33] and AZD[34] as demonstration drugs and successfully studied their migration inhibition effects on heterogeneous GBM (G55). We found a high dosage of AZD (500nM and 1000nM) provided reliable migration inhibition with an increased percentage of slow movers and decreased the percentage of fast movers. On the contrary, Dox had no inhibition of

migration and even could speed migration to a certain extent and increase the percentage of fast movers. While, when combined with CytoD, this effect could be minimized. Cytochalasin D's migration inhibition is due to preventing the polymerization of actin monomer and binding to F-actin polymer[14]. The results of this study showed that the combination of Dox and CytoD could minimize migration up-regulation effects, compared to simply using Dox. This finding has provided a potential combination of chemotherapeutic agents to improve GBM curability by reducing metastasis.

Besides, Hoechst/PI double staining enabled this system to carry out viability screening as well. Using free CellProfiler software the total cell number (Hoechst stain) and dead cell number (PI stain) were easily collected. Migrating cells have demonstrated the unique up-regulation of chemoresistance[35]. Screening the viability of cancer cells during confined-migration provides a more accurate model for specific drug selection. Viability difference between the 2D group and the migrating group when treated with different dosages of Dox and AZD substantiated the increased resistance of confined-migrating cells and proved the value of our mHTS system in anti-cancer study. The high viability of migrating cells proved the migration inhibition of AZD was not due to killing effects. Also, drug diffusion efficiency inside microchannel was tested by using autofluorescent Doxorubicin hydrochloride as a demonstrational molecule (supplementary data FigS2). No significant evidence indicated that migration speed and viability differences were due to the location of cancer cells inside the device. Furthermore, if necessary, we can also combine migrating screening and viability screening to study different velocity subgroups' chemotherapeutic sensitivities.

By comparing bulk level Z' between G55 (heterogeneous) and D54-EGFR (homogenous), we proved Z' based on bulk data has its limitation to judge the robustness of an HTS assay which is based on cancer tissue screening. Though statistical parameter - Z' is commonly used[36], it is significantly influenced by screening cell line's heterogeneity. However, the phenotypic and functional heterogeneity is one of the most important natures for tumors that mainly caused by genetic change, environmental differences and reversible changes in cell properties.[37] Therefore, the capability of carrying out single-cell-level is more important for cancer study. To applicate this single-cell-level screening method in HTS manner, we tried to classify the whole population into subgroups and then get single-cell-level Z' for each subpopulation. As expected, Z' had been improved. This proved that our mHTS platform is a successful trial to combine single-cell-level analysis and HTS and can be applied to heterogeneous cancer cells.

Conclusion

Our cell-based microchannel platform with individually addressable channels can separate confined-migrating cells to provide a single-cell-level analysis. The attempt of our microchannel platform revealed the possibility of single-cell-level mHTS, especially in migrating-inhibition related drug development for migratory cancer. The heterogeneity of cancer cells points out the necessity of combing single-cell-level study and high-throughput screening. Designing an efficient way to group heterogeneous cancer cells into subpopulations and provide more accuracy and robust analysis would be the next stage of cancer HTS study.

Acknowledgments

References

1. Bondy M L, Scheurer M E, Malmer B, Barnholtz-Sloan J S, Davis F G, Il'yasova D, Kruchko C, McCarthy B J, Rajaraman P, Schwartzbaum J A, Sadetzki S, Schlehofer B, Tihan T, Wiemels J L, Wrensch M, Buffler P A and Brain Tumor Epidemiology C 2008 Brain tumor epidemiology: consensus from the Brain Tumor Epidemiology Consortium *Cancer* **113** 1953-68
2. Giese A, Bjerkvig R, Berens M E and Westphal M 2003 Cost of migration: invasion of malignant gliomas and implications for treatment *J Clin Oncol* **21** 1624-36
3. Wells A, Grahovac J, Wheeler S, Ma B and Lauffenburger D 2013 Targeting tumor cell motility as a strategy against invasion and metastasis *Trends in pharmacological sciences* **34** 283-9
4. Szymański P, Markowicz M and Mikiciuk-Olasik E 2012 Adaptation of high-throughput screening in drug discovery—toxicological screening tests *International journal of molecular sciences* **13** 427-52
5. Gough W, Hulkower K I, Lynch R, McGlynn P, Uhlik M, Yan L and Lee J A 2011 A quantitative, facile, and high-throughput image-based cell migration method is a robust alternative to the scratch assay *J Biomol Screen* **16** 155-63
6. Kramer N, Walzl A, Unger C, Rosner M, Krupitza G, Hengstschläger M and Dolznig H 2013 In vitro cell migration and invasion assays *Mutation Research/Reviews in Mutation Research* **752** 10-24
7. Hulkower K I and Herber R L 2011 Cell migration and invasion assays as tools for drug discovery *Pharmaceutics* **3** 107-24
8. Lautscham L A, Kämmerer C, Lange J R, Kolb T, Mark C, Schilling A, Strissel P L, Strick R, Gluth C and Rowat A C 2015 Migration in confined 3D environments is determined by a combination of adhesiveness, nuclear volume, contractility, and cell stiffness *Biophys J* **109** 900-13
9. Tong Z, Balzer E M, Dallas M R, Hung W-C, Stebe K J and Konstantopoulos K 2012 Chemotaxis of cell populations through confined spaces at single-cell resolution *PloS one* **7**
10. Marshall J 2011 *Cell Migration*: Springer) pp 97-110

11. Saadatpour A, Lai S, Guo G and Yuan G-C 2015 Single-cell analysis in cancer genomics *Trends in Genetics* **31** 576-86

12. Mak M and Erickson D 2014 Mechanical decision trees for investigating and modulating single-cell cancer invasion dynamics *Lab on a Chip* **14** 964-71

13. Mak M, Reinhart-King C A and Erickson D 2013 Elucidating mechanical transition effects of invading cancer cells with a subnucleus-scaled microfluidic serial dimensional modulation device *Lab on a Chip* **13** 340-8

14. Schliwa M 1982 Action of cytochalasin D on cytoskeletal networks *The Journal of cell biology* **92** 79-91

15. Di Cosimo S and Baselga J 2008 Targeted therapies in breast cancer: where are we now? *European Journal of Cancer* **44** 2781-90

16. Kovalchuk O, Filkowski J, Meservy J, Ilnytskyy Y, Tryndyak V P, Vasyl'F C and Pogribny I P 2008 Involvement of microRNA-451 in resistance of the MCF-7 breast cancer cells to chemotherapeutic drug doxorubicin *Molecular cancer therapeutics* **7** 2152-9

17. Leakakos T, Ji C, Lawson G, Peterson C and Goodwin S 2003 Intravesical administration of doxorubicin to swine bladder using magnetically targeted carriers *Cancer chemotherapy and pharmacology* **51** 445-50

18. Nikpour M, Emadi-Baygi M, Fischer U, Niegisch G, Schulz W A and Nikpour P MTDH/AEG-1 contributes to central features of the neoplastic phenotype in bladder cancer. Elsevier) pp 670-7

19. Kolb E A, Gorlick R, Houghton P J, Morton C L, Neale G, Keir S T, Carol H, Lock R, Phelps D and Kang M H 2010 Initial testing (stage 1) of AZD6244 (ARRY‑142886) by the pediatric preclinical testing program *Pediatric blood & cancer* **55** 668-77

20. Muller C, Chatelut E, Gualano V, De Forni M, Huguet F, Attal M, Canal P and Laurent G 1993 Cellular pharmacokinetics of doxorubicin in patients with chronic lymphocytic leukemia: comparison of bolus administration and continuous infusion *Cancer chemotherapy and pharmacology* **32** 379-84

21. Paul C D, Mistriotis P and Konstantopoulos K 2017 Cancer cell motility: lessons from migration in confined spaces *Nature Reviews Cancer* **17** 131

22. Bui L S Q, Hill T, et al. 2018 Microchannel Device for Proteomic Analysis of Migrating Cancer Cells *Biomedical Physics & Engineering Express*

23. Bui L, Bhuiyan S H, Hendrick A, Chuong C J and Kim Y T 2017 Role of key genetic mutations on increasing migration of brain cancer cells through confinement *Biomed Microdevices* **19**

24. Zhang J-H, Chung T D Y and Oldenburg K R 1999 A simple statistical parameter for use in evaluation and validation of high throughput screening assays *J Biomol Screen* **4** 67-73

25. Sui Y and Wu Z 2007 Alternative statistical parameter for high-throughput screening assay quality assessment *J Biomol Screen* **12** 229-34

26. Abdi H 2010 Coefficient of variation *Encyclopedia of research design* **1** 169-71

27. Holland E C 2000 Glioblastoma multiforme: the terminator *Proceedings of the National Academy of Sciences* **97** 6242-4

28. Møller H G, Rasmussen A P, Andersen H H, Johnsen K B, Henriksen M and Duroux M 2013 A systematic review of microRNA in glioblastoma multiforme: micro-modulators in the mesenchymal mode of migration and invasion *Molecular neurobiology* **47** 131-44

29. Able Jr R A, Dudu V and Vazquez M 2011 Migration and invasion of brain tumors

30. Jiang X, Bruzewicz D A, Wong A P, Piel M and Whitesides G M 2005 Directing cell migration with asymmetric micropatterns *Proceedings of the National Academy of Sciences* **102** 975-8

31. Fisher R, Pusztai L and Swanton C 2013 Cancer heterogeneity: implications for targeted therapeutics *British journal of cancer* **108** 479

32. Meacham C E and Morrison S J 2013 Tumour heterogeneity and cancer cell plasticity *Nature* **501** 328

33. Pérez-Arnaiz C, Busto N, Leal J M and García B 2014 New insights into the mechanism of the DNA/doxorubicin interaction *The Journal of Physical Chemistry B* **118** 1288-95

34. H Tan F, L Putoczki T, S Stylli S and B Luwor R 2014 The role of STAT3 signaling in mediating tumor resistance to cancer therapy *Current drug targets* **15** 1341-53

35. Lefranc F, Brotchi J and Kiss R 2005 Possible future issues in the treatment of glioblastomas: special emphasis on cell migration and the resistance of migrating glioblastoma cells to apoptosis *Journal of clinical oncology* **23** 2411-22

36. An W F and Tolliday N 2010 Cell-based assays for high-throughput screening *Molecular biotechnology* **45** 180-6

37. Marusyk A, Almendro V and Polyak K 2012 Intra-tumour heterogeneity: a looking glass for cancer? *Nature Reviews Cancer* **12** 32

Supplementary Material

Supplementary Methods

Microchannel Device Design and Assembling

To make our device appropriate for a 96-well plate, the outside arc for each device was 6mm (FigS1. A). It just met the well size of a 96-well plate. The length of every microchannel was 2.5mm and the total number of channels was 110. The long channel size and the high number of channel arrays were aimed to hold sufficient migrating cells for analysis. When assembled to the 96-well plate, all devices' quality and assembling conditions were controlled by checking under a microscope before the cell culturing step. According to microchannels' color change (FigS1. B), we could maintain the channel's liquid-tight sealing property.
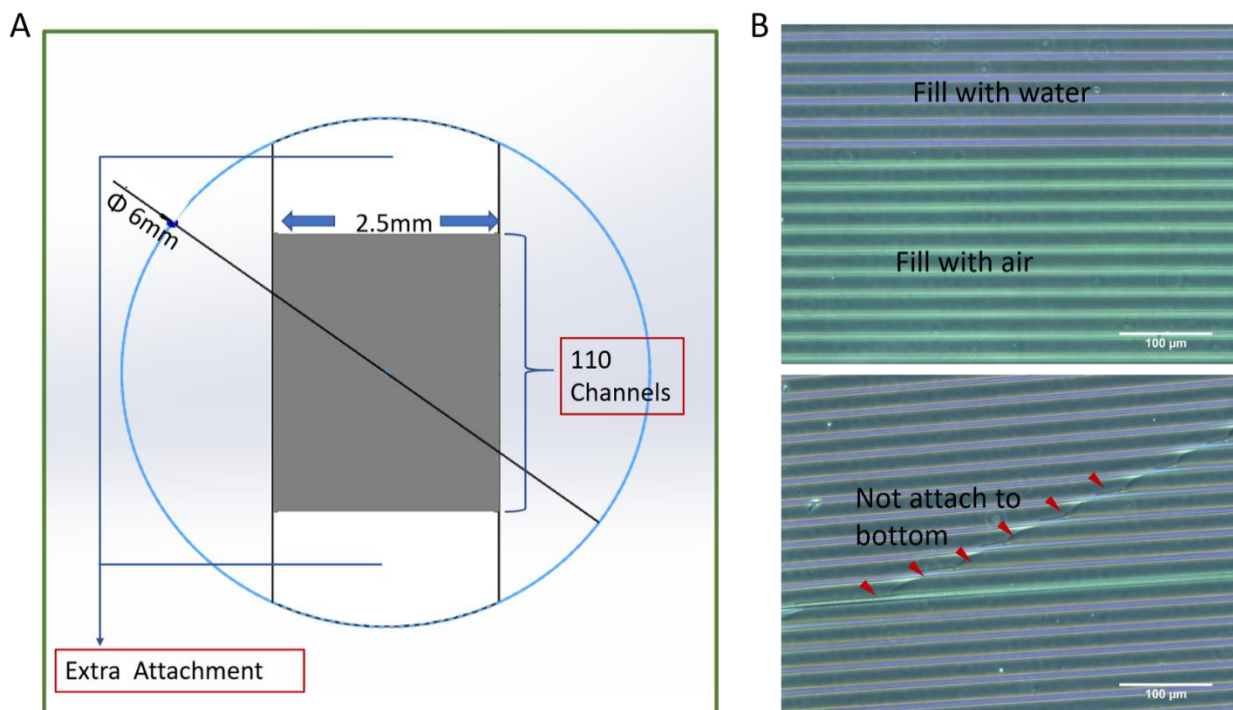
FigS1. Microchannel Device Design and Assembling A. The outside arc for each device had diameter of 6mm. The length of all channels was 2.5 mm. Both ends had extra an attachment area to enhance assembling (as indicated by arrow). Each microchannel device contained 110 separate microchannels. **B.** Microchannels were assembled to 96-well plate and attachment quality was controlled based on microchannel's color change. Top window shows microchannels' color difference between filled with water (pink) and filled with air (light blue). Bottom window shows peeling curve observed in non-sealing microchannels (labeled by red arrowhead).

Dox Diffusing and Uptake

Doxorubicin hydrochloride (DoxH, M.Wt:580, Sigma Aldrich) because of its autofluorescence was chosen as the demon drug. After enough G55 cells migrating inside the microchannel, 8μM (this concentration can ensure the signal is detectable) DoxH was added to plate and all plates were incubated for 30min. All wells were washed with fresh image medium right before taking the image. Fluorescent images were taken with excitation as 470 nm and emission as 595 nm. The intensity of the cell was measured by ImageJ.

CytoD 30min Incubation Viability Test

For the IC50 test, G55 and D54-EGFR cells were seeded to 96-well plate with seeding number as 5000 per well. Incubated cells overnight at 37°C, 5% CO2. Plates were treated with Cytochalasin D (CytoD, 0.001mM, 0.01mM, 0.1mM, 1mM, 10mM and 100mM in 0.1% DMSO) for 30 minutes. Cells' viabilities were checked by MTS assay. IC50 for both cell lines was calculated based on logistic function.

For the in-channel viability test, G55 cells were seeded 5 days before the test in a density of 15,000 per well. After 30min's CytoD incubation (0.095μM, 0.3μM, 0.95μM and 3μM) Hoechst/PI double staining was used to compare viability.

Supplementary Results

Dox Intensity of Migrating Cells at Different Locations

To observe drug diffuse efficiency we utilized autofluorescent drug Doxorubicin hydrochloride (DoxH, M.Wt:580) which has the highest molecular weight among all those tested drugs (Temozolomide M.Wt: 194; Cytochalasin D M.Wt: 507.63) in our study. After 30min incubation we compared intensity between cells at microchannel opening (within 0.2mm from both entrances) and middle area (≥1mm away from both entrances), no significant difference had been observed (FigS2). That provided the evidence to prove minimum influence has been addressed from diffusing issues and uptake imparity. However, it was difficult to including 2D ones into the comparation due to the PDMS roof may influence the intensity measurement. But according to our previous study, even cells under higher physical confinements (5 X 5 µm) the drug diffusive influx

can saturate the whole cell as quickly as 2 minutes[1]. Therefore, drug uptake will not be influenced a lot by the cell's location.
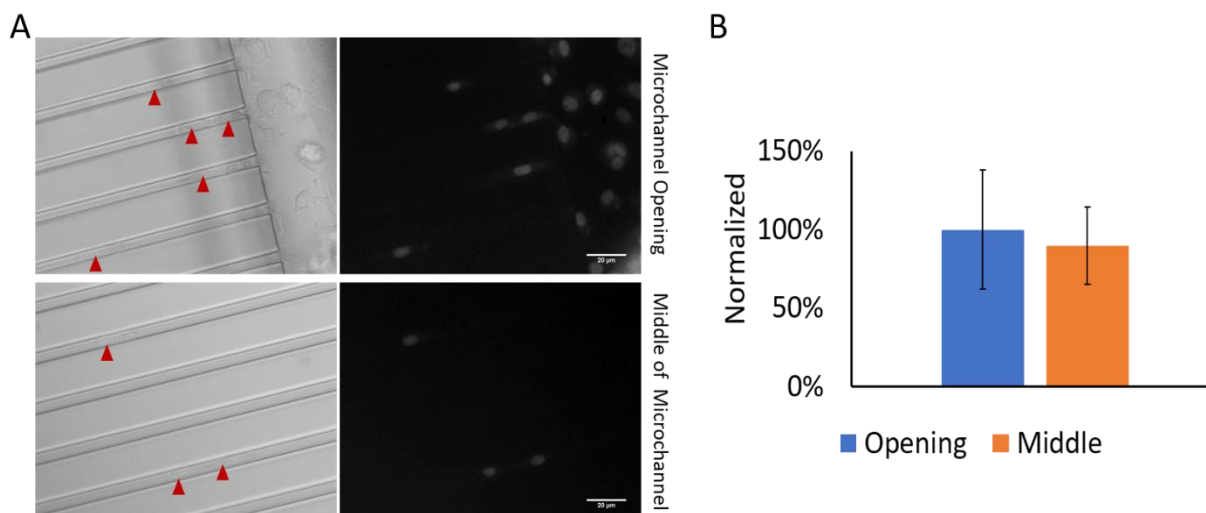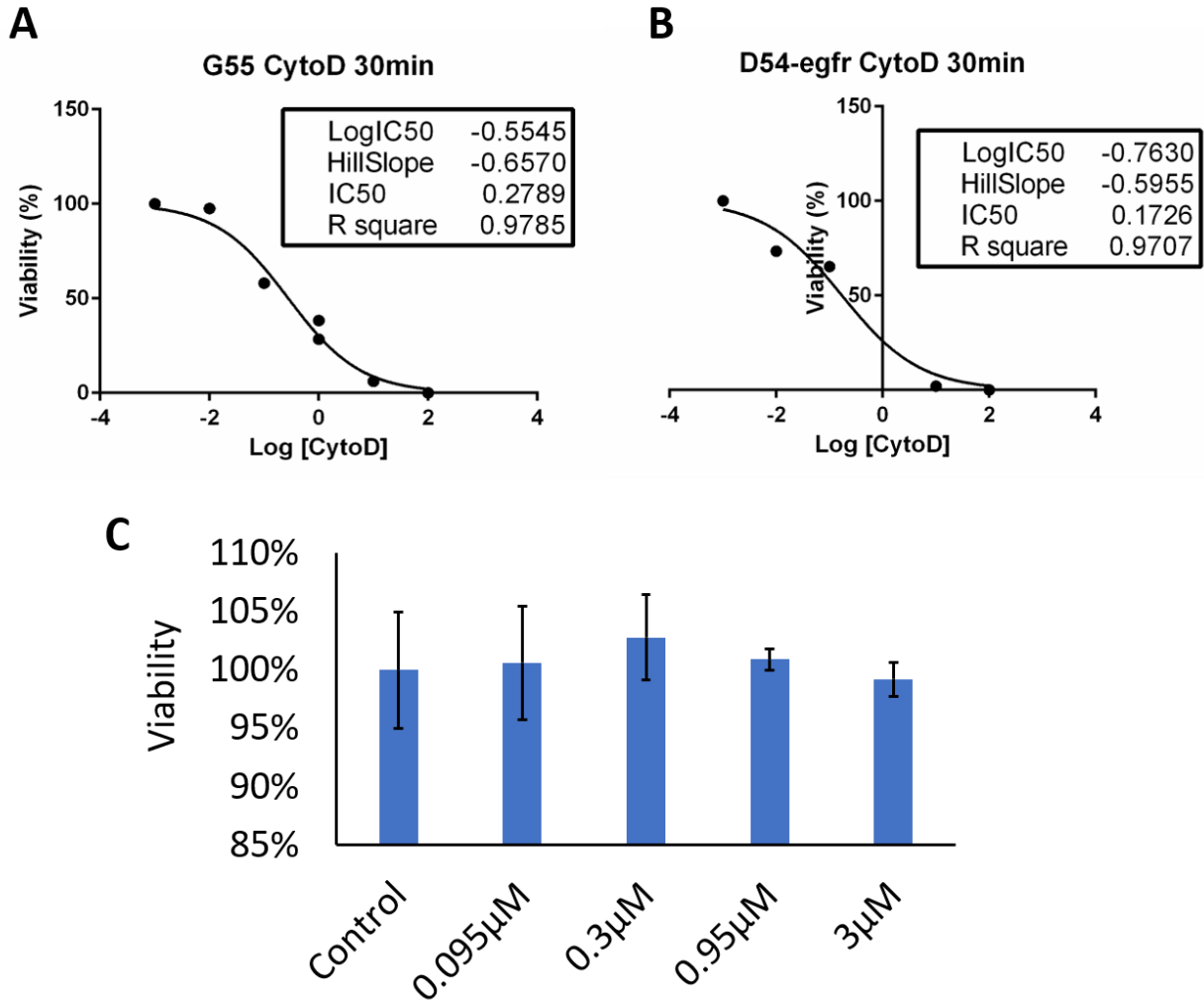

FigS2. Dox intensity was not significant different at opening and middle of microchannel. A. Representative DoxH image of cancer cells at different location of microchannel (opening (within 0.2mm from both entrances): top two; middle (≥1mm away from both entrances): bottom two). Left column are bright view images, right column are DoxH images. **B.** DoxH intensity of G55 cells at opening and middle. Data are normalized to opening cells' intensity. Average ± standard deviation. N≥50.

CytoD IC50 and In-channel Viability

CytoD 30min incubation's IC50 for G55 and D54-EGFR were tested by MTS assay. For G55 cells IC50 was around 0.2789mM and D54-egfr's IC50 was about 0.1726mM (FigS3 A & B). The in-channel viability was carried out by Hoechst/PI double staining and counting method. No significant killing effect was observed in all groups (FigS3 C).

A G55 CytoD 30min

LogIC50	-0.5545
HillSlope	-0.6570
IC50	0.2789
R square	0.9785

B D54-egfr CytoD 30min

LogIC50	-0.7630
HillSlope	-0.5955
IC50	0.1726
R square	0.9707

C

FigS3. IC50 for CytoD 30min Incubation. A. G55 cells treated for various doses of CytoD 30min and IC50 was around 0.2789mM. **B.** D54-egfr cells CytoD 30min IC50 was around 0.1726mM. N=3 per group. **C.** G55 cells in-channel viability. Data were normalized by DMSO control. Average ± standard deviation. N=3 per group.

References

1. Bui, Loan, et al. "Brain tumor genetic modification yields increased resistance to paclitaxel in physical confinement." *Scientific reports* 6 (2016): 26134.

Chapter 4. Summary and Future Works

The natural microenvironment of an organism is a complex three-dimensional structure[1]. Cells live inside the ECM need to make contact with surrounding components[2,3]. Therefore, they need to respond to various physical stimuli (e.g., matrix dimensionality and mechanical properties) and convert these extracellular physical signals into intracellular biochemical activity[4,5]. This process is known as mechanotransduction[6]. It is becoming increasingly apparent that physical cues within the cell's microenvironment directly impact tumor cell adhesion and migration during metastatic cascade and are also involved in therapeutic resistance. For example, gliomas notoriously invading and developing drug resistance after migrating to adjacent brain tissue is one of the biggest challenges for clinical treatment[7,8]. Therefore, stopping confined migration or break confined-migration triggered therapeutic resistance is an impotent component in developing modem anticancer strategies. To design a suitable platform for carrying out the confined-migration study is urgent. Because physical topography and confinement are necessary to induce a response of cells that is similar to the real microenvironment[9]. Also, due to its lack of reproducibility and complexity of performing, *in vivo* models are not widely used in cancer cell migration studies[10]. Hence, more bio-engineered platforms are applicable in this area. All projects presented here is aiming to applicate microchannel technology in cancer confined-migration study. By figure out how tumor cells integrate multiple physical cues simultaneously and respond accordingly, we attempt to understand the link between confined-migration and its triggered therapeutic resistance. On top of that, we try to search the potential value of the microchannel platform in an anticancer study.

In Chapter 1, we used different PDMS-based microchannel platforms to carry out detailed protein analysis and treatment response tests on several common cancer types. Based on those studies we reported that physically tight confinement during cancer cell migration could trigger therapeutic resistance and induce cancer stem cell-like behavior including up-regulation in efflux proteins and in cancer stem cell-related markers. We are the first group that focuses on the relationship between confined pressure and interaction from the surrounding environment during migration and tumor cells' up-regulated therapeutic resistance and the production of cancer stem cell-like features. Utilizing the microchannel device and forcing cells to migrate through physical confinement provides a potential new avenue for obtaining multifactorial therapeutic resistant cancer cells (having increased drug efflux and CSC-like behavior). This technique can be harnessed in the development of new anticancer treatments, specifically targeting metastatic, therapy-resistant cancer. Since a large number of PDMS-based devices are needed for every single experiment. The efficiency of the technology still needs to be improved. A new platform with high efficiency and low cost is needed for further investigation.

In Chapter 2, we created three conditional cell groups via three commonly used techniques: 1) migrating without confined impute via scratch assay; 2) receiving confined impute but with very limited migrating space by trans-well assay; 3) migrating under confinement via microchannel assay. Based on comparison among those three cell populations in both protein expression and chemotherapy sensitivity proves, we concluded that maintaining a certain distance of migration and receiving physical confinement during the migration period are two indispensables in triggering metastasis depended on therapeutic resistance. From another point of view, we proved the microchannel technique's unique value in cancer study especially in the metastatic cancer filed. However, since we only used highly malignant glioblastoma cell (G55) as the main test model, the

results right now had its limitation. In order to improve its broad significance additional tests on other tumor cells with different degree of malignancy is needed for further investigation.

In Chapter 3, we are the first group to try to carry out a confined-migration study in a high-throughput (HT) manner by using microchannel devices. We created a novel mHTS platform: single-cell-level high-throughput drug screening for targeting migratory cancer cells by using our own-designed microchannel devices. This mHTS platform can carry out both migration tracking and drug sensitivity test. Also, this platform is suitable for single-cell-level screening. It is well known that heterogeneity is one of the most important nature for tumors[11,12]. Therefore, combining single-cell-level study and HTS together is necessary for the next stage of cancer study. Out mHTS platform is a successful trial to combine single-cell-level analysis and HTS together and applicate on heterogeneous cancer cells. However, though we tried to use the subpopulation-classification method to improve this method's precision and repeatability in the HTS manner, the Z' number still hasn't reached an ideal value. The future work for this project is to design a more efficient classification method to group heterogeneous cancer cells into subpopulations and provide more accuracy and robust analysis. Besides, it is important to test this platform's feasibility of other cancer types.

Microchannel technology is a valuable tool in cancer study because of its capability to mimic distinct properties of the *in vivo* situation[13]. What's more, they can provide new perspectives on how tumor cells integrate multiple physical cues simultaneously and respond accordingly, because of their unique properties (e.g. easily to control mechanical stimulus in order to mimic mechanotransduction at various stages of the metastatic cascade)[14-16]. With the help of those engineered devices, we can carry out various targeted studies and filtrate different physical stimuli'

influence on tumor cell's behavior[17-19]. Then target signaling pathways involved in tumor cell mechanosensing of physical stimuli to find an efficient therapeutic strategy. Besides, its multiformity provides the possibility of application in modem cancer research such as HTS. It is no doubt that microchannel technology will have its new position and value in today's cancer research area.

Reference:

1   Bissell, M. J. *et al.* Tissue structure, nuclear organization, and gene expression in normal and malignant breast. *Cancer research* **59**, 1757s-1764s (1999).
2   Lynch, C. C. & Matrisian, L. M. Matrix metalloproteinases in tumor–host cell communication. *Differentiation: REVIEW* **70**, 561-573 (2002).
3   Even-Ram, S. & Yamada, K. M. Cell migration in 3D matrix. *Current opinion in cell biology* **17**, 524-532 (2005).
4   Uzieliene, I., Bernotas, P., Mobasheri, A. & Bernotiene, E. The role of physical stimuli on calcium channels in chondrogenic differentiation of mesenchymal stem cells. *International journal of molecular sciences* **19**, 2998 (2018).
5   Guilak, F. *et al.* Control of stem cell fate by physical interactions with the extracellular matrix. *Cell stem cell* **5**, 17-26 (2009).
6   Orr, A. W., Helmke, B. P., Blackman, B. R. & Schwartz, M. A. Mechanisms of mechanotransduction. *Developmental cell* **10**, 11-20 (2006).
7   Liu, C.-A. *et al.* Migration/invasion of malignant gliomas and implications for therapeutic treatment. *International journal of molecular sciences* **19**, 1115 (2018).
8   Viapiano, M. S. & Lawler, S. E. in *CNS Cancer*   1219-1252 (Springer, 2009).
9   Barthes, J. *et al.* Cell microenvironment engineering and monitoring for tissue engineering and regenerative medicine: the recent advances. *BioMed research international* **2014** (2014).
10   Hickman, J. A. *et al.* Three‑dimensional models of cancer for pharmacology and cancer cell biology: capturing tumor complexity in vitro/ex vivo. *Biotechnology journal* **9**, 1115-1128 (2014).
11   Marusyk, A. & Polyak, K. Tumor heterogeneity: causes and consequences. *Biochimica et Biophysica Acta (BBA)-Reviews on Cancer* **1805**, 105-117 (2010).
12   Alizadeh, A. A. *et al.* Toward understanding and exploiting tumor heterogeneity. *Nature medicine* **21**, 846 (2015).
13   Sung, K. E. & Beebe, D. J. Microfluidic 3D models of cancer. *Advanced drug delivery reviews* **79**, 68-78 (2014).
14   Xu, X., Farach-Carson, M. C. & Jia, X. Three-dimensional in vitro tumor models for cancer research and drug evaluation. *Biotechnology advances* **32**, 1256-1268 (2014).

15   (!!! INVALID CITATION !!!).

16   Boussommier-Calleja, A., Li, R., Chen, M. B., Wong, S. C. & Kamm, R. D. Microfluidics: a new tool for modeling cancer–immune interactions. *Trends in cancer* **2**, 6-19 (2016).

17   Stroka, K. M. & Konstantopoulos, K. Physical biology in cancer. 4. Physical cues guide tumor cell adhesion and migration. *American Journal of Physiology-Cell Physiology* **306**, C98-C109 (2014).

18   Ma, D. *et al.* Microfluidic platform for probing cancer cells migration property under periodic mechanical confinement. *Biomicrofluidics* **12**, 024118 (2018).

19   Ohashi, T., Mazalan, M. B., Ming, M. & Shin, J. H. S14: Cell mechanics and cell mechanobiology-1 S14-1 Effect of Physical Environment on Cell Migration Using Microchannel Device.

Biography

Qionghua Shen's research interests focus on using microchannel technology for cancer cell confined-migration and metastasis triggered therapeutic resistance study. She received her Bachelor's degree in Clinical Medicine from Nantong University: The Medical School, China, and a Master's degree in Biomedical Engineering from Wayne State University, U.S. She joined Dr. Young-tae Kim's group in the Bioengineering Department at UTA as a Ph.D. student and started to work on the application of microchannel devices in cancer confined-migration and metastasis triggered therapeutic resistance study.

Academic degrees

University of Texas at Arlington: Bioengineering   Arlington, Texas, U.S

     Ph.D. Degree in Biomedical Engineering

     Overall GPA: **4.0** / 4.0

Wayne State University: Biomedical Engineering   Detroit, Michigan, U.S

     Master's Degree in Biomedical Engineering

     Overall GPA: **3.75** / 4.0

Nantong University: The Medical School, Clinical Medicine   Nantong, Jiangsu, China

     Bachelor 's Degree in Clinical Medicine

     Overall GPA: **3.43** / 4.0

Publications and Awards

Publications:

1. **Shen, Q**., Niederstrasser, H., Barakat, R., … & Kim, Y. T. (2020). Single-cell-level screening method for migratory cancer cells and its potential feasibility in high-throughput manner. *Biofabrication*, *12*(3), 035019.

2. Bui, L., **Shen, Q**., Hill, T., Bhuiyan, S. H., ... & Kim, Y. T. (2018). Microchannel device for proteomic analysis of migrating cancer cells. *Biomedical Physics & Engineering Express*, *4*(6), 065026

3. **Shen, Q**., Bui, L., Barakat, R., …& Kim, Y.T. (2018, October). Multifunctional Drug Resistance Triggered by Creep Under 3D Confinement. *Paper presented at the BMES 2018 Annual Meeting in Atlanta, Georgia.*

4. **Shen, Q**., Haddadin, Z., Hill, Tamara., Bui, L., …& Kim, Y.T. (2017, October). High-throughput Cancer Drug Screening for Migratory Cancer Cells. *Paper presented at the BMES 2017 Annual Meeting in Phoenix, Arizona.*

5. **Shen, Q.**, Hill, Tamara., Bui, L., …& Kim, TY.T. (2017, May). High-throughput Screening In Migratory GBM. *Paper presented at the Brain Tumor Summit 2017 in Stephenson Cancer Center, Oklahoma city, Oklahoma.*

6. **Shen, Q.**, Hill, T., Cai, X., … & Kim, Y.T. (2020) Physical Confinement during Cancer Cell Migration Triggers Therapeutic Resistance and Cancer Stem Cell-like Behavior. (submitted).

7. **Shen, Q.**, Germain, A., Wolf, J., & Kim, Y.T. (2020) Confined Migration and Its Contribution to Therapeutic Resistance of GBM. (submitted)

8. **Shen, Q.**, Germain, A., & Kim, Y.T. (2020) Migration and Physical Confinement are Two Indispensable Elements for Upregulating GBM's Chemotherapeutic Resistance. (manuscript preparation).

9. Haider, N., **Shen, Q.**, Palencia, D., … & Kim, Y.T. (2020) Upregulate Drug Resistance of H460 Lung Cancer Cells via Microchannel Device. (manuscript finished).

Honor and Award:

a. 2017, recipient of **Franklyn Alexander PhD Scholarship**, College of Engineering, University of Texas at Arlington, Arlington, Texas.

b. 2020, recipient of **Alfred and Janet Potvin Award for Outstanding Bioengineering Students**, College of Engineering, University of Texas at Arlington, Arlington, Texas.

c. 2017-Present, recipient of **Bioengineering STEM Doctoral Fellowship,** Department of Bioengineering, University of Texas at Arlington, Arlington, Texas.